This is to certify that the
dissertation entitled

INVESTIGATING THE MOLECULAR PATHOGENESIS OF A NOVEL MITOFUSIN 2 MUTATION IN A CANINE NEUROAXONAL DYSTROPHY MODEL

presented by

Rabeah Abbas Al-Temaimi

has been accepted towards fulfillment
of the requirements for the

Ph.D degree in Genetics

Major Professor's Signature

August 20, 2010

Date

N

INVESTIGATING THE MOLECULAR PATHOGENESIS OF A NOVEL MITOFUSIN 2 MUTATION IN A CANINE NEUROAXONAL DYSTROPHY MODEL

By

Rabeah Abbas Al-Temaimi

A DISSERTATION

Submitted to
Michigan State University
In partial fulfillment of the requirement
For the degree of

DOCTOR OF PHILOSOPHY

Genetics

2010

ABSTRACT

INVESTIGATING THE MOLECULAR PATHOGENESIS OF A NOVEL MITOFUSIN 2 MUTATION IN A CANINE NEUROAXONAL DYSTROPHY MODEL

By

Rabeah Abbas Al-Temaimi

Mutations in mitofusin 2 (*MFN2*) gene are one of the underlying causes of the most common inherited neuropathy, Charcot-Marie-Tooth (CMT). A novel *MFN2* mutation (ΔE539) was detected as the cause for an autosomal recessive inherited fetal-onset neuroaxonal dystrophy (FNAD) in a dog model. FNAD pathology manifests in the nervous system, causing secondary effects on muscle functions. MFN2 is a nuclear encoded, mitochondrial outer membrane protein involved in maintaining mitochondrial shape, integrity, and dynamics through protein interaction networks. The aim of this thesis was to investigate the effects of the novel *MFN2* mutation at the molecular and cellular levels. Mutant MFN2 mRNA transcript analysis revealed active transcription of the mutant *MFN2* allele in tissues derived from both homozygous and heterozygous dogs. Immunoblotting, and immunocytochemistry revealed a decreased amount of mutant MFN2 protein in tissues of diseased dogs. Polarography performed on mitochondrial extracts derived from affected pups did not detect any mitochondrial respiratory dysfunctions. Mitochondrial structure and distribution assayed through live-cell imaging of *in-vitro* cultured primary canine fibroblasts in combination with mitochondria specific dyes showed maintained mitochondrial morphology and networks in cells derived from

affected pups. Analysis of mitochondrial membrane potential, an indicator of mitochondrial integrity and health, suggested a reduced membrane potential in affected pup mitochondria. Mitochondrial autophagy and recycling stress was not detected *in-vitro* under normal culture conditions. The mitochondrial fusion function of mutant MFN2 is lost as revealed by specific knock down of its fusion complementing cellular paralogue MFN1 in affected pup primary fibroblast cells. In conclusion, the ΔE539 mutation in MFN2 results in loss of protein expression which is proposed to affect an MFN2 function relevant to nervous system derived tissues. Mitochondrial structure and assayed functions are maintained in affected dog cultured primary fibroblast cells in spite of possible membrane potential declines.

This disse

This dissertation is dedicated to the young generation in my family, above all to Habeeb, my nephew.

ACKNOWLEDGEMENTS

First and foremost, I would like to acknowledge my mentor and friend, Dr. John Fyfe. His supervision and understanding made this work possible. Second, I would like to acknowledge my committee members for their support and guidance. Dr. Andrea Amalfitano, Dr. Karen Friderici, and Dr. Kyle Miller. I consider myself privileged to be envied by my peers for having the best committee. I would like to express my gratitude to other faculty members who have helped and supported me during my PhD, Prof. Shelagh M. Ferguson-Miller, Dr. Steven R. Heidemann, and Dr. Vilma Yuzbasiyan-Gurkan. I would like to extend special acknowledgement to Melinda Kay Frame, Carrie Hiser and Neil Bowlby who were exceptional in providing their time and experience.

I would like to extend heartfelt gratitude and love to my family away from home, all my dear friends and colleagues. Erin foremost has been the best comrade. Her help and thoughtfulness always surpassed my expectations. The Friderici and Schutte lab members who were the best neighbors. Ellen, Eric, Kathy, Meghan, Mei, Soumya, Ayo, Arriana and Walid. Thank you all for being yourselves. My deepest gratitude goes to my best friends away from lab Amal, Hanan, Cheryl, Rehan, Tejas and Pampa (Elizabeth). You have brought so much light into my life; I could not have survived this PhD without you. Special acknowledgment goes to my family and friends in Kuwait. I appreciate their

tolerance

persevere.

Altaf, Fatm

belief and

University

tolerance of my absence, but they never waned from encouraging me to persevere. My mother, my sisters, my nephews and nieces, and my best friends Altaf, Fatma, Fahd, and Sindhu. Thank you all, this work is the product of your belief and confidence in me. Lastly, I am grateful to Kuwait government and University for giving me the opportunity to pursue my PhD degree.

TABLE OF CONTENTS

LIST OF TABLES

LIST OF FIGURES

"Images in this dissertation are presented in color"

KEY TO ABBREVIATIONS

Bak	BCL2-Antagonist/Killer 1
Bax	BCL2-Associated X protein
BCL2	B-Cell Leukemia/Lymphoma 2
BMI	Body Mass Index
CF	Canine Fibroblast
CMT	Charcot-Marie-Tooth
CNS	Central Nervous System
CP	Ceruloplasmin
DMEM	Dulbecco's Modified Eagle Medium
DRG	Dorsal Root Ganglia
Drp1	Dynamin-Related Protein 1
DsiRNA	Double Stranded Interfering RNA
ER	Endoplasmic Reticulum
ERK	Extracellular signal-Regulated Kinase
ERRα	Estrogen Related Receptor-α

FBS	Fetal Bovine Serum
FNAD	Fetal-onset neuroaxonal dystrophy
FRET	Fluorescence resonance energy transfer
FTL	Ferritin light chain
Fzo	Fuzzy onion
GABA-A	Gamma aminobutyric acid-a
GRIF-1	GABA-A receptor interacting factor-1
HMSNVI	Hereditary motor and sensory neuropathy type VI
HPRT	Hypoxanthine phosphoribosyltransferase
HRP	Horse radish peroxidase
HSG	Hyperplasia suppressor gene
INAD	Infantile neuroaxonal dystrophy
KIF1B	Kinesin family member 1 beta
MARCH-V	Membrane-associated RING-CH
MARF	Mitochondrial assembly regulatory factor
MFN1	Mitofusin 1
MFN2	Mitofusin 2

Miro	Mitochondrial Rho
MPT	Membrane permeability transition
mtDNA	Mitochondrial DNA
NBIA	Neurodegenerative disorders with brain iron accumulation
NC1	Non-coding 1
NGF	Nerve growth factor
OIP106	O Glc NAc transferase- interacting protein 106
OMIM	Online Mendelian Inheritance of Man
OPA1	Optic atrophy 1
OXPHOS	Oxidative phosphorylation
PANK2	Pantothenate kinase 2
PGC-1	Peroxisome proliferator–activated receptor γ coactivator-1
PINK1	PTEN-induced putative kinase 1
PKA	Protein kinase A
PLA2G6	Phospholipase A_2, group VI
PMP22	Peripheral myelin protein 22
PMSF	Phenylmethylsulfonyl fluoride

qRT-PCR	Quantitative real-time polymerase chain reaction
Ras	Rat sarcoma protein
ROS	Reactive oxygen species
RT-PCR	Reverse transcriptase-polymerase chain reaction
SDS-PAGE	Sodium dodecyl sulfate –polyacrylamide gel electrophoresis
SEOAN	Severe early-onset axonal neuropathy
SNP	Single nucleotide polymorphism
STOML-2	Stomatin-like protein 2
TMRM	Tetramethyl rhodamine methyl ester
VDAC	Voltage dependent anion channel

CHAPTER I

INTRODUCTION

Chapter I

Introduction

The objective of my research was to characterize a novel mutation in the mitofusin 2 (*MFN2*) gene at the cellular and molecular levels in a dog model of fetal onset neuroaxonal dystrophy. To analyze the novel mutant *MFN2*, I will first briefly describe and review the phenotype observed and its human related disease phenotypes, mitochondrial structure and functions related to MFN2, MFN2 structure and functions, and MFN2 suspected roles in disease.

Understanding the molecular underpinnings of single gene disorders that cause neurological pathologies poses a number of challenges. The challenges can be in the form of phenocopies, phenotype heterogeneity, and nervous system-specific functions. Neuropathies can be primary or secondary. An approximate total of 6,500 inherited disease phenotypes with known molecular factors (2714 phenotypes), or suspected to be Mendelian in nature (1999 phenotypes) are catalogued in the Online Mendelian Inheritance of Man (OMIM). A search conducted in OMIM using "inherited neuropathy" as a keyword, and limited to records with descriptive phenotype resulted in 141inherited neuropathy phenotypes. Among the 141 hits, 54 known genetic factor(s) were recorded that contribute to or are associated with the incidence of an inherited neuropathy. Many of genes play a role in influencing more than one neuropathologic phenotype. Investigations focused on understanding the molecular factors involved in neuropathies to elucidate the pathogenesis of the lesion and to

discern a th

been potenti

and the com

to discern th

biological fu

discern a therapeutic strategy. However, progress in achieving either goal has been potentially hampered by the scarce accessibility of tissue in living subjects, and the complexity and poorly understood biology of neural networks. Therefore, to discern the role of a gene in an inherited neuronal disease and distinguish its biological functions, animal models are extremely important.

Canine Feta

Infant
Seitelberger
presents at
paralysis (1
spheroids ir
brain (6).
disorders a
heterogene
disease pr
neuroaxona
accumulati
towards ful
the other
phenotype
pantothena
enzyme A
disorders
mutation i
accumulat
the *PLA2*
INAD cas
phenocop

Canine Fetal onset Neuroaxonal Dystrophy (FNAD) Phenotype

Infantile neuroaxonal neuropathy (INAD) (INAD, OMIM #256600; a.k.a. Seitelberger disease) is an autosomal recessive neuroaxonal dystrophy that presents at infancy with motor deterioration, hypotonia, and a rapidly progressive paralysis (1-5). The classical diagnosis includes the presence of axonal spheroids in peripheral nerve biopsies, and frequent iron accumulations in the brain (6). INAD has been grouped with several other neurodegenerative disorders associated with brain iron accumulations (NBIA), which form a heterogeneous group of phenotypes classified based on age of onset, rate of disease progression and molecular findings (Figure 1). The major form of neuroaxonal dystrophy known as NBIA1 (OMIM #234200) presents with iron accumulation within the first decade of life (juvenile NAD), and rapid progression towards full paralysis within 15 years. NBIA1 comprises 50% of NBIA cases (7), the other NBIA disorders are disorders of iron metabolism and other NAD phenotypes (8). Mutations underlying NBIA1 disease have been mapped to the pantothenate kinase 2 (*PANK2*) gene that encodes the first enzyme in the co-enzyme A biosynthetic pathway (9). INAD is a second common form of NBIA disorders associated with early onset and rapid progression. The causative mutation in most of INAD cases, more specifically those associated with iron accumulation and an onset within the first 2-years of life, have been mapped to the *PLA2G6* gene that encodes a phospholipase A_2 protein (10, 11). However, INAD cases without *PLA2G6* mutations (~20%) suggest locus heterogeneity or phenocopies with different underlying molecular lesions (10-14). Those INAD

Figure 1-1. Classif

accumulation (NBI

Figure 1-1. Classification of neurodegenerative diseases with brain iron accumulation (NBIA).

NBIA

Early onset, rapid progression

- NBIA1 (*PANK2*)
- INAD (*PLA2G6*)
- Idiopathic NBIA (unknown)

Late onset, slow progression

- Atypical NBIA1 (*PANK2*)
- Atypical NAD (*PLA2G6*)
- Neuroferritinopathy (*FTL*)
- Aceruloplasminemia (*CP*)
- Idiopathic NBIA1 (unknown)

cases ass
conform to
here.

A
developme
(FNAD) a
affected b
soon after
phenotype
hypoplasia
nerve root
system, al
showed d
nuclei. Bra
evidence o
formation,
above mer
throughout
spheroids
material co
filaments,

cases associated with earlier onset and severe rapid progression of disease conform to the canine fetal onset neuroaxonal dystrophy phenotype discussed here.

A canine animal model with severe neurological impairment of development and fetal onset was identified as fetal onset neuroaxonal dystrophy (FNAD) and characterized anatomically (15) (Appendix A). Newborn pups affected by this phenotype exhibit fetal akinesia during late gestation and die soon after birth due to respiratory insufficiency. Physical characteristics of the phenotype include arthrogryposis, scoliosis, pulmonary hypoplasia, cerebellar hypoplasia, smaller brainstem, and reduced diameter of the spinal cord and nerve roots. Histological findings of pathology are restricted to the nervous system, albeit sparing the cerebral hemispheres. For example, the cerebellum showed delayed development and degeneration of Purkinje cells and deep nuclei. Brainstem, spinal cord and spinal nerve roots were found to demonstrate evidence of active neurodegeneration, axonal swelling and dystrophy. Spheroid formation, a characteristic feature of some axonal neuropathies, for example the above mentioned INAD (16) and sensory dominant ataxia (17), was also evident throughout the brainstem and spinal cord. Ultrastructural examination of spheroids using electron microscopy revealed accumulations of electron dense material consisting of fragmented organelles, disorganized arrays of intermediate filaments, and amorphous matter. Repeated matings revealed a simple

autosomal recessive mode of inheritance with full penetrance (15). Genetic exclusion of the *PLA2G6* gene as causative factor for canine FNAD was conducted even though no iron accumulation was detected. Alleles of markers flanking the canine *PLA2G6* did not segregate with deduced FNAD alleles, thus eliminating *PLA2G6* gene involvement (15), (Appendix A).

Canine Fetal onset Neuroaxonal Dystrophy (FNAD) Molecular Etiology

To assay for the underlying mutation causing FNAD, a combination of linkage mapping and SNP haplotype analyses was conducted, and a 200kb interval demonstrating zero recombination was detected (personal communication with supervisor John Fyfe). Sequencing of genes in the interval revealed a novel three base deletion mutation in the mitofusin-2 (*MFN2)* gene, a mutation inherited homozygosly only by animals demonstrating FNAD disease phenotype.

MFN2 is a nuclear encoded mitochondrial outer membrane protein. The mutation leads to a single amino acid deletion of a glutamic acid residue at position 539 (ΔE539). Mutations in the *MFN2* gene have been previously associated with motor and sensory neuropathies that include Charcot-Marie-Tooth (CMT2A2, OMIM #609260), hereditary motor and sensory neuropathy type VI (HMSNVI, OMIM #601152), and sporadic severe early onset axonal neuropathy (SEOAN) (18) (Figure 1-2). Charcot-Marie-Tooth (CMT) is one of the most common inherited neuropathies, with an estimated prevalence rate of 17-40 cases for every 100,000 individuals (19, 20). The clinical phenotype includes a progressive weakness and muscular atrophy in the most distal limbs that gradually progresses proximally. There is considerable loss of peripheral nerve axons resulting in loss of deep tendon reflexes and onset of foot deformities such as hammer toes or flat feet (21, 22). There are several different types of CMT. These phenotypes are classified according to electrophysiological analysis, histological analysis, and genetic findings (23). CMT can be transmitted in an

autosomal dominant, autosomal recessive, or X-linked mode of inheritance (24). The principal forms, CMT1 and CMT2, are distinguished by electrophysiology and neuronal pathology. Demyelinating CMT1 types A-F are autosomal dominant forms with characteristic demyelination of sensory and motor nerves, and slowed nerve conduction velocities. CMT2 types A-L are autosomal dominant forms with characteristic axonal degeneration and maintained or mildly reduced nerve conduction velocities. CMT1 forms with autosomal recessive transmission are classified as CMT4, and rare recessive forms of CMT2 are classified as AR-CMT2 (25). CMTX1 is X-linked dominant (26), whereas CMTX2-4 are X-linked recessive (27). Moreover, a dominant intermediate form of CMT (DI-CMTA-D) has been identified with an intermediate electrophysiological profile between CMT1 and CMT2 and different underlying molecular lesions (28, 29). Extensive classification criteria have been employed to arrive at this categorization, albeit it is not fixed.

Etiologic genetic factors and mutations underlying most of reported CMT phenotypes have been discovered, in total 17 genes and 25 chromosomal regions (30). However, varying degrees of disease severity (31, 32), age of onset (33), and ethnic patterning (19, 34) suggest modifier genes/environment involvement. Treatment of CMT forms is limited to management and corrective surgeries with few reports investigating possible molecular therapies (35-37). *MFN2* mutations have been associated with the most common form of CMT2 (38), CMT2A2, and are mostly point mutations leading to amino acid substitution (39). The CMT2 phenotype has been mapped to six different genes and two

Figure 1-2. The structure of MFN2 protein with highlighted known functional domains (block squares). SOEAN (**), HMSNVI (*), and CMT2A2 associated mutations are aligned based on their functional domain localization. Δ, deletion; fs, frame shift; X, premature stop codon.

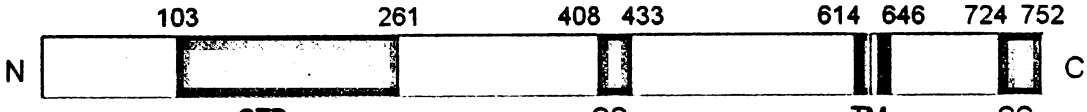

Q45R
V69F
L76P
L92P
R94Q
R94W*
K98E
A100G

R104W
T105M
P123L
G127V
A164V**
P165R
P165Y
T206I*
I213T
D214N**
F216S
F223L
T236M
V244M
R250Q
P251A

S263P
V273G
R274Q
Q276R*
H277R
R280H
F284Y
G298R
E347V
S350P
K357N
H361Y*
T362M
R364W*
M376I
ΔK379-M381
A383V
Q386P
C390R**
R400X

R418X*
E424G
P456L
R468H

D570S

V705I
R707W
K710P
A716T
W740S
Q751X
L753fs

associate

kinesin fa

with a la

KIF1B ge

most cor

including

reflexes,

sensory lo

(51, 52). M

and follow

that regio

hereditary

phenotype

and/or se

axonal ne

years of a

mild audito

MFN2 va

mutations

associated

nervous sy

between m

so far has

associated chromosomal loci (40-49). The first CMT2 gene to be discovered was kinesin family member 1 beta gene (*KIF1B*) (41, 50), however it did not associate with a large number of investigated families. Following exclusion of CMT2A1 *KIF1B* gene involvement, a uniform phenotypic subset of CMT2 patients with the most common characteristics of CMT2 was analyzed. Phenotype criteria including distal lower limb muscular atrophy, lower limb diminished or lost tendon reflexes, absent or slightly reduced nerve conduction velocity, along with mild sensory loss in lower extremities were used to map the CMT2A2 specific region (51, 52). Mapping results associated a region on human chromosome 1p35-p36, and follow up sequencing studies identified mutations in *MFN2* localized within that region (47). Another hereditary neuropathy caused by *MFN2* mutations is hereditary motor and sensory neuropathy type VI (HMSN VI). The associated phenotype is indistinguishable from CMT2A2 except for impaired nocturnal vision and/or sensorineural hearing loss involvement (53, 54). Severe early onset axonal neuropathy (SEOAN) is a sporadic form of CMT2 occurring before 5 years of age and progressing through adult life. The phenotype is associated with mild auditory impairment but not with nocturnal vision loss. Identified mutations in *MFN2* vary between homozygous and compound heterozygous missense mutations presenting a recessive mode of inheritance (18). Overall, the associated mutations in *MFN2* have varying degrees of pathogenic effect on the nervous system indicating a threshold effect of product toxicity or a relationship between mutation location and phenotype severity. However, no *MFN2* mutation so far has been associated with a neuroaxonal dystrophy phenotype.

Mitofusi

Mi

of structu

2 was fir

Onions (

formation

and the

analysis

Th

exons of

are hype

factor (M

paralogu

mitofusir

mitochor

participa

overall a

greater

different

upstrear

upstrear

activatic

prolifera

Mitofusion-2 Gene and Protein Structure

Mitofusin-2 (MFN2) belongs to the dynamin family of GTPases composed of structurally related but functionally varied proteins of different sizes. Mitofusin-2 was first identified in the fruit fly *Drosophila melanogaster* and termed Fuzzy Onions (Fzo) corresponding to its discovery during the onion stage of spermatid formation (55). Studies in yeast identified yeast Fzo orthologue Fzo1p (56, 57), and the mammalian orthologue was identified through sequence homology analysis and functional assays in-*vitro* (58).

The canine *MFN2* gene is located on chromosome 2 and consists of 19 exons of which 17 exons are protein coding. Alternative names for mitofusins are hyperplasia suppressor gene (HSG) and mitochondrial assembly regulatory factor (MARF). In conjunction with identifying the mammalian MFN2 a cellular paralogue to it has been identified; namely Mitofusin-1 (MFN1) (58). While both mitofusins are ubiquitously expressed, nuclear encoded, and are targeted to the mitochondrial outer membrane, each has different interaction partners and participate in various functional pathways. MFN1 shares approximately 66.2% overall amino acid sequence similarity to MFN2, and has an approximate 8-fold greater GTPase activity than MFN2 (59). *MFN2* gene expression is regulated by different transcription factors interacting with different regulatory elements upstream of the *MFN2* gene. A promoter sequence element has been identified upstream of the transcription start site at region -421 to -397 (60). Transcriptional activation of *MFN2* has been shown to be sensitive to inductions of peroxisome proliferator–activated receptor γ coactivator (PGC-1) α and β forms, and

estrogen r

skeletal mu

also been

binding to

MFN

membrane

identified i

domain in

made up o

functions:

(PKA) ph

domains,

the cytos

eukaryotic

GTPase

conservati

conserved

four conse

(Figure 1-

fusion and

coiled coil

with MFN2

estrogen related receptor-α (ERRα) through active binding at promoter sites in skeletal muscle and immortalized muscle derived cell-lines (60-62). PGC-1 δ has also been found to actively induce *MFN2* expression in heart, however via active binding to a different promoter element at -837 to -817 (63).

MFN2, like its cellular paralogue MFN1, is a mitochondrial outer membrane bound protein. MFN2 mitochondrial targeting sequences have been identified in the bipartite hydrophobic residues making up the transmembrane domain in the C-terminal portion of the protein (58, 64). Mammalian MFN2 is made up of 757 residues (86 KDa) and contains five distinct domains of known functions: N-terminus GTPase domain, a coiled coil domain, a protein kinase A (PKA) phosphorylation site at serine 442 (65), two short transmembrane domains, and a C-terminus coiled coil domain. The C- and N-termini both face the cytosol (Figure 1-3A) (64). Phylogenic comparison of MFN2 and its eukaryotic orthologues in different species revealed high conservation of the GTPase domain sequence, whereas other domains shared moderate conservation (66). Moreover, these studies revealed seven consistently conserved regions of which some overlapped with known functional domains and four conserved regions of unknown function on the cytosolic N-terminus of MFN2 (Figure 1-3B). Three of the unknown regions seem to contribute to mitochondrial fusion and interact with the C-terminal coiled coil domain. The abundance of coiled coil cellular proteins (67) suggests possible interactive protein partners with MFN2 through its coiled coil domain (66).

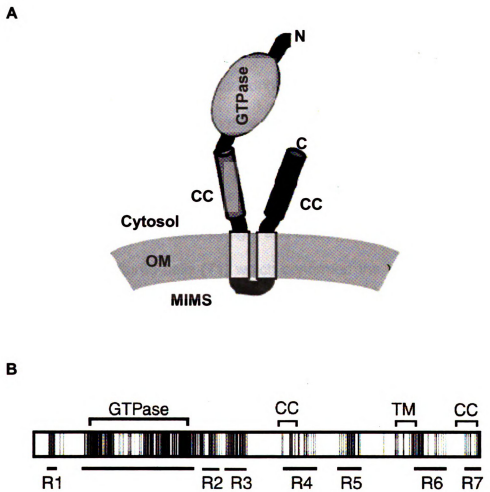

Figure1- 3. A) Predicted MFN2 protein structure as it localizes in the mitochondrial outer membrane (68). **B)** Highly conserved regions (R1-R7) derived from comparative sequence homology between mitofusins of mouse, *Drosophila melanogaster* (fruit fly) and *Caenorhabditis elegans* (66). OM, outer membrane; TM, transmembrane; MIMS, mitochondrial intermembrane space; CC, coiled coil; N, N-terminus; C, C-terminus.

The Mitochondrion

MFN2 is a nuclear encoded mitochondrial outer membrane protein. MFN2 functions as a key protein involved in regulating mitochondrial physical and biochemical properties. The mitochondrion is a eukaryotic subcellular organelle considered a multi-tasking powerhouse that conveys its vital cellular impacts via biochemical and physical interactions. Mitochondria were first described in the late 19th century as granular threads inside the sperm cell (69). Since then these observations were corroborated by light and electron microscopy observations of tissues (70) and cultured cells (71) which confirmed the reticular morphology of mitochondria. The mitochondrion is a double membrane bound organelle with a smooth outer mitochondrial membrane, and an undulating inner membrane with large surface area. Individual extended invaginations of the inner membrane are termed cristae and are anchored to the inner membrane by thin tubules (cristae junctions) (72). The inner membrane envelopes the mitochondrial matrix which harbor copies of mtDNA and matrix proteins, while the inter-membrane space allows for extended interaction between the inner and outer membrane proteins. The outer membrane is characterized by enhanced permeability due to its high lipid content and voltage gated channels (73), whereas the inner membrane is mostly protein in nature with restricted permeability (74, 75). The primary role of mitochondria is energy production via the oxidative phosphorylation pathway (76, 77) that acquires its substrates in the form of high energy intermediates from metabolic pathways (eg. glycolysis) to generate the energy coin of the cell, adenosine triphosphate (ATP) (78). The mitochondrion contains its own genome

that enco
mitochon
importanc
cellular p
cellular sig
thought to
mitochon
channels
buffering
85), meta
mitochon
external r

Tl
tubular n
alternatir
throughc
by cycle
are inde
The ma
potentia
electron
dictates
impact

that encodes 37 genes; 13 for subunits of respiratory complexes, 22 for mitochondrial tRNA, and 2 for rRNA (79). Additional functions of equal importance (80) include calcium buffering, control of apoptosis, regulation of cellular proliferation signals, regulation of cellular metabolism, propagation of cellular signals, and steroid synthesis (81). Calcium buffering, a property that was thought to be the province of endoplasmic reticulum, is a process by which mitochondria at sites of calcium flux take up calcium through outer membrane channels to dampen effects of calcium overload on the cell (82). Calcium buffering is of major importance since it directly affects vital cellular signaling (83-85), metabolism (86, 87), and survival (88). Aside from its protein content (89), mitochondrial structure, shape and dynamics also dictate the optimal internal and external responses within the cell.

The mitochondrion as its Latin name indicates can be tubular or extended tubular networks (Mitos = thread) or vesicular (chondros = grain) in shape. These alternating shapes allow for focal or uniform distribution of mitochondria throughout the cell. The dynamics of shape shifting and distribution is regulated by cycles of fusion, fission and transport of mitochondria (90). Fusion and fission are independent mechanisms mediated by their own sets of specific proteins. The majority of mitochondrial functions rely on an intact mitochondrial membrane potential that is maintained by a proton gradient formed in conjunction with electron transport through a serious of redox reactions. Membrane potential dictates fusion/fission capabilities and membrane permeability, thus directly impacting mitochondrial dynamics and biochemical efficiency. To date,

mitochondrial dysfunctions have been implicated in a wide array of neurodegenerative disorders and diseases of aging either as the causative factor (91) or a secondary factor contributing to disease.

Mitofusin-2 Functions and Interactions

Mitofusins as their name imply are major players in the mitochondrial fusion phenomenon. Mitochondrial fusion was thought to be restricted to formation of giant mitochondria during spermatogenesis (92), or under induced stressful conditions *in-vivo* (93-97), and *in-vitro* (98). However, the abundance of reports (99-101) describing long networks of mitochondria forming a reticulum in many eukaryotic cells established mitochondrial fusion as a physiological phenomenon required for cellular homeostasis (102). Mitochondrial fusion/fission cycles are thought to sustain efficient mitochondrial morphology, distribution, and biochemical competence to adapt to changing intrinsic and extrinsic parameters (103). The regulation of fusion/fission cycles are believed to be regulated by phosphorylation, sumoylation, and ubiquitination events, however pathways and proteins involved are unclear (104). Forming mitochondrial tubules through fusion is critical for maintaining respiratory efficiency (105). In addition, co-mixing of mitochondrial DNA (mtDNA) has been shown to occur during fusion, which also allows distribution of replicated mtDNA (106-109). Fusion is also postulated to buffer out reactive oxygen species (ROS) by dilution and by exposing ROS to a more abundant and healthy detoxifying mitochondrial environment (110).

Several proteins play a part in fusion, and their collaborative activity is antagonized by fission which involves a different set of proteins, resulting in a dynamic state of cellular mitochondria to establish cellular equilibrium and maintenance (90). The mitofusins are ubiquitously expressed but their expression levels vary differentially in different tissues (111). While MFN1

functions primarily in mitochondrial membrane fusion, it also tethers membrane more strongly than MFN2 through its direct interaction with the mitochondrial inner membrane dynamin related protein, optic atrophy 1 (OPA1) (59, 112). The mitofusins are believed to form hetrodimers and homodimers through their C-terminal coiled coil domains projecting from opposite mitochondria outer membranes (59, 68) to initiate fusion in a GTP dependent manner and in the presence of proper mitochondrial membrane potential (55, 56, 58, 113).

Both mitofusins are critical for embryonic development since knock out mouse models of either mitofusin are embryonic lethal during mid-gestation (114). Lethality highlights MFN2 essential role in formation of the placental trophoblast giant cell layer (114), while MFN1 is believed to have a function in placental maintenance (115). Moreover, evidence implicates MFN2 as an early stage critical protein in regulating embryonic preimplantation development; its expression is abundant in cytoplasm of oocytes and progresses in a spatio-temporal pattern throughout blastocyst maturation (116). Apoptosis is another physiological process that is influenced by mitofusins. During apoptosis mitochondria undergo increased fission that augments outer membrane permeability and release of proapoptotic factors that incite cell death. During apoptotic stimuli, pro-apoptotic BCL2-associated X protein (Bax) translocates from the cytosol to the mitochondrial outer membrane and forms porous clusters in association with several mitochondrial outer membrane proteins that include BCL2-antagonist/killer 1 (Bak), another pro-apoptotic protein (117). There is direct evidence that Bak binds both mitofusins under normal cellular conditions,

however
tightly to
(118). Alt
fragment
foci with I
apoptosis
unfavoral
MFN2 in
anti-apop
(BCL-xL)
apoptosis
suppress
cell fate r
rat sarco
inhibiting
cascade

MF
mitochon
degradati
lysosoma
for autop
fission, a
hyper fus

however once apoptotic signals are received it dissociates from MFN2 and binds tightly to MFN1 inhibiting mitochondrial fusion while promoting fragmentation (118). Although Bak is believed to be the key player in promoting mitochondrial fragmentation, Bax aids in the membrane permeability shift by forming protein foci with Bak and MFN2 (119, 120). In addition, activation mutants of MFN2 resist apoptosis via the Bax/Bak pathway by promoting mitochondrial fusion despite unfavorable loss in membrane potential, thus further establishing the role of MFN2 in inhibiting the mitochondrial pathway to apoptosis (121). Interestingly, anti-apoptotic factors B-cell leukemia/lymphoma 2 (BCL-2) and BCL2-like 1 (BCL-xL) proteins have been shown to directly interact with MFN2 to counteract apoptosis related mitochondrial fission, however this interaction does not suppress Bax mediated apoptosis or release of apoptotic factors (122). Another cell fate role pertinent to MFN2 is an anti-proliferative property through binding to rat sarcoma (Ras) proto-oncogene via its N-terminus p21 ras signature motif and inhibiting the extracellular signal-regulated kinases1/2 (ERK1/2) signaling cascade that promotes proliferation (123).

MFN2 is implicated in another cellular survival pathway, namely mitochondrial autophagy or mitophagy. Mitophagy is the cellular controlled degradation of dysfunctional mitochondria through autophagic factors and lysosomal recruitment. Sorting out dysfunctional mitochondria and targeting them for autophagy requires a complex mechanism that involves cycles of fusion, fission, and mitochondrial outer membrane ubiquitinylation (124-126). A cycle of hyper fusion is the first step in mitochondrial sorting to dilute the effects of

damaged mitochondria (106). Once irreversibly damaged mitochondria are singled out by loss of mitochondrial membrane potential (113), these mitochondria become enlarged through an unknown process and become unable to fuse and exchange their contents (127). Targeting dysfunctional mitochondria for mitophagy involves translocating the cytoplasmic ubiquitin ligase Parkin to mitochondrial outer membranes for active protein ubiquitinylation (128), an event dependent on PTEN-induced putative kinase 1 (PINK1) protein (129). Parkin mediated MFN2 ubiquitinylation results in two ubiquitinylated forms, single and multi-ubiquitinylated MFN2 (129). Patterned ubiquitinylation is thought to harbor functional attributes other than ubiquitin-mediated proteosome degradation (128, 130). A single MFN2 ubiquitinylation event targets MFN2 to proteosomal degradation, whereas multi-ubiquitinylated MFN2 destines mitochondria for mitophagy. This suggests that MFN2 is involved in two steps of mitophagy; inhibiting fusion via MFN2 degradation and branding dysfunctional mitochondria for mitophagy.

MFN2 interacts with other proteins in a tissue specific manner to promote mitochondrial tissue specific functions. Recent evidence show mitofusins directly interact with members of the axonal transport machinery in neurons (131). Mitochondrial Rho (Miro) is a protein identified in humans as an atypical Rho-GTPase localizing in mitochondrial outer membranes, and has two cellular paralogues Miro1 and 2 (132). Milton is a mitochondrial protein identified in *Drosophila* and found to have a predicted coiled-coil domain (133). Two human

orthologues of Milton were identified as GABA-A receptor-interacting factor 1 (GRIF-1) and O Glc NAc transferase- interacting protein 106 KDa (OIP106) (134). Miro and Milton interactions were predicted in *Drosophila* (135) and proven in their human orthologues to play a collaborative role in neuroaxonal transport of mitochondria (136). Miro and Milton human orthologues exhibit stronger MFN2:Miro2 interaction than Miro1, and a lesser interaction with Milton orthologues when compared to their MFN1 interaction (131). This finding supports an indirect functional role for MFN2 in mitochondrial axonal transport since no direct interaction with the Kinesin motor protein has been established (131).

There is direct evidence of novel interactions of MFN2 with protein partners mediating unknown functions, which proposes the possibility of undefined functions of MFN2. Novel interaction partners with MFN2 include human membrane-associated RING-CH (MARCH)-V, a mitochondrial outer membrane protein. MARCH-V is a novel mitochondrial ubiquitin ligase that inactivates the fission protein Drp1 via ubiquitinylation, while preserving its association with active MFN2 to promote mitochondrial fusion (137). Another novel protein was detected through its association with MFN2, stomatin-like protein 2 (STOML-2) that was previously believed to be an exclusively plasma membrane protein (138). However, evidence shows it to be targeted to mitochondrial inner membrane in a membrane potential dependent manner and processed to situate facing the mitochondrial intermembrane space and form

hetrodimers with MFN2 (139). The functional significance of this interaction is unknown; knock down of STOML2 only depolarizes mitochondria without any alteration to their morphology.

MFN2 has been shown to be a regulator of metabolism, cellular respiration and mitochondrial membrane potential. The role of MFN2 in regulating metabolism has been investigated primarily in skeletal muscle. Myogenesis is associated with upregulation of *MFN2* expression and increased mitochondrial fusion, enhanced aerobic glucose oxidation, enhanced cellular oxidative respiration, and maintenance of an optimal mitochondrial membrane potential (140). In addition, a noted upregulation in *MFN2* expression has been reported in skeletal muscle after physical exercise, most likely to promote similar effects as in myogenesis and to optimize cellular energy expenditure (60). In experiments where MFN2 deficiency has been imposed, marked reductions in glucose and lipid oxidation, in membrane potential, and in expression of nuclear encoded oxidative phosphorylation (OXPHOS) subunits have been observed (141). Conversely, overexpression of MFN2 in the same system enhanced mitochondrial membrane potential and promoted glucose oxidation, in addition to induced expression of OXPHOS subunits of complexes I, IV and V specifically, in a mode independent of its mitochondrial fusion function (141).

Mitochondria require spatial and temporal proximity to the endoplasmic reticulum (ER) for calcium exchange and utilization of ER lipid synthesis enzymes, events that are critical for mitochondrial functions (142-144). Calcium buffering itself is an emerging function of mitochondria. Mitochondrial functions affected by calcium levels include oxidative phosphorylation (145), outer membrane permeability, and apoptosis (146). MFN2 has been shown to localize in ER membranes and associate with mitofusins on opposing mitochondrial outer membranes, mediating the tethering of ER to mitochondria to form microdomains required for functional calcium ion exchange and ER morphological regulation based on cellular demands (147-150).

It has become clear that even though MFN2 has mitochondrial fusion abilities, its functions are not restricted to fusion alone (148). MFN2 is involved in many cellular survival and homeostasis pathways that greatly increase its significance as a major player in cell fate. This fact also highlights its possible role in disease and abnormal phenotypes and the varied complex mutant phenotypes that may result from perturbation of one or more of its functions.

Mitofusin-2 Mutations in Disease

MFN2 mutations in CMT2A2 as mentioned earlier are mostly missense mutations (39, 151), with a novel splicing mutation reported recently (152). Severity of phenotype seems to correlate with increased dysfunction caused by mutations within or close to the N-terminal GTPase domain of MFN2 (151). Mechanism of pathogenesis in CMT2A caused by *MFN2* mutations has been increasingly studied without a uniform conclusion, but rather varied findings depending on type of mutation investigated. *In-vitro* studies on CMT2A patients' fibroblasts showed no mitochondrial morphology, respiration, or fusion defects correlating with *MFN2* mutations (153). This finding is supported by studies that have proven MFN1 can complement some MFN2 functions in maintaining mitochondrial integrity and fusion (154), and the fact that in CMT2A only neuronal cells are affected with pathology. However, another study in CMT2A fibroblasts investigated mitochondrial membrane potential and mitochondrial coupling and found partial uncoupling in mitochondrial control of respiration causing ~ 30% reduction in mitochondrial membrane potential (155). These findings were insufficient to explain the severe pathology seen in neurons, a realization that prompted the need to investigate *MFN2* mutants in neuronal cells. A single study has attempted such a regimen by using cultured embryonic rat dorsal root ganglion cells transfected with two CMT2A *MFN2* mutations. Although no morphological or oxidative respiration changes were noted, there was mitochondrial aggregation and a significant disruption in axonal transport (156). The axonal transport distortion involved stationary mitochondrial aggregates

within the axon and lesser numbers of uniformly sized, individual mobile mitochondria (156). Mitochondrial movement has been shown to undergo a qualitative change in MFN2 knock out mouse embryonic fibroblasts (114) and in MFN2 mutants with abolished GTP hydrolysis capacity (121). However, it hasn't been documented in neuronal cells, and the recent report of mitofusins interacting with axonal transport machinery (131) might clarify this pathogenic mechanism. In a study that aimed at studying properties of mutant MFN2 proteins in maintaining their functions and stability, selected mutants were expressed in yeast (157). The mutant proteins with mutations within the GTPase domain, V196M and V327T, formed disorganized and clustered mitochondria respectively, while a mutation in the C-terminal coiled coil domain caused extensively tubular mitochondrial morphology. Moreover, discrepancies in mitochondrial fusion abilities were noted in only the V327T mutant, which was also the only mutant displaying loss of GTP hydrolysis. Interestingly, ubiquitinylation of MFN2 mutants was dictated by retaining GTP hydrolysis function, with the V327T being the most stable MFN2 mutant and exceeding that of wild type MFN2 (157). These results taken together reinforce the idea of different mutations cause different mechanisms of pathogenesis, resulting in similar outcomes but with varying severities in CMT2A and other *MFN2* related neuropathies.

To elucidate the role of MFN2 in neurodegeneration, conditional knockout mice were created that lack MFN2 expression in developing embryonic tissues after day 7 of gestation (115). Active neurodegeneretion was seen throughout the

developing cerebellum due to loss of MFN2 mediated mitochondrial fusion. Examining Purkinje cells lacking MFN2 by in-vivo, in-vitro, and ultra structural studies revealed a specific functional dependence on MFN2. Purkinje cells lacking MFN2 have altered mitochondrial distribution, altered structure, altered respiration, and loss of mtDNA nucleoids. Moreover, developing Purkinje cells have a preferred requirement of MFN2 but not MFN1 for maintaining spine formation, dendritic outgrowth, and cell survival (115). This conditional MFN2 knockout mouse model is of important value towards proving that different tissues have different MFN2 functions and different sensitivities to MFN2 aberrations.

Aside from actual mutations in functional MFN2 domains, quantitative changes in *MFN2* expression have been associated with obesity and type-2 diabetes. Noted reductions in *MFN2* expression have been detected in obese and type-2 diabetic patients in a manner correlated with Body-Mass-Index (BMI) (158). Inversely, analyzing *MFN2* levels following weight loss and exercise showed enhanced elevations in *MFN2* expression and enhanced metabolism and energy production (60, 158-160). Collectively these findings negate the idea of MFN2 being involved solely in mitochondrial fusion and maintaining morphology. It extends MFN2 functions to regulating cellular metabolism, bioenergetics, and homeostasis, in addition to cell type specific functions such as axonal transport in neuronal cells. It will be necessary to investigate the capacities of MFN2 functional domains in different tissues and in relevant cellular organelles to fully fathom the pleiotropy of MFN2 functions.

The subsequent chapters aim at investigating the novel MFN2 mutation of FNAD dogs in relation to its functions and protein associations mentioned here. Wild type and mutant *MFN2* mRNA and protein expression were analyzed simultaneously with MFN1 expression in different tissues. Mitochondrial functions with direct evidence of MFN2 protein involvement were assayed *in-vitro* to determine cellular affects of mutant MFN2. Mitochondrial respiration, mitochondrial morphology and distribution, mitochondrial autophagy, and mitochondrial membrane potential were analyzed for aberrations. Mitochondrial fusion ability of mutant MFN2 was tested in-vitro by knocking down MFN1 and assaying for mutant MFN2 fusion complementation. Finally, in light of reviewed MFN2 literature and all data generated by my thesis project, findings will be discussed and conclusions will be drawn to postulate new hypotheses to interpret the FNAD dog phenotype.

References

1 Janota, I. (1979) Neuroaxonal dystrophy in the neonate. A case report. *Acta Neuropathol*, **46**, 151-154.

2 Tachibana, H., Hayashi, T., Kajii, T., Takashima, S. and Sasaki, K. (1986) Neuroaxonal dystrophy of neonatal onset with unusual clinicopathological findings. *Brain Dev*, **8**, 605-609.

3 Hunter, A.G., Jimenez, C.L., Carpenter, B.F. and MacDonald, I. (1987) Neuroaxonal dystrophy presenting with neonatal dysmorphic features, early onset of peripheral gangrene, and a rapidly lethal course. *Am J Med Genet*, **28**, 171-180.

4 Chow, G. and Padfield, C.J. (2008) A case of infantile neuroaxonal dystrophy: connatal Seitelberger disease. *J Child Neurol*, **23**, 418-420.

5 Barlow, J.K., Sims, K.B. and Kolodny, E.H. (1989) Early cerebellar degeneration in twins with infantile neuroaxonal dystrophy. *Ann Neurol*, **25**, 413-415.

6 Gregory, A., Polster, B.J. and Hayflick, S.J. (2009) Clinical and genetic delineation of neurodegeneration with brain iron accumulation. *J Med Genet*, **46**, 73-80.

7 Hayflick, S.J., Westaway, S.K., Levinson, B., Zhou, B., Johnson, M.A., Ching, K.H. and Gitschier, J. (2003) Genetic, clinical, and radiographic delineation of Hallervorden-Spatz syndrome. *N Engl J Med*, **348**, 33-40.

8 Kurian, M.A., Morgan, N.V., MacPherson, L., Foster, K., Peake, D., Gupta, R., Philip, S.G., Hendriksz, C., Morton, J.E., Kingston, H.M., Rosser, E.M., Wassmer, E., Gissen, P. and Maher, E.R. (2008) Phenotypic spectrum of neurodegeneration associated with mutations in the PLA2G6 gene (PLAN). *Neurology*, **70**, 1623-1629.

9 Zhou, B., Westaway, S.K., Levinson, B., Johnson, M.A., Gitschier, J. and Hayflick, S.J. (2001) A novel pantothenate kinase gene (PANK2) is defective in Hallervorden-Spatz syndrome. *Nat Genet*, **28**, 345-349.

10 Morgan, N.V., Westaway, S.K., Morton, J.E., Gregory, A., Gissen, P., Sonek, S., Cangul, H., Coryell, J., Canham, N., Nardocci, N., Zorzi, G., Pasha, S., Rodriguez, D., Desguerre, I., Mubaidin, A., Bertini, E., Trembath, R.C., Simonati, A., Schanen, C., Johnson, C.A., Levinson, B., Woods, C.G., Wilmot, B., Kramer, P., Gitschier, J., Maher, E.R. and Hayflick, S.J. (2006) PLA2G6, encoding a phospholipase A2, is mutated in neurodegenerative disorders with high brain iron. *Nat Genet*, **38**, 752-754.

11 Gregory, A., Westaway, S.K., Holm, I.E., Kotzbauer, P.T., Hogarth, P., Sonek, S., Coryell, J.C., Nguyen, T.M., Nardocci, N., Zorzi, G., Rodriguez, D., Desguerre, I., Bertini, E., Simonati, A., Levinson, B., Dias, C., Barbot, C., Carrilho, I., Santos, M., Malik, I., Gitschier, J. and Hayflick, S.J. (2008) Neurodegeneration associated with genetic defects in phospholipase A(2). *Neurology*, **71**, 1402-1409.

12 Rakheja, D., Uddin, N., Mitui, M., Cope-Yokoyama, S., Hogan, R.N. and Burns, D.K. (2010) Fetal akinesia deformation sequence and neuroaxonal dystrophy without PLA2G6 mutation. *Pediatr Dev Pathol.*

13 Khateeb, S., Flusser, H., Ofir, R., Shelef, I., Narkis, G., Vardi, G., Shorer, Z., Levy, R., Galil, A., Elbedour, K. and Birk, O.S. (2006) PLA2G6 mutation underlies infantile neuroaxonal dystrophy. *Am J Hum Genet*, **79**, 942-948.

14 Wu, Y., Jiang, Y., Gao, Z., Wang, J., Yuan, Y., Xiong, H., Chang, X., Bao, X., Zhang, Y., Xiao, J. and Wu, X. (2009) Clinical study and PLA2G6 mutation screening analysis in Chinese patients with infantile neuroaxonal dystrophy. *Eur J Neurol*, **16**, 240-245.

15 Fyfe, J.C., Al-Tamimi, R.A., Castellani, R.J., Rosenstein, D., Goldowitz, D. and Henthorn, P.S. (2010) Inherited neuroaxonal dystrophy in dogs causing lethal, fetal-onset motor system dysfunction and cerebellar hypoplasia. *J Comp Neurol*, **518**, 3771-3784.

16 Itoh, K., Negishi, H., Obayashi, C., Hayashi, Y., Hanioka, K., Imai, Y. and Itoh, H. (1993) Infantile neuroaxonal dystrophy--immunohistochemical and ultrastructural studies on the central and peripheral nervous systems in infantile neuroaxonal dystrophy. *Kobe J Med Sci*, **39**, 133-146.

17 Moeller, J.J., Macaulay, R.J., Valdmanis, P.N., Weston, L.E., Rouleau, G.A. and Dupre, N. (2008) Autosomal dominant sensory ataxia: a neuroaxonal dystrophy. *Acta Neuropathol*, **116**, 331-336.

18 Vallat, J.M., Ouvrier, R.A., Pollard, J.D., Magdelaine, C., Zhu, D., Nicholson, G.A., Grew, S., Ryan, M.M. and Funalot, B. (2008) Histopathological findings in hereditary motor and sensory neuropathy of axonal type with onset in early childhood associated with mitofusin 2 mutations. *J Neuropathol Exp Neurol*, **67**, 1097-1102.

19 Martyn, C.N. and Hughes, R.A. (1997) Epidemiology of peripheral neuropathy. *J Neurol Neurosurg Psychiatry*, **62**, 310-318.

20 Skre, H. (1974) Genetic and clinical aspects of Charcot-Marie-Tooth's disease. *Clin Genet*, **6**, 98-118.

21 Walker, A.E., Laws, E.R. and Udvarhelyi, G.B. (1998) *The genesis of neuroscience*. American Association of Neurological Surgeons, Park Ridge, Ill.

22 Tooth, H.H. (1886) *The peroneal type of progressive muscular atrophy*. Lewis, London.

23 Banchs, I., Casasnovas, C., Alberti, A., De Jorge, L., Povedano, M., Montero, J., Martinez-Matos, J.A. and Volpini, V. (2009) Diagnosis of Charcot-Marie-Tooth disease. *J Biomed Biotechnol*, **2009**, 985415.

24 Dyck, P.J. and Lambert, E.H. (1968) Lower motor and primary sensory neuron diseases with peroneal muscular atrophy. I. Neurologic, genetic, and electrophysiologic findings in hereditary polyneuropathies. *Arch Neurol*, **18**, 603-618.

25 Berger, P., Young, P. and Suter, U. (2002) Molecular cell biology of Charcot-Marie-Tooth disease. *Neurogenetics*, **4**, 1-15.

26 Bergoffen, J., Trofatter, J., Pericak-Vance, M.A., Haines, J.L., Chance, P.F. and Fischbeck, K.H. (1993) Linkage localization of X-linked Charcot-Marie-Tooth disease. *Am J Hum Genet*, **52**, 312-318.

27 Kim, H.J., Hong, S.H., Ki, C.S., Kim, B.J., Shim, J.S., Cho, S.H., Park, J.H. and Kim, J.W. (2005) A novel locus for X-linked recessive CMT with deafness and optic neuropathy maps to Xq21.32-q24. *Neurology*, **64**, 1964-1967.

28 Fabrizi, G.M., Ferrarini, M., Cavallaro, T., Cabrini, I., Cerini, R., Bertolasi, L. and Rizzuto, N. (2007) Two novel mutations in dynamin-2 cause axonal Charcot-Marie-Tooth disease. *Neurology*, **69**, 291-295.

29 Claeys, K.G., Zuchner, S., Kennerson, M., Berciano, J., Garcia, A., Verhoeven, K., Storey, E., Merory, J.R., Bienfait, H.M., Lammens, M., Nelis, E., Baets, J., De Vriendt, E., Berneman, Z.N., De Veuster, I., Vance, J.M., Nicholson, G., Timmerman, V. and De Jonghe, P. (2009) Phenotypic spectrum of dynamin 2 mutations in Charcot-Marie-Tooth neuropathy. *Brain*, **132**, 1741-1752.

30 Lee, J.H. and Choi, B.O. (2006) Charcot-marie-tooth disease: seventeen causative genes. *J Clin Neurol*, **2**, 92-106.

31 Garcia, C.A., Malamut, R.E., England, J.D., Parry, G.S., Liu, P. and Lupski, J.R. (1995) Clinical variability in two pairs of identical twins with the Charcot-Marie-Tooth disease type 1A duplication. *Neurology*, **45**, 2090-2093.

32 Gouvea, S.P., VH, S.B., Bueno, K.C., Genari, A.B., Lourenco, C.M., Sobreira, C., Barreira, A.A. and Marques, W., Jr. (2010) Compound Charcot-

Marie-Tooth disease may determine unusual and milder phenotypes. *Neurogenetics*, **11**, 135-138.

33 Steiner, I., Gotkine, M., Steiner-Birmanns, B., Biran, I., Silverstein, S., Abeliovich, D., Argov, Z. and Wirguin, I. (2008) Increased severity over generations of Charcot-Marie-Tooth disease type 1A. *J Neurol*, **255**, 813-819.

34 Braathen, G.J., Sand, J.C., Lobato, A., Hoyer, H. and Russell, M.B. (2010) Genetic epidemiology of Charcot-Marie-Tooth in the general population. *Eur J Neurol*.

35 Hai, M., Bidichandani, S.I., Hogan, M.E. and Patel, P.I. (2001) Competitive binding of triplex-forming oligonucleotides in the two alternate promoters of the PMP22 gene. *Antisense Nucleic Acid Drug Dev*, **11**, 233-246.

36 Liu, N., Varma, S., Tsao, D., Shooter, E.M. and Tolwani, R.J. (2007) Depleting endogenous neurotrophin-3 enhances myelin formation in the Trembler-J mouse, a model of a peripheral neuropathy. *J Neurosci Res*, **85**, 2863-2869.

37 Dequen, F., Filali, M., Lariviere, R.C., Perrot, R., Hisanaga, S. and Julien, J.P. (2010) Reversal of neuropathy phenotypes in conditional mouse model of Charcot-Marie-Tooth disease type 2E. *Hum Mol Genet*, **19**, 2616-2629.

38 Verhoeven, K., Claeys, K.G., Zuchner, S., Schroder, J.M., Weis, J., Ceuterick, C., Jordanova, A., Nelis, E., De Vriendt, E., Van Hul, M., Seeman, P., Mazanec, R., Saifi, G.M., Szigeti, K., Mancias, P., Butler, I.J., Kochanski, A., Ryniewicz, B., De Bleecker, J., Van den Bergh, P., Verellen, C., Van Coster, R., Goemans, N., Auer-Grumbach, M., Robberecht, W., Milic Rasic, V., Nevo, Y., Tournev, I., Guergueltcheva, V., Roelens, F., Vieregge, P., Vinci, P., Moreno, M.T., Christen, H.J., Shy, M.E., Lupski, J.R., Vance, J.M., De Jonghe, P. and Timmerman, V. (2006) MFN2 mutation distribution and genotype/phenotype correlation in Charcot-Marie-Tooth type 2. *Brain*, **129**, 2093-2102.

39 Cartoni, R. and Martinou, J.C. (2009) Role of mitofusin 2 mutations in the physiopathology of Charcot-Marie-Tooth disease type 2A. *Exp Neurol*, **218**, 268-273.

40 Evgrafov, O.V., Mersiyanova, I., Irobi, J., Van Den Bosch, L., Dierick, I., Leung, C.L., Schagina, O., Verpoorten, N., Van Impe, K., Fedotov, V., Dadali, E., Auer-Grumbach, M., Windpassinger, C., Wagner, K., Mitrovic, Z., Hilton-Jones, D., Talbot, K., Martin, J.J., Vasserman, N., Tverskaya, S., Polyakov, A., Liem, R.K., Gettemans, J., Robberecht, W., De Jonghe, P. and Timmerman, V. (2004) Mutant small heat-shock protein 27 causes axonal Charcot-Marie-Tooth disease and distal hereditary motor neuropathy. *Nat Genet*, **36**, 602-606.

41 Zhao, C., Takita, J., Tanaka, Y., Setou, M., Nakagawa, T., Takeda, S., Yang, H.W., Terada, S., Nakata, T., Takei, Y., Saito, M., Tsuji, S., Hayashi, Y. and Hirokawa, N. (2001) Charcot-Marie-Tooth disease type 2A caused by mutation in a microtubule motor KIF1Bbeta. *Cell*, **105**, 587-597.

42 Ismailov, S.M., Fedotov, V.P., Dadali, E.L., Polyakov, A.V., Van Broeckhoven, C., Ivanov, V.I., De Jonghe, P., Timmerman, V. and Evgrafov, O.V. (2001) A new locus for autosomal dominant Charcot-Marie-Tooth disease type 2 (CMT2F) maps to chromosome 7q11-q21. *Eur J Hum Genet*, **9**, 646-650.

43 Verhoeven, K., De Jonghe, P., Coen, K., Verpoorten, N., Auer-Grumbach, M., Kwon, J.M., FitzPatrick, D., Schmedding, E., De Vriendt, E., Jacobs, A., Van Gerwen, V., Wagner, K., Hartung, H.P. and Timmerman, V. (2003) Mutations in the small GTP-ase late endosomal protein RAB7 cause Charcot-Marie-Tooth type 2B neuropathy. *Am J Hum Genet*, **72**, 722-727.

44 Mersiyanova, I.V., Perepelov, A.V., Polyakov, A.V., Sitnikov, V.F., Dadali, E.L., Oparin, R.B., Petrin, A.N. and Evgrafov, O.V. (2000) A new variant of Charcot-Marie-Tooth disease type 2 is probably the result of a mutation in the neurofilament-light gene. *Am J Hum Genet*, **67**, 37-46.

45 Antonellis, A., Ellsworth, R.E., Sambuughin, N., Puls, I., Abel, A., Lee-Lin, S.Q., Jordanova, A., Kremensky, I., Christodoulou, K., Middleton, L.T., Sivakumar, K., Ionasescu, V., Funalot, B., Vance, J.M., Goldfarb, L.G., Fischbeck, K.H. and Green, E.D. (2003) Glycyl tRNA synthetase mutations in Charcot-Marie-Tooth disease type 2D and distal spinal muscular atrophy type V. *Am J Hum Genet*, **72**, 1293-1299.

46 Klein, C.J., Cunningham, J.M., Atkinson, E.J., Schaid, D.J., Hebbring, S.J., Anderson, S.A., Klein, D.M., Dyck, P.J., Litchy, W.J. and Thibodeau, S.N. (2003) The gene for HMSN2C maps to 12q23-24: a region of neuromuscular disorders. *Neurology*, **60**, 1151-1156.

47 Zuchner, S., Mersiyanova, I.V., Muglia, M., Bissar-Tadmouri, N., Rochelle, J., Dadali, E.L., Zappia, M., Nelis, E., Patitucci, A., Senderek, J., Parman, Y., Evgrafov, O., Jonghe, P.D., Takahashi, Y., Tsuji, S., Pericak-Vance, M.A., Quattrone, A., Battaloglu, E., Polyakov, A.V., Timmerman, V., Schroder, J.M. and Vance, J.M. (2004) Mutations in the mitochondrial GTPase mitofusin 2 cause Charcot-Marie-Tooth neuropathy type 2A. *Nat Genet*, **36**, 449-451.

48 Tang, B.S., Luo, W., Xia, K., Xiao, J.F., Jiang, H., Shen, L., Tang, J.G., Zhao, G.H., Cai, F., Pan, Q., Dai, H.P., Yang, Q.D., Xia, J.H. and Evgrafov, O.V. (2004) A new locus for autosomal dominant Charcot-Marie-Tooth disease type 2 (CMT2L) maps to chromosome 12q24. *Hum Genet*, **114**, 527-533.

49 Nelis
V., Comba
dominant
chromosom

50 Saito
(1997) Link
chromosom
1630-1635.

51 Ben
F., Rozear,
and et al.
Charcot-Ma
heterogene

52 Mug
Conforti, F.
Patitucci, A
Clinical an
southern Ita

53 Zuch
V., Chemin
Toumev, I.
Timmerma
atrophy is

54 Del
S., Airoldi,
Federico,
with intrafa
1959-1966

55 Hal
mitochond
90, 121-12

56 Her
Nunnari,
transmem

57 Rap
is a mito
functional
20155.

49 Nelis, E., Berciano, J., Verpoorten, N., Coen, K., Dierick, I., Van Gerwen, V., Combarros, O., De Jonghe, P. and Timmerman, V. (2004) Autosomal dominant axonal Charcot-Marie-Tooth disease type 2 (CMT2G) maps to chromosome 12q12-q13.3. *J Med Genet*, **41**, 193-197.

50 Saito, M., Hayashi, Y., Suzuki, T., Tanaka, H., Hozumi, I. and Tsuji, S. (1997) Linkage mapping of the gene for Charcot-Marie-Tooth disease type 2 to chromosome 1p (CMT2A) and the clinical features of CMT2A. *Neurology*, **49**, 1630-1635.

51 Ben Othmane, K., Middleton, L.T., Loprest, L.J., Wilkinson, K.M., Lennon, F., Rozear, M.P., Stajich, J.M., Gaskell, P.C., Roses, A.D., Pericak-Vance, M.A. and et al. (1993) Localization of a gene (CMT2A) for autosomal dominant Charcot-Marie-Tooth disease type 2 to chromosome 1p and evidence of genetic heterogeneity. *Genomics*, **17**, 370-375.

52 Muglia, M., Zappia, M., Timmerman, V., Valentino, P., Gabriele, A.L., Conforti, F.L., De Jonghe, P., Ragno, M., Mazzei, R., Sabatelli, M., Nicoletti, G., Patitucci, A.M., Oliveri, R.L., Bono, F., Gambardella, A. and Quattrone, A. (2001) Clinical and genetic study of a large Charcot-Marie-Tooth type 2A family from southern Italy. *Neurology*, **56**, 100-103.

53 Zuchner, S., De Jonghe, P., Jordanova, A., Claeys, K.G., Guergueltcheva, V., Cherninkova, S., Hamilton, S.R., Van Stavern, G., Krajewski, K.M., Stajich, J., Tournev, I., Verhoeven, K., Langerhorst, C.T., de Visser, M., Baas, F., Bird, T., Timmerman, V., Shy, M. and Vance, J.M. (2006) Axonal neuropathy with optic atrophy is caused by mutations in mitofusin 2. *Ann Neurol*, **59**, 276-281.

54 Del Bo, R., Moggio, M., Rango, M., Bonato, S., D'Angelo, M.G., Ghezzi, S., Airoldi, G., Bassi, M.T., Guglieri, M., Napoli, L., Lamperti, C., Corti, S., Federico, A., Bresolin, N. and Comi, G.P. (2008) Mutated mitofusin 2 presents with intrafamilial variability and brain mitochondrial dysfunction. *Neurology*, **71**, 1959-1966.

55 Hales, K.G. and Fuller, M.T. (1997) Developmentally regulated mitochondrial fusion mediated by a conserved, novel, predicted GTPase. *Cell*, **90**, 121-129.

56 Hermann, G.J., Thatcher, J.W., Mills, J.P., Hales, K.G., Fuller, M.T., Nunnari, J. and Shaw, J.M. (1998) Mitochondrial fusion in yeast requires the transmembrane GTPase Fzo1p. *J Cell Biol*, **143**, 359-373.

57 Rapaport, D., Brunner, M., Neupert, W. and Westermann, B. (1998) Fzo1p is a mitochondrial outer membrane protein essential for the biogenesis of functional mitochondria in Saccharomyces cerevisiae. *J Biol Chem*, **273**, 20150-20155.

58 Santel, A. and Fuller, M.T. (2001) Control of mitochondrial morphology by a human mitofusin. *J Cell Sci*, **114**, 867-874.
59 Ishihara, N., Eura, Y. and Mihara, K. (2004) Mitofusin 1 and 2 play distinct roles in mitochondrial fusion reactions via GTPase activity. *J Cell Sci*, **117**, 6535-6546.

60 Cartoni, R., Leger, B., Hock, M.B., Praz, M., Crettenand, A., Pich, S., Ziltener, J.L., Luthi, F., Deriaz, O., Zorzano, A., Gobelet, C., Kralli, A. and Russell, A.P. (2005) Mitofusins 1/2 and ERRalpha expression are increased in human skeletal muscle after physical exercise. *J Physiol*, **567**, 349-358.

61 Soriano, F.X., Liesa, M., Bach, D., Chan, D.C., Palacin, M. and Zorzano, A. (2006) Evidence for a mitochondrial regulatory pathway defined by peroxisome proliferator-activated receptor-gamma coactivator-1 alpha, estrogen-related receptor-alpha, and mitofusin 2. *Diabetes*, **55**, 1783-1791.

62 Liesa, M., Borda-d'Agua, B., Medina-Gomez, G., Lelliott, C.J., Paz, J.C., Rojo, M., Palacin, M., Vidal-Puig, A. and Zorzano, A. (2008) Mitochondrial fusion is increased by the nuclear coactivator PGC-1beta. *PLoS One*, **3**, e3613.

63 Li, Y., Yin, R., Liu, J., Wang, P., Wu, S., Luo, J., Zhelyabovska, O. and Yang, Q. (2009) Peroxisome proliferator-activated receptor delta regulates mitofusin 2 expression in the heart. *J Mol Cell Cardiol*, **46**, 876-882.

64 Rojo, M., Legros, F., Chateau, D. and Lombes, A. (2002) Membrane topology and mitochondrial targeting of mitofusins, ubiquitous mammalian homologs of the transmembrane GTPase Fzo. *J Cell Sci*, **115**, 1663-1674.

65 Zhou, W., Chen, K.H., Cao, W., Zeng, J., Liao, H., Zhao, L. and Guo, X. (2010) Mutation of the protein kinase A phosphorylation site influences the anti-proliferative activity of mitofusin 2. *Atherosclerosis*.

66 Honda, S., Aihara, T., Hontani, M., Okubo, K. and Hirose, S. (2005) Mutational analysis of action of mitochondrial fusion factor mitofusin-2. *J Cell Sci*, **118**, 3153-3161.

67 Walshaw, J. and Woolfson, D.N. (2001) Socket: a program for identifying and analysing coiled-coil motifs within protein structures. *J Mol Biol*, **307**, 1427-1450.

68 Koshiba, T., Detmer, S.A., Kaiser, J.T., Chen, H., McCaffery, J.M. and Chan, D.C. (2004) Structural basis of mitochondrial tethering by mitofusin complexes. *Science*, **305**, 858-862.

69 Mazzarello, P. (1999) A unifying concept: the history of cell theory. *Nat Cell Biol*, **1**, E13-15.

70 Bakeeva, L.E., Chentsov Yu, S. and Skulachev, V.P. (1978) Mitochondrial framework (reticulum mitochondriale) in rat diaphragm muscle. *Biochim Biophys Acta*, **501**, 349-369.

71 Lewis, M.R. and Lewis, W.H. (1914) Mitochondria in Tissue Culture. *Science*, **39**, 330-333.

72 Mannella, C.A., Marko, M., Penczek, P., Barnard, D. and Frank, J. (1994) The internal compartmentation of rat-liver mitochondria: tomographic study using the high-voltage transmission electron microscope. *Microsc Res Tech*, **27**, 278-283.

73 Bay, D.C. and Court, D.A. (2002) Origami in the outer membrane: the transmembrane arrangement of mitochondrial porins. *Biochem Cell Biol*, **80**, 551-562.

74 Schwerzmann, K., Cruz-Orive, L.M., Eggman, R., Sanger, A. and Weibel, E.R. (1986) Molecular architecture of the inner membrane of mitochondria from rat liver: a combined biochemical and stereological study. *J Cell Biol*, **102**, 97-103.

75 Allen, R.D., Schroeder, C.C. and Fok, A.K. (1989) An investigation of mitochondrial inner membranes by rapid-freeze deep-etch techniques. *J Cell Biol*, **108**, 2233-2240.

76 Chance, B. and Williams, G.R. (1956) The respiratory chain and oxidative phosphorylation. *Adv Enzymol Relat Subj Biochem*, **17**, 65-134.

77 Mitchell, P. (1961) Coupling of phosphorylation to electron and hydrogen transfer by a chemi-osmotic type of mechanism. *Nature*, **191**, 144-148.

78 Racker, E. (1980) From Pasteur to Mitchell: a hundred years of bioenergetics. *Fed Proc*, **39**, 210-215.

79 Cantatore, P., Roberti, M., Rainaldi, G., Gadaleta, M.N. and Saccone, C. (1989) The complete nucleotide sequence, gene organization, and genetic code of the mitochondrial genome of Paracentrotus lividus. *J Biol Chem*, **264**, 10965-10975.

80 McBride, H.M., Neuspiel, M. and Wasiak, S. (2006) Mitochondria: more than just a powerhouse. *Curr Biol*, **16**, R551-560.

81 Rossier, M.F. (2006) T channels and steroid biosynthesis: in search of a link with mitochondria. *Cell Calcium*, **40**, 155-164.

82 Contreras, L., Drago, I., Zampese, E. and Pozzan, T. (2010) Mitochondria: The calcium connection. *Biochim Biophys Acta*, **1797**, 607-618.

83 Cao, X. and Chen, Y. (2009) Mitochondria and calcium signaling in embryonic development. *Semin Cell Dev Biol*, **20**, 337-345.

84 Buchholz, J.N., Behringer, E.J., Pottorf, W.J., Pearce, W.J. and Vanterpool, C.K. (2007) Age-dependent changes in Ca2+ homeostasis in peripheral neurones: implications for changes in function. *Aging Cell*, **6**, 285-296.

85 Lukyanenko, V., Chikando, A. and Lederer, W.J. (2009) Mitochondria in cardiomyocyte Ca2+ signaling. *Int J Biochem Cell Biol*, **41**, 1957-1971.

86 Griffiths, E.J. and Rutter, G.A. (2009) Mitochondrial calcium as a key regulator of mitochondrial ATP production in mammalian cells. *Biochim Biophys Acta*, **1787**, 1324-1333.

87 Graier, W.F., Frieden, M. and Malli, R. (2007) Mitochondria and Ca(2+) signaling: old guests, new functions. *Pflugers Arch*, **455**, 375-396.

88 Bernardi, P. and Rasola, A. (2007) Calcium and cell death: the mitochondrial connection. *Subcell Biochem*, **45**, 481-506.

89 Gibson, B.W. (2005) The human mitochondrial proteome: oxidative stress, protein modifications and oxidative phosphorylation. *Int J Biochem Cell Biol*, **37**, 927-934.

90 Bereiter-Hahn, J. and Voth, M. (1994) Dynamics of mitochondria in living cells: shape changes, dislocations, fusion, and fission of mitochondria. *Microsc Res Tech*, **27**, 198-219.

91 DiMauro, S. (2004) Mitochondrial diseases. *Biochim Biophys Acta*, **1658**, 80-88.

92 Kakinuma, T., Abe, H. and Nomura, Y. (1955) On the mitochondrial structure in the spermatogenic cells of the rats. *Okajimas Folia Anat Jpn*, **27**, 97-101.

93 Asano, M., Wakabayashi, T., Ishikawa, K. and Kishimoto, H. (1977) Induction of megamitochondria in mouse hepatocytes by nialamide. *J Electron Microsc (Tokyo)*, **26**, 141-144.

94 Wakabayashi, T. and Green, D.E. (1977) Membrane fusion in mitochondria. I. Ultrastructural basis for fusion. *J Electron Microsc (Tokyo)*, **26**, 305-320.

95 Wakabayashi, T., Asano, M., Ishikawa, K. and Kishimoto, H. (1977) Cuprizone-induced megamitochondrial formation and membrane fusion. *J Electron Microsc (Tokyo)*, **26**, 137-140.

96 Svoboda, D.J. and Higginson, J. (1963) Ultrastructural Hepatic Changes in Rats on a Necrogenic Diet. *Am J Pathol*, **43**, 477-495.

97 Lantos, P.L., Ketterer, B. and Holt, S.J. (1973) The ultrastructure of the hepatocyte of the vitamin E deficient rat and the effect of a single intraperitoneal dose of N,N-dimethyl-4-aminoazobenzene on the stability of its fractionated polysomes. *Exp Mol Pathol*, **18**, 68-79.

98 Guveli, D.E. (1987) Fusion of mitochondria. *J Biochem*, **102**, 1329-1332.

99 Hayashida, Y. (1973) Rat spinal ganglion cells characterized by atypical mitochondria. *Experientia*, **29**, 460-461.

100 Rancourt, M.W., McKee, A.P. and Pollack, W. (1975) Mitochondrial profile of a mammalian lymphocyte. *J Ultrastruct Res*, **51**, 418-424.

101 Kirkwood, S.P., Munn, E.A. and Brooks, G.A. (1986) Mitochondrial reticulum in limb skeletal muscle. *Am J Physiol*, **251**, C395-402.

102 Skulachev, V.P. (1990) Power transmission along biological membranes. *J Membr Biol*, **114**, 97-112.

103 Berman, S.B., Pineda, F.J. and Hardwick, J.M. (2008) Mitochondrial fission and fusion dynamics: the long and short of it. *Cell Death Differ*, **15**, 1147-1152.

104 Knott, A.B., Perkins, G., Schwarzenbacher, R. and Bossy-Wetzel, E. (2008) Mitochondrial fragmentation in neurodegeneration. *Nat Rev Neurosci*, **9**, 505-518.

105 Chen, H., Chomyn, A. and Chan, D.C. (2005) Disruption of fusion results in mitochondrial heterogeneity and dysfunction. *J Biol Chem*, **280**, 26185-26192.

106 Ono, T., Isobe, K., Nakada, K. and Hayashi, J.I. (2001) Human cells are protected from mitochondrial dysfunction by complementation of DNA products in fused mitochondria. *Nat Genet*, **28**, 272-275.

107 Chen, H., Vermulst, M., Wang, Y.E., Chomyn, A., Prolla, T.A., McCaffery, J.M. and Chan, D.C. (2010) Mitochondrial fusion is required for mtDNA stability in skeletal muscle and tolerance of mtDNA mutations. *Cell*, **141**, 280-289.

108 Detmer, S.A. and Chan, D.C. (2007) Functions and dysfunctions of mitochondrial dynamics. *Nat Rev Mol Cell Biol*, **8**, 870-879.

109 Nakada, K., Inoue, K., Ono, T., Isobe, K., Ogura, A., Goto, Y.I., Nonaka, I. and Hayashi, J.I. (2001) Inter-mitochondrial complementation: Mitochondria-specific system preventing mice from expression of disease phenotypes by mutant mtDNA. *Nat Med*, **7**, 934-940.

110 Jezek, P. and Plecita-Hlavata, L. (2009) Mitochondrial reticulum network dynamics in relation to oxidative stress, redox regulation, and hypoxia. *Int J Biochem Cell Biol*, **41**, 1790-1804.

111 Santel, A., Frank, S., Gaume, B., Herrler, M., Youle, R.J. and Fuller, M.T. (2003) Mitofusin-1 protein is a generally expressed mediator of mitochondrial fusion in mammalian cells. *J Cell Sci*, **116**, 2763-2774.

112 Cipolat, S., Martins de Brito, O., Dal Zilio, B. and Scorrano, L. (2004) OPA1 requires mitofusin 1 to promote mitochondrial fusion. *Proc Natl Acad Sci U S A*, **101**, 15927-15932.

113 Legros, F., Lombes, A., Frachon, P. and Rojo, M. (2002) Mitochondrial fusion in human cells is efficient, requires the inner membrane potential, and is mediated by mitofusins. *Mol Biol Cell*, **13**, 4343-4354.

114 Chen, H., Detmer, S.A., Ewald, A.J., Griffin, E.E., Fraser, S.E. and Chan, D.C. (2003) Mitofusins Mfn1 and Mfn2 coordinately regulate mitochondrial fusion and are essential for embryonic development. *J Cell Biol*, **160**, 189-200.

115 Chen, H., McCaffery, J.M. and Chan, D.C. (2007) Mitochondrial fusion protects against neurodegeneration in the cerebellum. *Cell*, **130**, 548-562.

116 Jiang, G.J., Pan, L., Huang, X.Y., Han, M., Wen, J.K. and Sun, F.Z. (2005) Expression of HSG is essential for mouse blastocyst formation. *Biochem Biophys Res Commun*, **335**, 351-355.

117 Nechushtan, A., Smith, C.L., Lamensdorf, I., Yoon, S.H. and Youle, R.J. (2001) Bax and Bak coalesce into novel mitochondria-associated clusters during apoptosis. *J Cell Biol*, **153**, 1265-1276.

118 Brooks, C., Wei, Q., Feng, L., Dong, G., Tao, Y., Mei, L., Xie, Z.J. and Dong, Z. (2007) Bak regulates mitochondrial morphology and pathology during apoptosis by interacting with mitofusins. *Proc Natl Acad Sci U S A*, **104**, 11649-11654.

119 Karbowski, M., Lee, Y.J., Gaume, B., Jeong, S.Y., Frank, S., Nechushtan, A., Santel, A., Fuller, M., Smith, C.L. and Youle, R.J. (2002) Spatial and temporal

association of Bax with mitochondrial fission sites, Drp1, and Mfn2 during apoptosis. *J Cell Biol*, **159**, 931-938.

120 Karbowski, M., Arnoult, D., Chen, H., Chan, D.C., Smith, C.L. and Youle, R.J. (2004) Quantitation of mitochondrial dynamics by photolabeling of individual organelles shows that mitochondrial fusion is blocked during the Bax activation phase of apoptosis. *J Cell Biol*, **164**, 493-499.

121 Neuspiel, M., Zunino, R., Gangaraju, S., Rippstein, P. and McBride, H. (2005) Activated mitofusin 2 signals mitochondrial fusion, interferes with Bax activation, and reduces susceptibility to radical induced depolarization. *J Biol Chem*, **280**, 25060-25070.

122 Delivani, P., Adrain, C., Taylor, R.C., Duriez, P.J. and Martin, S.J. (2006) Role for CED-9 and Egl-1 as regulators of mitochondrial fission and fusion dynamics. *Mol Cell*, **21**, 761-773.

123 Chen, K.H., Guo, X., Ma, D., Guo, Y., Li, Q., Yang, D., Li, P., Qiu, X., Wen, S., Xiao, R.P. and Tang, J. (2004) Dysregulation of HSG triggers vascular proliferative disorders. *Nat Cell Biol*, **6**, 872-883.

124 Ziviani, E. and Whitworth, A.J. (2010) How could Parkin-mediated ubiquitination of mitofusin promote mitophagy? *Autophagy*, **6**.

125 Twig, G., Hyde, B. and Shirihai, O.S. (2008) Mitochondrial fusion, fission and autophagy as a quality control axis: the bioenergetic view. *Biochim Biophys Acta*, **1777**, 1092-1097.

126 Twig, G., Elorza, A., Molina, A.J., Mohamed, H., Wikstrom, J.D., Walzer, G., Stiles, L., Haigh, S.E., Katz, S., Las, G., Alroy, J., Wu, M., Py, B.F., Yuan, J., Deeney, J.T., Corkey, B.E. and Shirihai, O.S. (2008) Fission and selective fusion govern mitochondrial segregation and elimination by autophagy. *EMBO J*, **27**, 433-446.

127 Navratil, M., Terman, A. and Arriaga, E.A. (2008) Giant mitochondria do not fuse and exchange their contents with normal mitochondria. *Exp Cell Res*, **314**, 164-172.

128 Narendra, D., Tanaka, A., Suen, D.F. and Youle, R.J. (2008) Parkin is recruited selectively to impaired mitochondria and promotes their autophagy. *J Cell Biol*, **183**, 795-803.

129 Ziviani, E., Tao, R.N. and Whitworth, A.J. (2010) Drosophila parkin requires PINK1 for mitochondrial translocation and ubiquitinates mitofusin. *Proc Natl Acad Sci U S A*, **107**, 5018-5023.

130 Matsuda, N. and Tanaka, K. (2009) Does Impairment of the Ubiquitin-Proteasome System or the Autophagy-Lysosome Pathway Predispose Individuals to Neurodegenerative Disorders such as Parkinson's Disease? *J Alzheimers Dis.*

131 Misko, A., Jiang, S., Wegorzewska, I., Milbrandt, J. and Baloh, R.H. (2010) Mitofusin 2 is necessary for transport of axonal mitochondria and interacts with the Miro/Milton complex. *J Neurosci*, **30**, 4232-4240.

132 Fransson, A., Ruusala, A. and Aspenstrom, P. (2003) Atypical Rho GTPases have roles in mitochondrial homeostasis and apoptosis. *J Biol Chem*, **278**, 6495-6502.

133 Stowers, R.S., Megeath, L.J., Gorska-Andrzejak, J., Meinertzhagen, I.A. and Schwarz, T.L. (2002) Axonal transport of mitochondria to synapses depends on milton, a novel Drosophila protein. *Neuron*, **36**, 1063-1077.

134 Brickley, K., Smith, M.J., Beck, M. and Stephenson, F.A. (2005) GRIF-1 and OIP106, members of a novel gene family of coiled-coil domain proteins: association in vivo and in vitro with kinesin. *J Biol Chem*, **280**, 14723-14732.

135 Giot, L., Bader, J.S., Brouwer, C., Chaudhuri, A., Kuang, B., Li, Y., Hao, Y.L., Ooi, C.E., Godwin, B., Vitols, E., Vijayadamodar, G., Pochart, P., Machineni, H., Welsh, M., Kong, Y., Zerhusen, B., Malcolm, R., Varrone, Z., Collis, A., Minto, M., Burgess, S., McDaniel, L., Stimpson, E., Spriggs, F., Williams, J., Neurath, K., Ioime, N., Agee, M., Voss, E., Furtak, K., Renzulli, R., Aanensen, N., Carrolla, S., Bickelhaupt, E., Lazovatsky, Y., DaSilva, A., Zhong, J., Stanyon, C.A., Finley, R.L., Jr., White, K.P., Braverman, M., Jarvie, T., Gold, S., Leach, M., Knight, J., Shimkets, R.A., McKenna, M.P., Chant, J. and Rothberg, J.M. (2003) A protein interaction map of Drosophila melanogaster. *Science*, **302**, 1727-1736.

136 Fransson, S., Ruusala, A. and Aspenstrom, P. (2006) The atypical Rho GTPases Miro-1 and Miro-2 have essential roles in mitochondrial trafficking. *Biochem Biophys Res Commun*, **344**, 500-510.

137 Nakamura, N., Kimura, Y., Tokuda, M., Honda, S. and Hirose, S. (2006) MARCH-V is a novel mitofusin 2- and Drp1-binding protein able to change mitochondrial morphology. *EMBO Rep*, **7**, 1019-1022.

138 Wang, Y. and Morrow, J.S. (2000) Identification and characterization of human SLP-2, a novel homologue of stomatin (band 7.2b) present in erythrocytes and other tissues. *J Biol Chem*, **275**, 8062-8071.

139 Hajek, P., Chomyn, A. and Attardi, G. (2007) Identification of a novel mitochondrial complex containing mitofusin 2 and stomatin-like protein 2. *J Biol Chem*, **282**, 5670-5681.

140 Bach, D., Pich, S., Soriano, F.X., Vega, N., Baumgartner, B., Oriola, J., Daugaard, J.R., Lloberas, J., Camps, M., Zierath, J.R., Rabasa-Lhoret, R., Wallberg-Henriksson, H., Laville, M., Palacin, M., Vidal, H., Rivera, F., Brand, M. and Zorzano, A. (2003) Mitofusin-2 determines mitochondrial network architecture and mitochondrial metabolism. A novel regulatory mechanism altered in obesity. *J Biol Chem*, **278**, 17190-17197.

141 Pich, S., Bach, D., Briones, P., Liesa, M., Camps, M., Testar, X., Palacin, M. and Zorzano, A. (2005) The Charcot-Marie-Tooth type 2A gene product, Mfn2, up-regulates fuel oxidation through expression of OXPHOS system. *Hum Mol Genet*, **14**, 1405-1415.

142 Rizzuto, R., Brini, M., Murgia, M. and Pozzan, T. (1993) Microdomains with high Ca2+ close to IP3-sensitive channels that are sensed by neighboring mitochondria. *Science*, **262**, 744-747.

143 Vance, J.E. (1990) Phospholipid synthesis in a membrane fraction associated with mitochondria. *J Biol Chem*, **265**, 7248-7256.

144 Hajnoczky, G., Csordas, G., Madesh, M. and Pacher, P. (2000) The machinery of local Ca2+ signalling between sarco-endoplasmic reticulum and mitochondria. *J Physiol*, **529 Pt 1**, 69-81.

145 Moreno-Sanchez, R. (1985) Regulation of oxidative phosphorylation in mitochondria by external free Ca2+ concentrations. *J Biol Chem*, **260**, 4028-4034.

146 Deniaud, A., Sharaf el dein, O., Maillier, E., Poncet, D., Kroemer, G., Lemaire, C. and Brenner, C. (2008) Endoplasmic reticulum stress induces calcium-dependent permeability transition, mitochondrial outer membrane permeabilization and apoptosis. *Oncogene*, **27**, 285-299.

147 de Brito, O.M. and Scorrano, L. (2008) Mitofusin 2 tethers endoplasmic reticulum to mitochondria. *Nature*, **456**, 605-610.

148 de Brito, O.M. and Scorrano, L. (2008) Mitofusin 2: a mitochondria-shaping protein with signaling roles beyond fusion. *Antioxid Redox Signal*, **10**, 621-633.

149 de Brito, O.M. and Scorrano, L. (2009) Mitofusin-2 regulates mitochondrial and endoplasmic reticulum morphology and tethering: the role of Ras. *Mitochondrion*, **9**, 222-226.

150 Csordas, G. and Hajnoczky, G. (2009) SR/ER-mitochondrial local communication: calcium and ROS. *Biochim Biophys Acta*, **1787**, 1352-1362.

151 Calvo, J., Funalot, B., Ouvrier, R.A., Lazaro, L., Toutain, A., De Mas, P., Bouche, P., Gilbert-Dussardier, B., Arne-Bes, M.C., Carriere, J.P., Journel, H., Minot-Myhie, M.C., Guillou, C., Ghorab, K., Magy, L., Sturtz, F., Vallat, J.M. and Magdelaine, C. (2009) Genotype-phenotype correlations in Charcot-Marie-Tooth disease type 2 caused by mitofusin 2 mutations. *Arch Neurol*, **66**, 1511-1516.

152 Boaretto, F., Vettori, A., Casarin, A., Vazza, G., Muglia, M., Rossetto, M.G., Cavallaro, T., Rizzuto, N., Carelli, V., Salviati, L., Mostacciuolo, M.L. and Martinuzzi, A. (2010) Severe CMT type 2 with fatal encephalopathy associated with a novel MFN2 splicing mutation. *Neurology*, **74**, 1919-1921.

153 Amiott, E.A., Lott, P., Soto, J., Kang, P.B., McCaffery, J.M., DiMauro, S., Abel, E.D., Flanigan, K.M., Lawson, V.H. and Shaw, J.M. (2008) Mitochondrial fusion and function in Charcot-Marie-Tooth type 2A patient fibroblasts with mitofusin 2 mutations. *Exp Neurol*, **211**, 115-127.

154 Detmer, S.A. and Chan, D.C. (2007) Complementation between mouse Mfn1 and Mfn2 protects mitochondrial fusion defects caused by CMT2A disease mutations. *J Cell Biol*, **176**, 405-414.

155 Loiseau, D., Chevrollier, A., Verny, C., Guillet, V., Gueguen, N., Pou de Crescenzo, M.A., Ferre, M., Malinge, M.C., Guichet, A., Nicolas, G., Amati-Bonneau, P., Malthiery, Y., Bonneau, D. and Reynier, P. (2007) Mitochondrial coupling defect in Charcot-Marie-Tooth type 2A disease. *Ann Neurol*, **61**, 315-323.

156 Baloh, R.H., Schmidt, R.E., Pestronk, A. and Milbrandt, J. (2007) Altered axonal mitochondrial transport in the pathogenesis of Charcot-Marie-Tooth disease from mitofusin 2 mutations. *J Neurosci*, **27**, 422-430.

157 Amiott, E.A., Cohen, M.M., Saint-Georges, Y., Weissman, A.M. and Shaw, J.M. (2009) A mutation associated with CMT2A neuropathy causes defects in Fzo1 GTP hydrolysis, ubiquitylation, and protein turnover. *Mol Biol Cell*, **20**, 5026-5035.

158 Bach, D., Naon, D., Pich, S., Soriano, F.X., Vega, N., Rieusset, J., Laville, M., Guillet, C., Boirie, Y., Wallberg-Henriksson, H., Manco, M., Calvani, M., Castagneto, M., Palacin, M., Mingrone, G., Zierath, J.R., Vidal, H. and Zorzano, A. (2005) Expression of Mfn2, the Charcot-Marie-Tooth neuropathy type 2A gene, in human skeletal muscle: effects of type 2 diabetes, obesity, weight loss, and the regulatory role of tumor necrosis factor alpha and interleukin-6. *Diabetes*, **54**, 2685-2693.

159 Gastaldi, G., Russell, A., Golay, A., Giacobino, J.P., Habicht, F., Barthassat, V., Muzzin, P. and Bobbioni-Harsch, E. (2007) Upregulation of peroxisome proliferator-activated receptor gamma coactivator gene (PGC1A) during weight loss is related to insulin sensitivity but not to energy expenditure. *Diabetologia*, **50**, 2348-2355.

160 Mingrone, G., Manco, M., Calvani, M., Castagneto, M., Naon, D. and Zorzano, A. (2005) Could the low level of expression of the gene encoding skeletal muscle mitofusin-2 account for the metabolic inflexibility of obesity? *Diabetologia*, **48**, 2108-2114.

CHAPTER II

ASSAYING MITOFUSIN 2 EXPRESSION AND LOCALIZATION IN NEONATAL DOGS WITH NEUROAXONAL DYSTROPHY PHENOTYPE

Assayi

ABSTRA

Mitof
neuropathie
type 2A2 (C
in *MFN2*
dystrophy (
an MFN2 c
of mutant *M*
transcripts
unaffected
and cDNA
western blo
and brainst
lysates. Ho
cells, signif
than in DR
mutation ca
that is likely

Chapter II

Assaying Mitofusin 2 expression and localization in neonatal dogs with neuroaxonal dystrophy phenotype

ABSTRACT

Mitofusin 2 (*MFN2*) mutations have been implicated in four human neuropathies, but most commonly as a causative lesion in Charcot-Marie-Tooth type 2A2 (CMT2A2). Here we decribe a novel in-frame three nucleotide deletion in *MFN2* that results in an autosomal recessive, fetal onset neuroaxonal dystrophy (FNAD) in dogs. A single glutamic acid residue (ΔE539) is deleted in an MFN2 conserved domain of unknown function. Assaying transcript expression of mutant *MFN2* using quantitative-Real Time-PCR (qRT-PCR) detected *MFN2* transcripts in tissues from diseased pups. Moreover, the mutant allele in unaffected carrier pups was determined to be actively expressed using RT-PCR and cDNA restriction digest patterns. MFN2 protein expression analysis by western blotting in several tissues in affected pups was undetectable in brain, and brainstem, and only trace amounts were observed in kidney and fibroblast lysates. However, in lysates derived from cultured dorsal root ganglion (DRG) cells, significant amounts of mutant MFN2 protein were detectable, though less than in DRG cells cultured from normal littermates. Our data suggest the ΔE539 mutation causes decreased MFN2 protein levels by an undetermined mechanism that is likely post-transcriptional.

Introduction

MFN2 is a protein involved in numerous vital cellular functions. *MFN2* knockout mouse models are embryonic lethal which supports the perceived importance of MFN2 for cellular development and survival (1, 2). *MFN2* is a nuclear encoded gene whose expression is governed by at least two promoter sequences, each of which is sensitive to isoforms of PGC-1 transcriptional coactivator (3-6). Once translated, MFN2 is targeted to the mitochondrial outer membrane via its non-canonical mitochondrial targeting sequence in the transmembrane domain (7). In addition, MFN2 localizes to the endoplasmic reticulum membranes in a manner that juxtaposes other MFN molecules on mitochondria to promote ER-mitochondrial tethering (8). The susceptibility of the nervous system to MFN2 mutations suggests sensitivity to abnormal MFN2 that is not shared by other systems. MFN2 is essential for cerebellar development and preservation, while MFN1 is not (9). In MFN2 knock out cerebellum the Purkinje cell layer showed increased degeneration, while other cerebellar structures were thought to be degenerating as a secondary event to Purkinje cell death. Although MFN1 does complement fusion defects of MFN2 (10), its expression in the mouse Purkinje cells is low in comparison to MFN2. However, Purkinje cell degeneration was reversible when transduced with wild type copies of either mitofusin in cerebellar cultures derived from MFN2 conditional knockout mice (9). Therefore, a differential expression pattern of mitofusins in the nervous system is a plausible explanation for nervous system sensitivity to *MFN2* mutations.

In this chapter I analyzed the steady-state RNA transcript and protein levels of mutant *MFN2* in several different tissues, and subcellular fractions.

Materials and Methods

Animals

Dogs segregating the FNAD phenotype were maintained in a breeding colony at Michigan State University under Animal Use Forms 02/21/2001 and 10/07-161-00. All protocols were approved by the Institutional Animal Use and Care Committee at MSU. Euthanasia was performed by administration of an overdose of sodium pentobarbital prior to dissection and preservation of tissues. Tissues were variably snap frozen in liguid nitrogen, fixed in neutral buffer formalin, or submerged in tissue culture medium.

Total RNA extractions

Total RNA extractions were performed using Qiagen RNeasy kit (Qiagen Inc., Valencia, CA), except for nervous system derived tissues which were extracted with Qiagen's Lipid tissue kit (Qiagen Inc., Valencia, CA). Manufacturers' protocols were followed in both. For non-nervous system tissues no more than 30 mg of frozen tissues were used. Excised tissues were immersed in RLT lysis buffer for homogenization using sonication for 15 seconds on ice. Lysates were centrifuged for 3 minutes at 10,000xg, supernatants were transferred to fresh centrifuge tubes, and 1 volume of 70% ethanol was added and mixed. The suspension was transferred into supplied columns and centrifuged at 10,000xg for 15 seconds. Sample was washed with supplied RW1 buffer to remove protein contaminants and centrifuged as above. Columns were washed twice with ethanol supplemented RPE buffer at 10,000xg for 5 seconds

and 2 minutes, respectively. Bound total RNAs were eluted in fresh microcentrifuge tubes with RNase-free water by centrifugation at 10,000xg for 1 minute. All centrifugations were performed at room temperature.

Similarly, for nervous system derived tissues, no more than 30 mg of frozen tissues were used for Qiagen Lipid tissue kit. Tissues were immersed in QIAzol lysis reagent and homogenized with a Polytron (Heidolph Brinkmann LLC, Elk Grove Village, IL). Homogenates were left at room temperature for 5 minutes, followed by addition of 1/5 volume of chloroform and vigorous shaking for 15 seconds. Tubes were incubated at room temperature for 3 minutes and centrifuged at 12,000xg for 10 minutes at 4°C for phase separation. Upper phases were transferred to fresh tubes, and an equal volume of 70% ethanol was added and mixed by vortex. Samples were transferred to mini spin columns supplied and centrifuged at 8,000xg for 15 seconds at room temperature. The remaining steps follow the same as mentioned above for non-nervous system tissue. Total RNA yields were determined using a microspectrophotometer (NanoDrop, Thermo Fisher Scientific Inc., Waltham, MA). Tissue samples used for total RNA preparations were derived from different normal and affected animals.

Reverse Transcription, and quantitative Real-Time PCR

Invitrogen's SuperSript III Reverse Transcriptase kit (Invitrogen Corp., Carlsbad, CA) was used for all cDNA synthesis reactions according to manufacturer's protocol. One normal and affected animal total RNA extract was

used for each tissue type reverse transcriptase reaction. Three micrograms of total RNA was used for each cDNA synthesis reaction containing 10mM dNTPs mix, Oligo-dT_{12-18}, 5X First-strand buffer, 0.1M DTT, Recombinant RNAsin Ribonuclease Inhibitor (Promega, Madison, WI) and SuperScript III RT. Reactions were incubated at 55°C for 60 minutes followed by 70°C incubation for 15 minutes for enzyme deactivation.

For quantitative Real-Time PCR (qRT-PCR), cDNA reactions were purified using a QiaQuick PCR purification kit (Qiagen Inc., Valencia, CA), and dilutions were made from normal brain stem cDNA to create standard curves for gene targets and endogenous control. Applied Biosystems' Fast SYBR Green master mix (Life Technologies Corp., Carlsbad, CA) was used to assay for *MFN1* and *MFN2* transcripts in selected tissues. I used the StepOnePlus™ Real-Time PCR system (Life Technologies Corp., Carlsbad, CA) for running the reactions and analysis. For estimating *MFN1*:*MFN2* ratios in different tissues of normal and affected pups, *HPRT* was used as an endogenous control (11), MFN1 and MFN2 as targets (table 2-1), and relative standard curve method for expression analysis. Each sample was assayed in triplicate, and qRT-PCR experiments were performed twice with different cDNA of the same total RNA stocks.

Allelic determination of mutant and wild type *MFN2* expression utilized restriction enzyme specific banding pattern of RT-PCR products. Following *MFN2* transcript specific amplification using the same primers as above (table 2-1) from cDNA of normal, carrier and mutant brainstem, *MFN2* cDNA was incubated with *MnlI* restriction enzyme (New England Biolabs, Ipswich, MA) that

recognizes a restriction site in *MFN2* wild type allele which has been abolished in the mutant allele. Restriction digests were electrophoresed on a 3.5% agarose gel stained with ethidium bromide.

Table 2-1: Exon-exon boundaries spanning primers used to assay for mitofusins transcription.

Gene (***Canis familiaris***)		**Primer sequence**	**T_M (°C)**
MFN1	Forward Primer	5'-CCCATGCCCTTCATATGGACAA-3'	59
	Reverse Primer	5'-TGCTGTCTGCGTACGTCTTCCA-3'	
MFN2	Forward Primer	5'-CAGCAGGACATGATAGATGGCTTGAA-3'	59
	Reverse Primer	5'-ACAACGAGAATGCCCATGGAGGT-3'	
HPRT	Forward Primer	5'-CCCAGCGTCGTGATTAGTGA-3'	59
	Reverse Primer	5'-GATGGCCTCCCATTTCCTTC-3'	

Kidney tissue fractionation

Fresh kidneys were excised and immersed in ice-cold tissue homogenization buffer (220mM mannitol, 70mM sucrose, 5mM MOPS; pH 7.4). Kidneys were weighed, minced and washed three times in homogenization buffer. Minced tissue was homogenized in 5 wet weight volumes of homogenization buffer supplemented with 0.1mM phenylmethylsulfonyl fluoride

(PMSF) and 2mM EGTA (isolation buffer) using a motor driven Teflon pestle in a glass homogenizer (5-7 strokes). Homogenate was centrifuged in swinging buckets at 700xg for 10 minutes at 4°C. An aliquot of the collected supernatant was designated the whole tissue lysate fraction, while the remainder was centrifuged at 7,000xg for 10 minutes at 4°C in a fixed angle rotor. Resultant mitochondrial pellets were resuspended in isolation buffer (mitochondrial fractions), while supernatants were ultra-centrifuged at 80,000xg for 1 hour at 4°C. Resultant pellets were resuspended in isolation buffer as the microsomal fractions, while final supernatants were stored as cytosolic fractions. All fractions were stored at -20°C until further processing. Fractions' protein concentrations were quantified using BioRad's protein assay dye reagent (Bio-Rad laboratories, Hercules, CA) by the Bradford protein assay method (12).

Nervous system tissue fractionation

Brain and brain stem tissue subcellular fractionation was performed according to a method adapted from Sujkovic *et al.* (13). At necropsy, whole brain and brain stem tissues were immediately submerged in homogenization buffer containing 5mM HEPES buffer (pH 7.4), 0.32M sucrose, and 0.1mM PMSF, and kept on ice till processing. After two rinses with homogenization buffer, tissues were immersed in homogenization buffer and homogenized using a motor driven Teflon pestle in a glass homogenizer with five loose strokes followed by five tight strokes. An aliquot of total homogenate was reserved and the remaining was centrifuged at 1,000xg for 10 minutes at 4°C. The pellets were discarded, and supernatants were centrifuged at 8,000xg for 10 minutes at 4°C

yielding the mitochondrial pellets and post-mitochondrial supernatants. Mitochondrial pellets were resuspended in homogenization buffer and stored, while the supernatants were further ultra-centrifuged at 110,000xg for 60 min at 4°C to generate cytosolic fraction supernatants and microsomal pellets. All samples were stored at -20°C for further analysis. Protein concentrations were quantified using BioRad's protein assay dye reagent (Bio-Rad laboratories, Hercules, CA) and the Bradford protein assay method (12).

Primary cell culture protein extraction

Primary canine fibroblasts (CF) and dorsal root ganglion (DRG) cell cultures were established and maintained according to methods in chapter III. Confluent cell cultures were trypsinized and collected in full growth medium. Cell pellets were collected by centrifugation at 700xg for 5 minutes. Pellets were washed in 1X PBS (137mM NaCl, 2.7mM KCl, 4.3mM Na2HPO4, and 1.47mM KH2PO4, pH 7.4) once. Resultant pellets were resuspended in cold protein extraction buffer (0.3M mannitol, 0.2mM EDTA, 10mM HEPES, 0.1mM PMSF, pH 7.4). Fibroblast cell pellets were homogenized using a glass homogenizer on ice. Fibroblast suspensions were centrifuged at 1,000xg for 10 minutes at 4°C. Resultant supernatant was aliquoted as total lysate, and the remaining portion was centrifuged at 14,000xg for 15 minutes at 4°C to generate mitochondrial pellet and post-mitochondrial supernatant. DRG cell pellets were sonicated for 10seconds on ice and centrifuged at 1,000xg for 10 minutes at 4°C. Resultant supernatant was stored as total DRG protein lysate. Protein concentrations of

collected fractions were determined using BioRad's protein assay dye reagent (Bio-Rad laboratories, Hercules, CA) according to Bradford protein assay (12).

Western blotting

All SDS-PAGE gels followed Laemmli gel method (14) and 10% polyacrylamide in the separating gel matrix. Detailed description of primary antibodies used in western blotting are listed in table 2-2. All antibodies were purchased from Abcam (Cambridge, CA). Lysates and sub-cellular fractions were probed for MFN2 using mouse monoclonal antibody to MFN2 (working concentration 3μg/mL). A chicken polyclonal antibody to MFN1 (1.5μg/mL) was used where indicated. Rabbit polyclonal antibody to VDAC/porin (40ng/mL) was used as a mitochondria loading control. Chicken polyclonal antibody to calreticulin (330ng/mL) was used as a loading control for ER membranes or microsomal fraction. Mouse monoclonal antibody to α-tubulin (500ng/mL) was used as a loading control for whole lysates and cytosolic fraction. Horse radish peroxidase (HRP) conjugated secondary antibodies used were rabbit anti-mouse IgG (diluted 1:80,000), rabbit anti-chicken IgY (diluted 1:180,000), and goat anti-rabbit IgG (diluted 1:80,000) (Sigma Aldrich, St. Louis, MO). Proteins were detected by chemiluminescence (Western lightning detection kit, Perkin-Elmer, Waltham, MA) on X-ray film. For semi-quantitation serial dilutions of subcellular fractions from kidney and brain were loaded on the same blot and probed with all the primary antibodies above. In addition, densitometry was performed on x-ray films that were not over-exposed, scanned and analyzed for MFN1 level of expression in brainstem tissues and DRG cells using Adobe Photoshop CS3

software (Adobe Systems Inc., San Jose, CA). Bands were highlighted using the lasso tool to determine mean intensity and total pixel values of selected band. Absolute intensity was calculated in Microsoft Excel (2007) by multiplying both values. Relative intensity was generated by dividing absolute intensity of target (numerator) and loading control (denominator) (15, 16).

Table 2-2. Detailed description of primary antibodies used in western blot and immunohistochemistry experiments.

Target	Immunogen	Abcam Product #
MFN2	Recombinant fragment of Human Mitofusin 2 residues 661 - 758	ab56889
MFN1	A fusion protein against mouse Mitofusin 1 residues 348 - 579	ab30939
Calreticulin	Synthetic peptide of human calreticulin residues 353 - 416	ab14234
α-Tubulin	Rat brain tubulin	ab28037
VDAC/Porin	Synthetic peptide derived from Human VDAC1 / Porin residues 150 - 250	ab15895

Results

Mitofusin transcript levels in different tissues

MFN1 is a cellular paralogue of MFN2 that has a primary function of mediating outer mitochondrial membrane fusion during mitochondrial fusion. This MFN1 function is considered an overlap with MFN2 fusion function, as MFN1 can mediate the process in the absence of MFN2 (10). However, no evidence shows that MFN1 can also compensate for other MFN2 functions. Although both mitofusins are ubiquitously expressed, their tissue pattern of expression varies from tissue to tissue. MFN1:MFN2 ratios were compared in normal and affected tissues to estimate tissue dependence of one mitofusin on the other under normal and pathologic conditions. Different tissue samples were collected from different affected and normal pups to assay for *MFN* transcripts levels. Results are representative of only one animal per tissue per genotype. Table 2-3 shows increased expression of *MFN2* in nervous system derived tissues and skeletal muscle under normal and FNAD pathology conditions when compared to *MFN1* expression. Tissues affected by FNAD related pathology,brainstem and spinal cord tissues, have increased levels of *MFN2* mRNA compared to *MFN1* mRNA. Thymus tissues show increased *MFN1* expression when compared to *MFN2* in normal pup tissues. However, in affected tissues the ratio is slightly reversed as mutant *MFN2* expression is increased.

Table 2-3. Quantitative Real-time PCR was used to determine *MFN1*:*MFN2* ratio is different tissues to establish tissue specific mitofusin expression, and any changes influenced by the FNAD phenotype.

Tissue		*MFN1* expression normalized to *HPRT*	*MFN2* expression normalized to *HPRT*	*MFN1*:*MFN2* ratio
Cerebellum	Normal Affected	2.3 2.7	2.7 3.0	0.8 0.9
Brainstem	Normal Affected	0.9 1.2	1.3 2.1	0.7 0.5
Spinal cord	Normal Affected	1.2 1.5	1.9 3.0	0.6 0.5
Skeletal muscle	Normal Affected	2.5 2.2	8.2 6.1	0.3 0.3
Thymus	Normal Affected	1.0 2.5	0.7 2.7	1.4 0.9

MFN2 allelic mRNA expression

The aim was to ascertain whether the mutant *MFN2* allele is being transcribed in isolated tissues from heterozygous and homozygous pups for the ΔE539 *MFN2* mutation. The selected tissue of interest was dog brainstem since observed pathology was restricted to the nervous system. The novel mutation in *MFN2* abolishes *MnlI* restriction enzyme cutting site in *MFN2* cDNA. Therefore, digestion of *MFN2* cDNA with *MnlI* restriction enzyme distinguishes the mutant allele from the wild type *MFN2* allele. Figure 2-1 shows the resultant banding pattern of digested *MFN2* cDNA of mutant *MFN2* allele in homozygous affected and heterozygous normal pups.

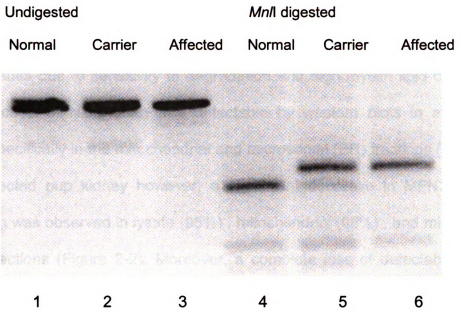

Figure 2-1. Allelic mRNA expression of mutant *MFN2*. Total RNA from homozygous normal *MFN2*, heterozygous, and homozygous mutant *MFN2* pups brainstem were used to amplify partial *MFN2* cDNA sequence spanning the novel mutation site. Lanes 1-3 represent amplified sequence, while lanes 4-6 represent amplified products after restriction digest with *MnlI* restriction enzyme. Lanes 5 and 6 distinguish the loss of *MnlI* cut site in mutant *MFN2* allele.

Mutant MFN2 protein expression and localization

We next analyzed mutant MFN2 protein abundance and localization in several tissues. Nervous system tissues assayed were brain and brain stem, which required a different sub-cellular fractionation protocol from that used for kidney tissues due to sensitivity to degradation and high myelin lipid content of neuronal cells. MFN2 protein was detectable by western blots in all normal tissues, specifically in the mitochondrial and microsomal (ER) fractions (Figure 2-2). In affected pup kidney however, a significant decrease in MFN2 protein expression was observed in lysate (95%) , mitochondrial (98%) , and microsomal (100%) fractions (Figure 2-2). Moreover, a complete loss of detectable MFN2 protein expression was evident in brain and brain stem fractions (Figure 2-3). Parallel analysis of MFN1 expression in brainstem tissues and subcellular fractions also from affected pups demonstrated maintained MFN1 expression in mutant tissues (Figure 2-4). MFN1 protein levels were normalized to calreticulen protein levels in different fractions. In total lysate MFN1 protein level increased by 19% in affected tissues, and in mitochondrial fraction of affected brainstem tissue MFN1 protein level was increased 41% of normal fraction level. MFN1 was detectable in microsomal fractions in both normal and mutant brainstem tissues, indicating a trace of mitochondrial outer membrane contamination in the microsomal fraction.

Subcellular fractionation of cultured primary cells total protein extracts was more challenging, and only feasible with primary dog fibroblast cells. In fibroblast total lysate, mitochondrial, and post-mitochondrial fractions, MFN2 was detectable in normal fibroblasts but only traces were observed in mutant fibroblasts (Figure 2-5). In DRG total lysate, however, a visible though reduced amount of MFN2 was detected in both normal and mutant cells (Figure 2-6). Mutant MFN2 protein level was 58% less than wild type MFN2 protein level in DRG cell total lysate. MFN1 protein level was 43% higher in affected pup DRG lysate when compared to normal pup DRG lysate and normalized with VDAC/Porin signal in DRG lysates of both genotypes.

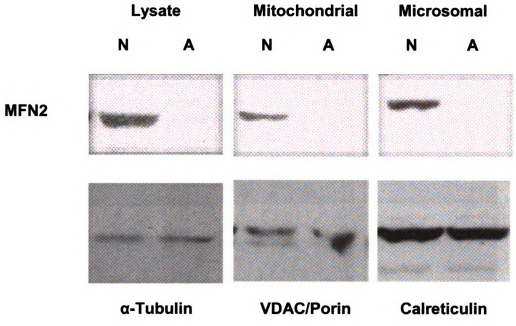

Figure 2-2. Kidney tissue fractions from normal (N) and affected (A) pups were assayed for MFN2 expression. Significant decrease in MFN2 expression was observed in affected fractions, albeit for trace amount in affected kidney lysate. In lysate and mitochondrial fractions 30μg of protein were used, whereas 40μg of microsomal fraction was used.

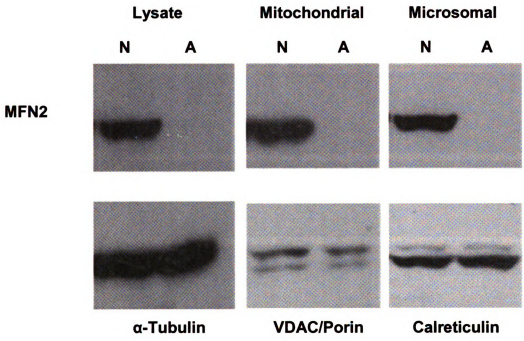

Figure 2-3. Brain tissue fractions from normal (N) and affected (A) pups were assayed for MFN2 expression. Significant loss of MFN2 detection was observed in all affected fractions. In lysate and mitochondrial fractions 30μg of protein were used, whereas 40μg of microsomal fraction was used.

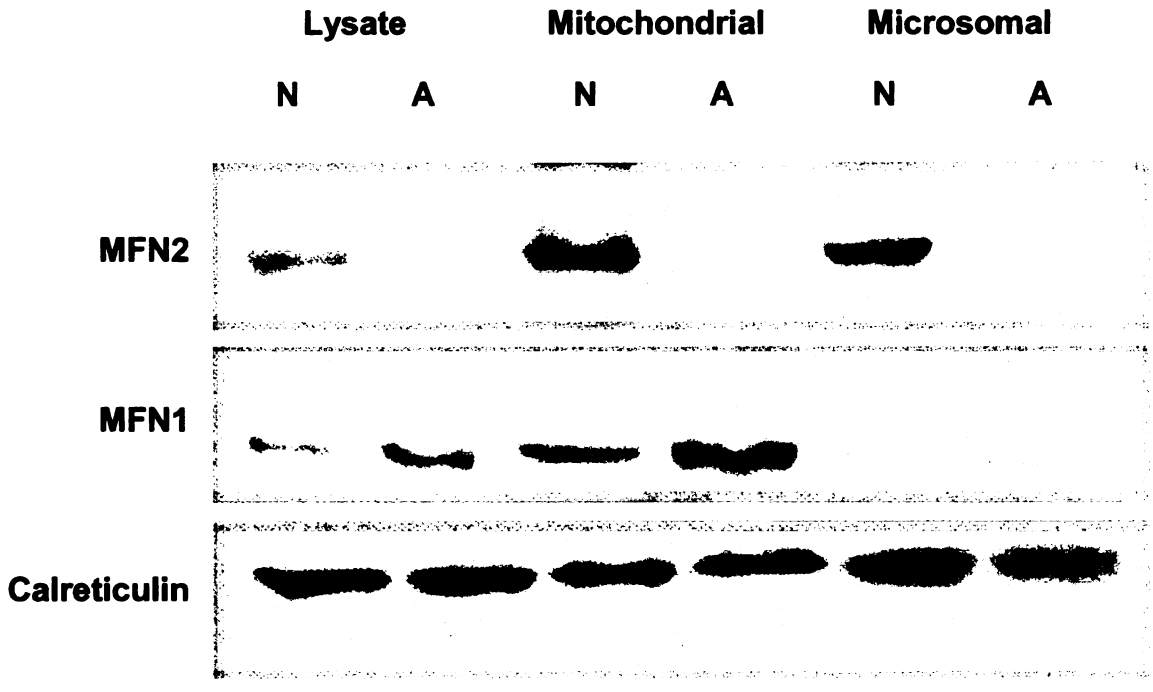

Figure 2-4. Brainstem tissue fractions from normal (N) and affected (A) pups were assayed for MFN2 and MFN1expression. Significant loss in MFN2 expression was observed in all affected fractions; however, MFN1 maintained expression in mitochondria. MFN1 expression increased in affected brainstem fractions when compared to normal pup brainstem fractions. All fractions were used at a concentration of 30µg/well.

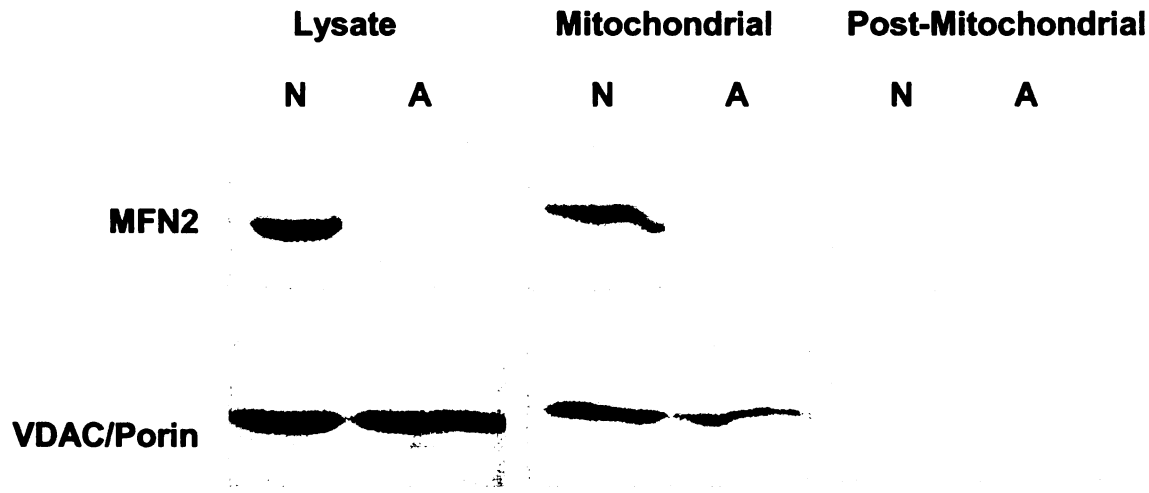

Figure 2-5. Cultured fibroblasts fractions from normal (N) and affected (A) pups were assayed for MFN2 expression. Trace amounts of MFN2 protein were observed in affected fractions when compared to normal cultured fibroblasts. Mitochondrial and post-mitochondrial fractions were used at a 10µg/well, while 20µg of total fibroblasts lysate was used.

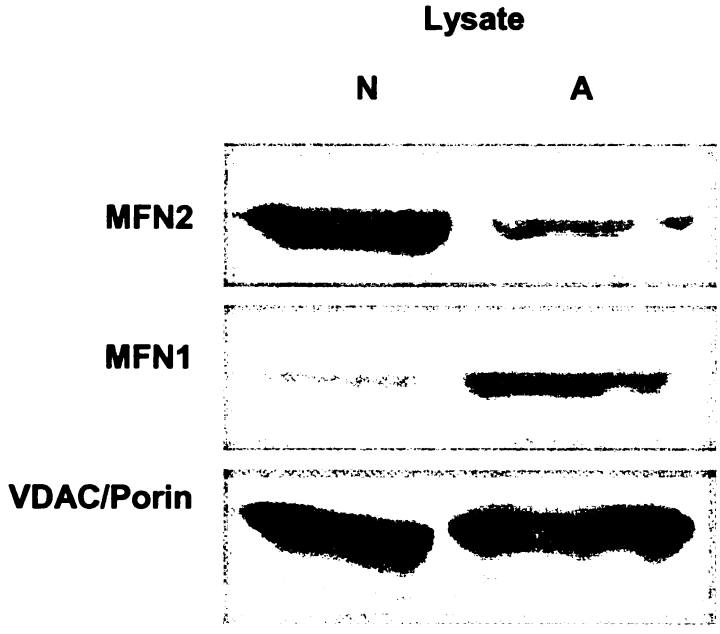

Figure 2-6. Cultured DRG lysates (25µg/well) from normal (N) and affected (A) pups were assayed for MFN2 and MFN1expression. MFN2 expression was detectable in affected DRG lysate albeit in decreased amounts when compared to normal DRG lysate. MFN1 was increased in affected DRG lysate when compared to normal DRG lysate.

Discussion

To characterize the pathogenesis of any mutation it is of primary interest to assay transcript and protein expression. Transcript expression might be of suggestive value in relation to protein expression but is not definitive. Assessment of mRNA levels is often taken as a proxy for gene expression, but RNA editing and regulation of translation, post-translational modifications, and subcellular localization renders this inaccurate for some genes. An example is CMT1A in which PMP22 gene duplication is the underlying cause. Interrogating *PMP-22* mRNA expression in nerve biopsies (17, 18) and skin (19) of CMT1A patients with *PMP-22* duplication resulted in a varied pattern of expression from normal to mild or high over-expression with overexpression correlating with less severe CMT1A phenotypes in nerves but not in skin. Protein expression and localization using immunohistochemistry was also variable in CMT1A patients with *PMP-22* duplications. Protein expression was reduced (17) or normal (20, 21) or varied in CMT1A patients with no correlation to disease severity (19). Therefore, only assumptions can be drawn from transcript analysis, and protein expression is the more significant assessment.

Mitofusins are ubiquitously expressed proteins but with tissue to tissue variability. For example, *MFN1* is expressed at similar levels in most human tissues, while *MFN2* has higher expression levels in heart and skeletal muscles (22). Our qRT-PCR data suggest that *MFN1* is transcribed in different affected pup tissues at comparable levels to normal pup levels, except for thymus tissue. *MFN1* transcription was slightly increased in tissues displaying FNAD related

pathology such as brain stem and spinal cord. Other tissues with strong mitochondrial dependence such as thymus and liver also showed marked increases in *MFN1* transcription in affected dogs. *MFN2* expression exhibited notable variation between tissues, and higher expression was noted in normal skeletal muscle relative to thymus tissue. Mutant *MFN2* expression in nervous system derived tissues was similar to those noted in wild type derived tissues except in spinal cord, which showed increased expression of mutant *MFN2*. Similar to *MFN1*, *MFN2* expression was notably increased in thymus tissues derived from affected pup. Mutant *MFN2* expression was decreased in skeletal muscle as was *MFN1*. This last observation is possibly attributable to lack of movement in late gestation due to motor neuron degeneration in diseased pups (23). There is a positive correlation between metabolic demands and mitochondrial dynamics that ultimately impacts gene expression levels of mitochondrial proteins. *MFN1* and *MFN2* observed expression levels might be in response to such demands in affected tissues undergoing active development and degeneration events. *MFN1*:*MFN2* ratio analysis in different tissues showed a possible tissue specific change in transcription levels of one mitofusin relative to the other. Nervous system derived tissues and skeletal muscle seem to favor *MFN2* expression when compared to *MFN1* expression. This phenomenon was suggested previously to explain nervous system tissue susceptibility to *MFN2* mutations while sparing other tissues (9). Affected pup tissues seem to respond to the presence of a mutation in *MFN2* by increasing *MFN2* expression when compared to *MFN1* levels, most noticeably in nervous system tissues. Among

those tissues the cerebellum only showed a slight increase. This might be attributed to the hypoplasia and degenerating cerebellar tissues being collected at an end point where *MFN2* level changes are no longer representative of the degenerative FNAD phenotype.

MFN2 wild type and mutant allele's expression was analyzed by restriction fragment length polymorphism technique. Gel based analysis showed active expression of the mutant allele in carrier brainstem tissues. However, carrier dogs lead a normal, healthy life without any signs of disease. Expression data at the RNA level is only suggestive of what cellular gene products are in demand at a given moment; RNA expression does not necessarily reflect translation of a transcript into a protein, its proper folding, targeting, or function.

Despite increased or normal MFN2 mRNA expression in affected dog tissues, analyzing mutant MFN2 protein expression demonstrated significant decreases. While wild type MFN2 localized to mitochondrial and ER fractions, mutant MFN2 was undetected in either. However, cultured primary DRG cells do show detectable amounts of mutant MFN2. Whether this is ascribed to cell-culture conditions or lack of proper tissue structure and signaling or altered protein turnover mechanism remains to be investigated. Enhanced MFN2 expression induced by *in-vitro* culturing might be attributed to addition of nerve growth factor (NGF). NGF specifically suppresses apoptotic signals and continues to suppress them despite accumulating pro-apoptotic signals (24). Relieving cellular stress might ameliorate the need for a strict cellular homeostasis control. Cellular mechanisms that control cellular fate include

apoptosis, necrosis, ubiquitin-mediated protein turnover and autophagy, each of which might be subdued in a pro-survival *in-vitro* culture system. Another culture induced condition is addition of glucose. Neurons depend almost entirely on glucose to provide energy for protein synthesis. High glucose conditions increase reactive oxygen species (ROS) stress. MFN2 is upregulated in response to oxidative stress at least in muscle tissues (25, 26). Neuronal dependence on maintained functions of mutant MFN2 might be favored in a culture system in comparison to *in-vivo*. Nervous system hierarchical signaling during systemic development is lost *in-vitro*, abolishing fundamental control over clearing dysfunctional neurons or proteins observed *in-vivo*.

This is the first report of an in frame single amino acid deletion within MFN2 that leads to complete loss of detectable protein. CMT2A2 MFN2 mutations analyzed for their functional attributes are detectable at the protein level and promote their altered functions depending on the site of mutation (27-31). The novel deletion of E539 residue falls within a conserved domain of MFN2 of unknown function (32). At this point only a speculation of the critical nature of this residue for maintaining an intact MFN2 protein with an accurate conformation and localization can be made. The impact of this mutation might influence transcript translation, protein modification, protein folding and conformation, protein targeting, or protein turn-over. Another possibility is that it might affect MFN2 ability to form stable interactions with protein partners. Further experiments to analyze these possibilities are required to fully describe the affect of this novel MFN2 mutant.

References

1 Chen, H., Detmer, S.A., Ewald, A.J., Griffin, E.E., Fraser, S.E. and Chan, D.C. (2003) Mitofusins Mfn1 and Mfn2 coordinately regulate mitochondrial fusion and are essential for embryonic development. *J Cell Biol*, **160**, 189-200.

2 Misko, A., Jiang, S., Wegorzewska, I., Milbrandt, J. and Baloh, R.H. (2010) Mitofusin 2 is necessary for transport of axonal mitochondria and interacts with the Miro/Milton complex. *J Neurosci*, **30**, 4232-4240.

3 Cartoni, R., Leger, B., Hock, M.B., Praz, M., Crettenand, A., Pich, S., Ziltener, J.L., Luthi, F., Deriaz, O., Zorzano, A., Gobelet, C., Kralli, A. and Russell, A.P. (2005) Mitofusins 1/2 and ERRalpha expression are increased in human skeletal muscle after physical exercise. *J Physiol*, **567**, 349-358.

4 Soriano, F.X., Liesa, M., Bach, D., Chan, D.C., Palacin, M. and Zorzano, A. (2006) Evidence for a mitochondrial regulatory pathway defined by peroxisome proliferator-activated receptor-gamma coactivator-1 alpha, estrogen-related receptor-alpha, and mitofusin 2. *Diabetes*, **55**, 1783-1791.

5 Liesa, M., Borda-d'Agua, B., Medina-Gomez, G., Lelliott, C.J., Paz, J.C., Rojo, M., Palacin, M., Vidal-Puig, A. and Zorzano, A. (2008) Mitochondrial fusion is increased by the nuclear coactivator PGC-1beta. *PLoS One*, **3**, e3613.

6 Li, Y., Yin, R., Liu, J., Wang, P., Wu, S., Luo, J., Zhelyabovska, O. and Yang, Q. (2009) Peroxisome proliferator-activated receptor delta regulates mitofusin 2 expression in the heart. *J Mol Cell Cardiol*, **46**, 876-882.

7 Rojo, M., Legros, F., Chateau, D. and Lombes, A. (2002) Membrane topology and mitochondrial targeting of mitofusins, ubiquitous mammalian homologs of the transmembrane GTPase Fzo. *J Cell Sci*, **115**, 1663-1674.

8 de Brito, O.M. and Scorrano, L. (2008) Mitofusin 2 tethers endoplasmic reticulum to mitochondria. *Nature*, **456**, 605-610.

9 Chen, H., McCaffery, J.M. and Chan, D.C. (2007) Mitochondrial fusion protects against neurodegeneration in the cerebellum. *Cell*, **130**, 548-562.

10 Detmer, S.A. and Chan, D.C. (2007) Complementation between mouse Mfn1 and Mfn2 protects mitochondrial fusion defects caused by CMT2A disease mutations. *J Cell Biol*, **176**, 405-414.

11 Etschmann, B., Wilcken, B., Stoevesand, K., von der Schulenburg, A. and Sterner-Kock, A. (2006) Selection of reference genes for quantitative real-time

PCR analysis in canine mammary tumors using the GeNorm algorithm. *Vet Pathol*, **43**, 934-942.

12 Bradford, M.M. (1976) A rapid and sensitive method for the quantitation of microgram quantities of protein utilizing the principle of protein-dye binding. *Anal Biochem*, **72**, 248-254.

13 Sujkovic, E., Mileusnic, R. and Fry, J.P. (2009) Metabolism of neuroactive steroids in day-old chick brain. *J Neurochem*, **109**, 348-359.

14 Laemmli, U.K. (1970) Cleavage of structural proteins during the assembly of the head of bacteriophage T4. *Nature*, **227**, 680-685.

15 Luhtala, N. and Parker, R. (2009) LSM1 over-expression in Saccharomyces cerevisiae depletes U6 snRNA levels. *Nucleic Acids Res*, **37**, 5529-5536.

16 Miller, R.K., Qadota, H., Stark, T.J., Mercer, K.B., Wortham, T.S., Anyanful, A. and Benian, G.M. (2009) CSN-5, a component of the COP9 signalosome complex, regulates the levels of UNC-96 and UNC-98, two components of M-lines in Caenorhabditis elegans muscle. *Mol Biol Cell*, **20**, 3608-3616.

17 Hanemann, C.O., Stoll, G., D'Urso, D., Fricke, W., Martin, J.J., Van Broeckhoven, C., Mancardi, G.L., Bartke, I. and Muller, H.W. (1994) Peripheral myelin protein-22 expression in Charcot-Marie-Tooth disease type 1a sural nerve biopsies. *J Neurosci Res*, **37**, 654-659.

18 Yoshikawa, H., Nishimura, T. and Yanagihara, T. (1995) [Molecular pathology of Charcot-Marie-Tooth disease type 1A: abnormal expression of PMP-22]. *Rinsho Shinkeigaku*, **35**, 1441-1443.

19 Katona, I., Wu, X., Feely, S.M., Sottile, S., Siskind, C.E., Miller, L.J., Shy, M.E. and Li, J. (2009) PMP22 expression in dermal nerve myelin from patients with CMT1A. *Brain*, **132**, 1734-1740.

20 Fabrizi, G.M., Simonati, A., Morbin, M., Cavallaro, T., Taioli, F., Benedetti, M.D., Edomi, P. and Rizzuto, N. (1998) Clinical and pathological correlations in Charcot-Marie-Tooth neuropathy type 1A with the 17p11.2p12 duplication: a cross-sectional morphometric and immunohistochemical study in twenty cases. *Muscle Nerve*, **21**, 869-877.

21 Nishimura, T., Yoshikawa, H., Fujimura, H., Sakoda, S. and Yanagihara, T. (1996) Accumulation of peripheral myelin protein 22 in onion bulbs and Schwann cells of biopsied nerves from patients with Charcot-Marie-Tooth disease type 1A. *Acta Neuropathol*, **92**, 454-460.

22 Santel, A., Frank, S., Gaume, B., Herrler, M., Youle, R.J. and Fuller, M.T. (2003) Mitofusin-1 protein is a generally expressed mediator of mitochondrial fusion in mammalian cells. *J Cell Sci*, **116**, 2763-2774.

23 Fyfe, J.C., Al-Tamimi, R.A., Castellani, R.J., Rosenstein, D., Goldowitz, D. and Henthorn, P.S. (2010) Inherited neuroaxonal dystrophy in dogs causing lethal, fetal-onset motor system dysfunction and cerebellar hypoplasia. *J Comp Neurol*, **518**, 3771-3784.

24 Chu, C.T. (2006) Autophagic stress in neuronal injury and disease. *J Neuropathol Exp Neurol*, **65**, 423-432.

25 Shen, T., Zheng, M., Cao, C., Chen, C., Tang, J., Zhang, W., Cheng, H., Chen, K.H. and Xiao, R.P. (2007) Mitofusin-2 is a major determinant of oxidative stress-mediated heart muscle cell apoptosis. *J Biol Chem*, **282**, 23354-23361.

26 Ding, H., Jiang, N., Liu, H., Liu, X., Liu, D., Zhao, F., Wen, L., Liu, S., Ji, L.L. and Zhang, Y. (2010) Response of mitochondrial fusion and fission protein gene expression to exercise in rat skeletal muscle. *Biochim Biophys Acta*, **1800**, 250-256.

27 Ouvrier, R. and Grew, S. (2010) Mechanisms of disease and clinical features of mutations of the gene for mitofusin 2: an important cause of hereditary peripheral neuropathy with striking clinical variability in children and adults. *Dev Med Child Neurol*, **52**, 328-330.

28 Cartoni, R. and Martinou, J.C. (2009) Role of mitofusin 2 mutations in the physiopathology of Charcot-Marie-Tooth disease type 2A. *Exp Neurol*, **218**, 268-273.

29 Amiott, E.A., Cohen, M.M., Saint-Georges, Y., Weissman, A.M. and Shaw, J.M. (2009) A mutation associated with CMT2A neuropathy causes defects in Fzo1 GTP hydrolysis, ubiquitylation, and protein turnover. *Mol Biol Cell*, **20**, 5026-5035.

30 Amiott, E.A., Lott, P., Soto, J., Kang, P.B., McCaffery, J.M., DiMauro, S., Abel, E.D., Flanigan, K.M., Lawson, V.H. and Shaw, J.M. (2008) Mitochondrial fusion and function in Charcot-Marie-Tooth type 2A patient fibroblasts with mitofusin 2 mutations. *Exp Neurol*, **211**, 115-127.

31 Baloh, R.H., Schmidt, R.E., Pestronk, A. and Milbrandt, J. (2007) Altered axonal mitochondrial transport in the pathogenesis of Charcot-Marie-Tooth disease from mitofusin 2 mutations. *J Neurosci*, **27**, 422-430.

32 Honda, S., Aihara, T., Hontani, M., Okubo, K. and Hirose, S. (2005) Mutational analysis of action of mitochondrial fusion factor mitofusin-2. *J Cell Sci*, **118**, 3153-3161.

CHAPTER III

FUNCTIONAL AND MORPHOLOGICAL ASSESSMENT OF MUTANT MFN2 MITOCHONDRIA

Chapter III

Functional and morphological assessment of mutant MFN2 mitochondria

ABSTRACT

MFN2 is a multi-function protein involved in various cellular processes. A primary MFN2 role is mitochondrial fusion, but additional roles including control of apoptosis and mitophagy, mitochondrial respiration, ER tethering, and axonal transport have also been established. To assay for the effect of the $MFN2^{\Delta E539}$ mutation several *in-vitro* assays were designed. Polarography was used to measure mitochondrial respiration in crude mitochondrial preparations. Live cell imaging in primary canine fibroblasts with organelle specific dyes were used to assay for mitochondrial morphology, distribution, and mitophagy. Moreover, membrane potential analysis in fibroblasts employed membrane potential sensitive mitochondrial dye, and fluorescence resonance energy transfer (FRET) technique. Results show unchanged mitochondrial respiration, morphology, and distribution. No increase of mitophagy was observed for mutant mitochondria when compared to wild type MFN2 mitochondria. Mitochondrial membrane potential appeared reduced in MFN2 mutant mitochondria assessed by FRET approaching statistical significance (p-value = 0.057). In conclusion, the novel MFN2 mutation does not affect the mitochondrial functions assayed here, nor did it induce mitophagy in cultured primary canine fibroblasts.

Introduction

Mitofusins are mitochondrial outer membrane GTPases involved primarily in mitochondrial fusion. MFN1 has 8-fold higher GTPase activity than MFN2 and promotes outer mitochondrial membrane fusion (1). MFN1 interacts with the inner mitochondrial membrane protein OPA1 resulting in tighter tethering of mitochondrial membranes and coordinating of inner and outer membrane fusion (2). MFN2 is involved in mitochondrial outer membrane fusion via interaction with mitofusin proteins on juxtaposed mitochondrial membranes (3). Canine mitofusin 1 and 2 proteins have ~66% amino acid similarity, far lower than the similarity of each to orthologues in disparate species. Structural disparities between mitofusins suggest different functions in addition to known overlapping functions. Mitofusin 1 and 2 knockout mice are embryonic lethal, however differing phenotypes and mitochondrial morphology and dynamics were observed in embryonic fibroblast cultures derived from each knockout (4). MFN2 has been shown to be involved in different functions and pathways that result in different outcomes in different cell types (5). There are seven highly conserved regions on MFN2, four of which have evidence of functional and structural activities (6). The four domains of known function are the N-terminus GTPase domain, transmembrane domain, and two coiled-coil domains. To some degree mutant forms of MFN2 are expected to exhibit dysfunctions correlating to their mutational site. The novel MFN2 mutation analyzed here (ΔE539) is within a conserved region of unknown function. The aim of the experiments detailed in this chapter is to identify a cellular phenotype related to the mutant MFN2. In summary, MFN2

functions include maintaining mitochondrial morphology and network through fusion (3, 7), a role in mitochondrial respiration (8, 9), a role in cell survival and mitophagy (10, 11), and a role in axonal transport (12). Evidence shows MFN2 as either a direct inducer, or an interactive partner with members of a cascade promoting a certain function. For example, overexpression of MFN2 is considered a signal for enhanced oxidative phosphorylation (9). Whereas MFN2 interactions with pro-apoptotic factors Bax and Bak can transmit a pro-apoptotic signal and determine cell survival (13, 14). Mitochondrial membrane potential is a direct sensor of mitochondrial health (15-17). The interplay between most of MFN2 functions depend on the mitochondrial state of polarization or depolarization (18-21).

In this chapter, experiments are focused on analyzing mitochondrial dynamics in $MFN2^{\Delta E539}$ mutant mitochondria that might directly influence cell survival. Mitochondrial respiration was used as a functional mitochondrial competency assay. Mitochondrial morphology and distribution were analyzed to determine mitochondrial structural integrity. Mitochondrial autophagy (mitophagy) was assayed to detect the clearance of dysfunctional mitochondria, and their abundance. Lastly, the electro-chemical property of mitochondria was assayed by analyzing the mitochondrial membrane potential in cultured primary canine fibroblasts.

Materials and Methods

Mitochondrial preparations and polarography

Excised kidneys were immersed in MSH buffer (210mM mannitol, 0.75M sucrose, 20mM HEPES, pH 7.4), minced and rinsed three times with MSH buffer. Kidney mince was resuspended in MSH buffer with 1mM EDTA and 0.1mM PMSF and homogenized using a glass Teflon homogenizer. Homogenates were centrifuged at 600x*g* for 10 min, and resultant supernatants were centrifuged at 7,500x*g* for 10 min. Pellets representing crude mitochondria fractions were washed with MSH buffer without EDTA twice. Final pellets were resuspended in respiration media (220mM mannitol, 68mM sucrose, 1.9mM HEPES, 2.4mM potassium phosphate buffer, 0.5mM EDTA, 1.8mM $MgCl_2$, 5.2mM succinate, 0.7g/l BSA, pH 7.4). Mitochondrial respiration was measured as a function of oxygen consumption from medium. A Gilson Model K-IC oxygen polarograph (Gilson Medical Electronics, Middleton, WI) equipped with 0.5cm-diameter Clark oxygen electrode and a water-jacketed 1.75-ml glass reaction chamber was used. Temperature was maintained at a constant 37°C using a circulating water bath. Medium was saturated with oxygen for 5 minutes with constant stirring. Aliquots of mitochondrial suspension were added and basal respiration recorded. Active respiration was recorded following addition of 0.45µM ADP. Total oxygen consumption was determined based on slope of active respiration and normalized by protein concentration of mitochondrial fractions added (22). Mitochondrial fraction protein concentrations were determined with BioRad's

protein assay dye reagent (Bio-Rad laboratories, Hercules, CA) according to Bradford protein assay method (23).

***In-vitro* culture system**

Primary canine fibroblasts (CF) were cultured from excised pup umbilical cord tissue. Excised tissues were washed three times in full CF growth medium for 3 minutes per wash. Tissues were minced with sterile scalpels, and tissue fragments were transferred to 60mm culture dishes containing full growth medium. Full CF growth medium contained high glucose DMEM (Invitrogen Corp., Carlsbad, CA), 10% fetal bovine serum, 1% glutamine, and 1% penicillin/streptomycin solution.

Primary dorsal root ganglia (DRG) were excised following complete dissection of spinal cord and its nerve roots. Isolated ganglia were collected in 1X HBSS (Invitrogen Corp., Carlsbad, CA) supplemented with 10mM HEPES (pH 7.4), and incubated with collagenase I-A (500U/ml) for 15 minutes at 37°C in a water bath. A second incubation with trypsin (1mg/ml) for 30 minutes at 37°C was terminated by addition of equal volume of full DRG growth medium. Mechanical triturations were repeated five times using a sterile glass Pasteur pipette. Each trituration was followed by a brief low speed centrifugation and supernatant was collected in a fresh tube. Pellets were resuspended in 1XPBS (137mM NaCl, 2.7mM KCl, 4.3mM Na_2HPO_4, and 1.47mM KH_2PO_4, pH 7.4) prior to each trituration repeat. Collected supernatants were centrifuged 1,000xg for 5 minutes. Resultant pellet was suspended in 3ml full DRG growth medium.

DRG growth medium contains L-15 medium (Invitrogen Corp., Carlsbad, CA), 10% fetal bovine serum, 2 mM L-glutamine, 24 mM $NaHCO_3$, 38 mM glucose, 1% penicillin/streptomycin solution, and 50ng/ml NGF (Sigma Aldrich, St. Louis, MO). DRG suspensions were plated on 60mm dishes pre-coated with 0.01% poly-L-ornithine (Sigma Aldrich, St. Louis, MO). Both types of cultures were maintained at 37°C and 5% CO_2 incubation conditions.

Live cell imaging of mitochondrial morphology and distribution

Cells were cultured in 35mm glass cover slip bottom dishes (MatTek corp., Ashland, MA). Cell cultures were incubated with 0.5μM mitotracker green (MTG) (Invitrogen Corp., Carlsbad, CA) for 1 hour in 2ml of full growth medium at 37°C and 5% CO_2 conditions. Cells were washed three times in fresh full medium and mounted in a disc incubator at 37°C. Images were captured with Olympus Fluoview 1500 confocal microscope (Olympus America Inc., Center Valley, PA) using 60X PlanApo objectives at 1.0 or higher digital zoom when magnification was required.

FRET for mitochondrial membrane potential analysis

Förster's fluorescence energy transfer (FRET) is a technique that has been modified to analyze mitochondrial polarization in living cells. When two dyes are within the same mitochondrion the fluorescence of the general mitochondrial dye (MTG, donor) becomes quenched upon laser excitation as energy of its excitation is transferred non-radiatively to a second dye (TMRM, acceptor) in close proximity, which will fluoresce instead of the donor emitting its

color (red) (24). CF cultures of homozygous wild type MFN2 and homozygous mutant $MFN2^{\Delta E539}$ genotypes (N = 6), were grown to ~70-80% confluence. Cells were incubated with 0.5μM MTG for 1 hour at 37°C and 5% CO_2. Cells were washed three times in full growth medium and imaged for uniform staining and cross-over emission. Cells were then incubated with 0.8μM TMRM (Invitrogen Corp., Carlsbad, CA) for 30 minutes at 37°C and 5% CO_2. Cells were washed three times with full growth medium. Cells were excited at 488nm wavelength and imaged using z-stack setting at 0.8μm focal plane thickness in parallel for green and red emissions. Eleven z-stacks per channel were captured for each culture. Cultures were incubated with 2.5mM KCN for 1 hour at 37°C and 5% CO_2 to depolarize mitochondria. At least six subsequent z-stacks were captured per channel. Images were analyzed with ImageJ software (U. S. National Institutes of Health, Bethesda, MD) to generate maximum intensity projections. FRET experiments were conducted in duplicate for each primary CF cell culture.

Analysis of FRET data involved generating polarized mitochondria:all mitochondria (red:green) ratios for each image captured. Ratios were corrected by dividing the ratio by the averaged KCN depolarized red:green ratio of the same cell line. This correction allows for subtracting green signal from polarized mitochondria for a finer estimate of polarized mitochondria within the cell. To account for experiment to experiment variability a linear mixed model statistical analysis method was employed using SPSS v.17 software (SPSS Inc., Chicago, IL). The linear mixed model allows for inclusion of random effects that might exhibit correlation and variability of non-constant magnitude that might be

obscured by variability between experimental sets (25). The model is flexible enough to include means of variables as well as covariance structures. Genotypes were selected as category for fixed effects, while number of animals (cell-lines) assayed was selected for random effects, and corrected ratio as the dependent variable.

Live cell imaging of mitophagy

Primary CF cultures were incubated with 0.5μM mitotracker green for two time points of 20 and 24 hours, at 37°C and 5% CO_2. Cells were washed three times with full growth medium and incubated with 50nM lysotracker blue-DND 22 (Invitrogen Corp., Carlsbad, CA) for 30minutes. Cells were imaged with an Olympus Fluoview 1500 confocal microscope (Olympus America Inc., Center Valley, PA) using 60X PlanApo objectives at 1.0 or higher digital zoom when magnification was required. Images were processed with Adobe Photoshop CS3 software (Adobe Systems Inc., San Jose, CA).

Results

Mitochondrial respiration

Kidney mitochondrial extracts from four pups of each homozygous wild type and mutant $MFN2^{\Delta E539}$ genotypes were assayed for mitochondrial respiration in duplicates. Polarographs generated on thermal graph paper were analyzed by hand and quantitative measurements were used in the following formula to estimate oxygen consumption rate;

$$\text{Rate}\left(\frac{\text{nmoles } O_2}{\text{Min}}\right) = \frac{\#\text{verti. sq.}}{\#\text{ hori. sq.}} \times \frac{1\text{hori. sq}}{4\text{ sec}} \times \frac{60\text{s}}{\text{min}} \times \frac{240\text{ nmoles } O_2}{\text{ml}} \times \frac{1.8\text{ ml}}{200\text{ verti. sq}}$$

(# Vert.sq.= number of vertical squares under the slope, #hori. Sq. = number of horizontal squares under the slope, each square on graph = 4 seconds, oxygen saturation in medium = 240 nmoles O_2, total glass chamber volume = 1.8ml)

Oxygen consumption rates were adjusted according to amount of input mitochondrial extract total protein concentration ((nmoles O_2/minute) /µg). Results comparing basal and active respiration in both genotypes were not significantly different. Homozygous normal genotype mean basal mitochondrial respiration was 16.32 (nmoles O_2/minute) /µg (SD_{Normal_Basal} = 5.2), while in

homozygous mutants it was 15.31 (nmoles O_2/minute) /µg ($SD_{Affected\_Basal}$= 7.6). Homozygous normal genotype mean active mitochondrial respiration was 30.04 (nmoles O_2/minute) /µg (SD_{Normal_Active}= 9), while in homozygous mutants it was 27.46 (nmoles O_2/minute) /µg ($SD_{Affected\_Active}$= 10.2). Both genotypes maintained similar respiration levels indicative of intact mitochondrial respiration. ATP production from medium supplemented with succinate as substrate for complex II proceeded similarly in both genotypes as revealed by oxygen consumption analysis. ATP production from added ADP to stimulate maximal respiration was also similarly induced in both genotypes as determined through oxygen consumption analysis. Therefore, ATP production and mitochondrial respiration are not affected by the $MFN2^{\Delta E539}$ mutation.

Mitochondrial morphology and distribution

Mitochondria can be found in different shapes depending on cellular conditions and requirements. Mitochondria can be spherical or tubular in shape. Spherical mitochondria can vary in diameter while maintaining mitochondrial structural integrity. Tubular mitochondrial can vary in lengths between short, intermediate, and long tubules. Multiple morphological phases are products of dynamic fusion/fission cycles. Distribution of mitochondria is governed by cell type and organelle-specific ATP demands. In primary CF cultures, no distinguishable differences were noted in mitochondrial shape between normal and $MFN2^{\Delta E539}$ mutants. Both cultures contained spherical and tubular mitochondrial in comparable quantities (Figure 3-1). Tubular mitochondria were of different lengths in both cell culture genotypes without any apparent differences. Mitochondrial distribution within cells was equally random in appearance without any obvious clustering attributed to mutant phenotype. Increased density of peri-nuclear mitochondrial was observed in some cells of both genotypes.

Neurons display various mitochondrial morphologies and distribution depending on their tissue environment, maturity and neural connections. Mitochondrial shape in neurons has been documented to change under excitotoxic, apoptotic, and injurious conditions (26). Mitochondrial morphology and distribution in primary DRG cultures of homozygous wt MFN2 and homozygous $MFN2^{\Delta E539}$ genotypes were comparable (Figure 3-2). Mitochondria

formed discrete entities along axons with increased densities at growth cones. The cell bodies were crowded with mitochondria of different shape. No detectable changes were observed related to mutant $MFN2^{\Delta E539}$ in primary DRG culture.

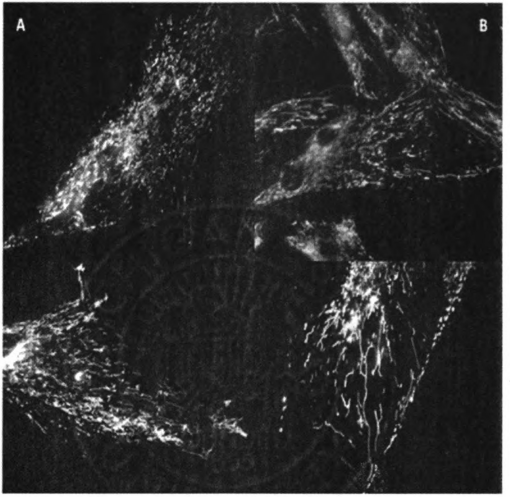

Figure 3-1. Fibroblast cells mitochondria are stained with MTG fluorescent dye. (**A**) Normal fibroblast cells; (**B**) Affected fibroblast cells. Upper panel captured at 40 x magnification; lower panel at 60x magnification.

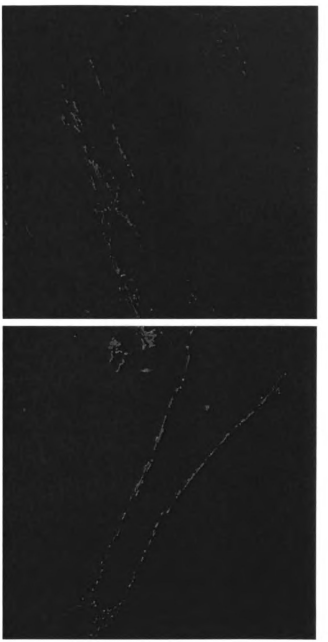

Figure 3-2. Dorsal root ganglia cells mitochondria are stained with MTG fluorescent dye. **Top**, normal DRG cells. **Bottom**, affected DRG cells.

Analysis of mitochondrial membrane potential

Mitochondrial membrane potential is an indicator of overall mitochondrial health (27). It is an electrical potential formed by the proton-gradient generated by electron transport chain complex activities in mitochondrial inner membranes. Mitochondria become depolarized upon membrane permeability transition (MPT). MPT endogenous inhibition is achieved by ATP or ADP production (28). MPT is induced in response to apoptotic or necrotic death stimuli (29), or due to outer membrane rupture or seepage (30), or calcium overload (31), or oxidative stress (32). In each case the general outcome is loss of mitochondrial outer membrane integrity, inhibition of ATP production, and loss of mitochondrial membrane potential. The state of mitochondrial depolarization cannot be rescued by fusion since a state of polarization is a fusion prerequisite (3, 33, 34). The only disposition for depolarized mitochondria is through targeted organelle autophagy (mitophagy) (35, 36). Here we used FRET, a sensitive fluorescence based method to detect membrane potential changes. Figure 3-3 is a representative of maximal intensity projections of captured z-stacks of fibroblasts cells doubly stained with MTG and TMRM. Different animals and experiments being performed on different days unavoidably generated variability in the results. To account for this variability and minimize its affect on significance, animal to animal variability was included to estimate random effects. The random effects were estimated based on animal to animal variance regardless of genotype to = 0.169 around the mean of corrected ratios, at a standard deviation of 0.082, and a significance p-value = 0.04. Inclusion of this estimate in pair wise comparisons of both genotypes resulted in a mean difference indicative of reduced membrane

potential in mutant CF cells approaching a significant p-value of 0.057 (Table 3-1).

Table 3-1. Statistical analysis of data generated from mitochondrial membrane potential assay. Descriptive statistics of estimated marginal means after accounting for random effects variation (upper table) and their pairwise comparisons (lower table).

Category	Mean	Std. Error	df	95% Confidence Interval	
				Lower Bound	Upper Bound
A	1.767	.175	9.999	1.377	2.157
N	2.299	.175	10.010	1.908	2.689

(I)	(J)	Mean Difference (I-J)	Std. Error	df	Sig.[a]	95% Confidence Interval for Difference[a]	
						Lower Bound	Upper Bound
N	A	.532	.248	10.004	.057	-.020	1.084

a. Adjustment for multiple comparisons: Least Significant Difference (equivalent to no adjustments).

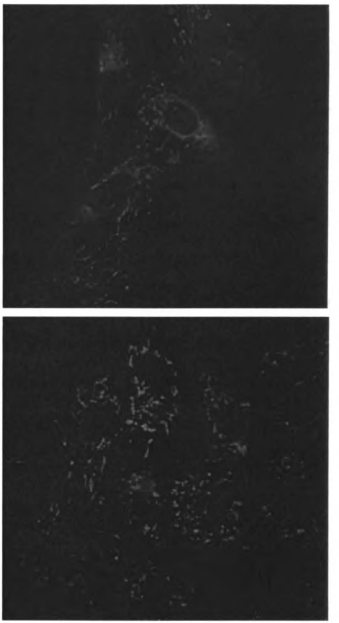

Figure 3-3. Mitochondrial membrane potential was assayed in normal (**A**) and affected (**B**) fibroblast cells using FRET technique. Mitochondria are doubly stained with general mitochondrial dye MTG (green) and polarized mitochondria specific dye TMRM (red). Green mitochondria are depolarized mitochondria.

Analysis of mitophagy

Mitochondria in living cells undergo recycling and mitophagy according to cellular fitness and stimuli (37, 38). Primary CF cells were incubated with MTG for 20 and 24 hours. Long incubation time should permit detection of mitochondria at different phases of degradation. Lysotracker DND-blue specifically stains acidic vacuoles, and thus identifies lysosomes and autophagosomes. Colocalization of green mitochondria within lysotracker detected lysosomes would signify active mitophagy. Comparison of mitophagy profiles of normal and mutant $MFN2^{\Delta E539}$ primary CF cells at two time points did not identify a significant mutant phenotype (Figure 3-3). Both cell types were equally lacking of any evidence of mitophagic stress. Therefore, at least in primary CF cells mutant $MFN2^{\Delta E539}$ mitochondria are not being targeted for specific degradation.

Figure 3-4. Mitochondrial degradation and recycling through mitophagy was assayed using mitochondrial and lysosomal specific fluorescent dyes at two time points. **A.** After 20 hrs normal (upper panel) and affected (lower panel) fibroblasts were imaged. **B.** After 24 hrs normal (upper panel) and affected (lower panel) fibroblasts were imaged. Both time points showed very little colocalization of mitochondria with lysosomes in either assayed fibroblasts genotypes.

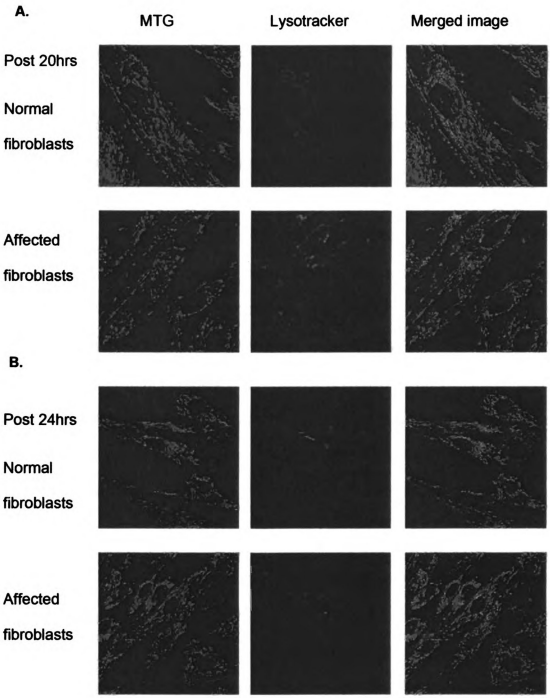
A.
MTG
Lysotracker
Merged image
Post 20hrs
Normal
fibroblasts
Affected
fibroblasts
B.
Post 24hrs
Normal
fibroblasts
Affected
fibroblasts

Discussion

Mitochondria are multi-functional organelles of the eukaryotic cell. Mitochondrial functions dictate cellular survival and homeostasis. A primary function of mitochondria is energy production through catalytic oxidation of intermediate metabolites. Enzyme complexes localized in the mitochondrial inner membrane catalyze the process efficiently in the presence of oxygen. Oxygen consumption is a direct indicator of active oxidative phosphorylation and formation of ATP. Evidence implicates MFN2 upregulation coincident with increased mitochondrial energy production after exercise (39), cold treatment (40), and insulin stimuli (41). Direct evidence implicates MFN2 overexpression in increasing expression of complexes I, IV, and V (9). Loss of function mutants and obesity induced MFN2 suppression and down regulated expression of complexes I, II, III and V. While mitochondrial fusion promoted by mitofusins is directly involved in promoting energy production (42), MFN2 effects on respiration are separate from its fusion function (9). Mutant $MFN2^{\Delta E539}$ is expressed on the transcript level; however only trace amounts of MFN2 were observed in kidney and fibroblast protein extracts. Oxygen consumption does not seem to be affected by this loss of MFN2 protein expression. No significant changes were observed in basal or active respiration. It was expected that this mutant would exhibit a respiration phenotype similar to loss of function or knock out/down of MFN2. To date there is no respiration data reported on MFN2 knock out mitochondria; however data for double mitofusin knock out suggest considerable loss of basal and active respiration (42). In contrast, reported MFN2 knock down

experiments did not show any significant coupled respiration deficiencies (8). Ten different MFN2 mutants causing CMT2A2 have been assayed for their respiration capabilities and have been found to retain their mitochondrial respiration capabilities (43-45). Therefore, it is not unforeseen that mitochondria lacking or harboring mutant forms of MFN2 retain their coupled respiratory control. However, uncoupled respiration was not included in our assay. Uncoupled respiration is the rapid procession of oxygen consumption into the electron transport chain without related ATP synthesis under the influence of potent uncoupling agents. This assay would relate more to the metabolic efficiency of mitochondria than respiration and ATP production. MFN2 knock down and CMT2A2 MFN2 mutant cells exhibit altered uncoupled respiration (8, 46). How this relates to the pathogenesis of CMT2A2 is still unknown. However, it is reported to be attributed to reductions in mitochondrial membrane potential, a process dependant on the inner mitochondrial membrane structure and function (46).

Mitochondrial morphology and distribution is controlled by at least four GTPases involved in fission and fusion cycles (47). MFN2 is one of three GTPases involved in mitochondrial fusion; the other two are MFN1 and OPA1. MFN2 knock out embryonic mouse derived fibroblasts contained predominantly spherical and oval mitochondria, with a minor fraction (4.5%) that maintained tubular shape (4). Mitochondrial shape in $MFN2^{\Delta E539}$ mutant fibroblasts did not display any aberrant mitochondrial shape. Moreover, tubular mitochondrial networks were observed throughout the cell. Minor subsets of spherical

mitochondria have been observed but are not in comparable quantities to normal wild type MFN2 mitochondria. Given the lack of MFN2 protein expression in fibroblasts an aberrant mitochondrial shape was expected as in the MFN2 knockout embryonic mouse derived fibroblasts. However, this is not the result observed. A possible explanation is that mouse embryonic derived fibroblasts were harvested at day e10.5, whereas our fibroblasts are from born pups. Embryonic fibroblasts might be showing an overall phenotype attributed to losing all of MFN2 functions not just fusion. MFN2 expression has been reported to be upregulated in mouse oocytes and preimplantation embryos accumulating in the cytoplasm at early stages and at sub-membranes, spindle and chromosomal structures at later stages of oocyte maturation (48). This early requirement of MFN2 suggests that its complete loss generates a defective embryo in which aberrant mitochondrial shape is a secondary event. In our novel MFN2 mutant however, pups survive the entire duration of gestation and although displaying an abnormal phenotype they are born alive and may survive for some time given respiratory support. Whether or not the mutant MFN2 is expressed at early stages of development remains to be investigated. In addition, it is possible that an amount of MFN2 is expressed below detectable abilities of western blotting and is sufficient to prevent embryonic death. Moreover, several CMT2A2 MFN2 mutants have been assayed for mitochondrial shape either in patient derived fibroblasts (43) or by transfection into mitofusin null mouse embryonic fibroblasts (49). In patient fibroblasts no abnormal mitochondrial shape has been noted. In cells transfected with CMT2A mutants of MFN2, mitochondria showed various

shapes corresponding to different mutants. A result from these reports is that MFN1 complements defective MFN2 whereas wild type MFN2 does not which correlates with CMT2A2 dominant inheritance (49). MFN1 rescues fusion defects of mutant MFN2 and restores mitochondrial shape. In DRG cells no abnormal mitochondrial shape or distribution was noted in $MFN2^{\Delta E539}$ mutants. It should be mentioned that in neurons mitochondrial shape and distribution changes in each subcompartment within a neuron (26). $MFN2^{\Delta E539}$ mutant DRG cells maintained mitochondrial dynamics in comparable measure to wild type MFN2 mitochondria.

Mitochondrial membrane potential is a critical discriminator for mitochondrial health. Our results indicate a slight reduction in mitochondrial polarization in $MFN2^{\Delta E539}$ mutant fibroblasts when compared to wild type MFN2. This change did not reach significance but was suggestive (p-value 0.057). This minor change might not contribute to cell death directly but might be an indicator of dysfunctional mitochondria. Fusion is maintained in fibroblast cells suggesting that the membrane potential decrease is not sufficient to alter mitochondrial shape. Depolarized mitochondria are specifically targeted to degradation through cellular organelle autophagy, or mitophagy but analyzing mitophagy in $MFN2^{\Delta E539}$ mutant primary CF cells did not result in any observed increase in the disposal machinery.

MFN2 plays an important role in mitochondrial clearance via mitophagy. Parkin, a ubiquitin ligase is targeted specifically to dysfunctional mitochondria destined for autophagic degradation (50). The recruitment of Parkin to mitochondrial membranes is guided by interactions with PINK1, a mitochondrial kinase (51-54). When recruited, Parkin specifically ubiquitinylates mitofusins to prevent re-fusion of dysfunctional mitochondria and labels them for degradation (55). It was expected that cells lacking either mitofusin that display aberrant mitochondrial shape and fragmentation would have increased Parkin recruitment. However that was not the case when analyzing fibroblasts null for either MFN1 or MFN2 (55). In fact, only a fraction (3.33%) of MFN2 null cells with aberrant mitochondria sequestered Parkin for active mitophagy (50). Double MFN null cells showed active recruitment indicative that suppression of more than one fusion factor destines mitochondria for autophagy. In light of these findings, lack of induction of mitophagy in our novel MFN2 mutant is not surprising.

Pathology presented in animal models is hard to translate *in-vitro.* Neuropathies are especially difficult to analyze due to the structural and functional complexity of the nervous system. The lack of any structural anomaly in $MFN2^{\Delta E539}$ mutant cultured primary CF and DRG cells, or functional anomaly in primary CF cells could simply mean that they are not affected by the mutation in any way. Or it could be interpreted as a state of *in-vitro* induced equilibrium. It has been reported that optimal rates of fusion and fission events can sustain mitochondrial functions and integrity regardless of continuous stress (56). Convenient *in-vitro* conditions can easily alleviate levels of stress and allow for

steady state mitochondrial resilience. Testing several stressors might generate a phenotype *in-vitro* but how that might correlate with *in-vivo* conditions will need to be investigated.

References

1 Ishihara, N., Eura, Y. and Mihara, K. (2004) Mitofusin 1 and 2 play distinct roles in mitochondrial fusion reactions via GTPase activity. *J Cell Sci*, **117**, 6535-6546.

2 Cipolat, S., Martins de Brito, O., Dal Zilio, B. and Scorrano, L. (2004) OPA1 requires mitofusin 1 to promote mitochondrial fusion. *Proc Natl Acad Sci U S A*, **101**, 15927-15932.

3 Legros, F., Lombes, A., Frachon, P. and Rojo, M. (2002) Mitochondrial fusion in human cells is efficient, requires the inner membrane potential, and is mediated by mitofusins. *Mol Biol Cell*, **13**, 4343-4354.

4 Chen, H., Detmer, S.A., Ewald, A.J., Griffin, E.E., Fraser, S.E. and Chan, D.C. (2003) Mitofusins Mfn1 and Mfn2 coordinately regulate mitochondrial fusion and are essential for embryonic development. *J Cell Biol*, **160**, 189-200.

5 de Brito, O.M. and Scorrano, L. (2008) Mitofusin 2: a mitochondria-shaping protein with signaling roles beyond fusion. *Antioxid Redox Signal*, **10**, 621-633.

6 Honda, S., Aihara, T., Hontani, M., Okubo, K. and Hirose, S. (2005) Mutational analysis of action of mitochondrial fusion factor mitofusin-2. *J Cell Sci*, **118**, 3153-3161.

7 de Brito, O.M. and Scorrano, L. (2009) Mitofusin-2 regulates mitochondrial and endoplasmic reticulum morphology and tethering: the role of Ras. *Mitochondrion*, **9**, 222-226.

8 Bach, D., Pich, S., Soriano, F.X., Vega, N., Baumgartner, B., Oriola, J., Daugaard, J.R., Lloberas, J., Camps, M., Zierath, J.R., Rabasa-Lhoret, R., Wallberg-Henriksson, H., Laville, M., Palacin, M., Vidal, H., Rivera, F., Brand, M. and Zorzano, A. (2003) Mitofusin-2 determines mitochondrial network architecture and mitochondrial metabolism. A novel regulatory mechanism altered in obesity. *J Biol Chem*, **278**, 17190-17197.

9 Pich, S., Bach, D., Briones, P., Liesa, M., Camps, M., Testar, X., Palacin, M. and Zorzano, A. (2005) The Charcot-Marie-Tooth type 2A gene product, Mfn2, up-regulates fuel oxidation through expression of OXPHOS system. *Hum Mol Genet*, **14**, 1405-1415.

10 Berman, S.B., Pineda, F.J. and Hardwick, J.M. (2008) Mitochondrial fission and fusion dynamics: the long and short of it. *Cell Death Differ*, **15**, 1147-1152.

11 Ziviani, E. and Whitworth, A.J. (2010) How could Parkin-mediated ubiquitination of mitofusin promote mitophagy? *Autophagy*, **6**.

12 Misko, A., Jiang, S., Wegorzewska, I., Milbrandt, J. and Baloh, R.H. (2010) Mitofusin 2 is necessary for transport of axonal mitochondria and interacts with the Miro/Milton complex. *J Neurosci*, **30**, 4232-4240.

13 Neuspiel, M., Zunino, R., Gangaraju, S., Rippstein, P. and McBride, H. (2005) Activated mitofusin 2 signals mitochondrial fusion, interferes with Bax activation, and reduces susceptibility to radical induced depolarization. *J Biol Chem*, **280**, 25060-25070.

14 Brooks, C., Wei, Q., Feng, L., Dong, G., Tao, Y., Mei, L., Xie, Z.J. and Dong, Z. (2007) Bak regulates mitochondrial morphology and pathology during apoptosis by interacting with mitofusins. *Proc Natl Acad Sci U S A*, **104**, 11649-11654.

15 Gonzalez-Polo, R.A., Boya, P., Pauleau, A.L., Jalil, A., Larochette, N., Souquere, S., Eskelinen, E.L., Pierron, G., Saftig, P. and Kroemer, G. (2005) The apoptosis/autophagy paradox: autophagic vacuolization before apoptotic death. *J Cell Sci*, **118**, 3091-3102.

16 Jezek, P. and Plecita-Hlavata, L. (2009) Mitochondrial reticulum network dynamics in relation to oxidative stress, redox regulation, and hypoxia. *Int J Biochem Cell Biol*, **41**, 1790-1804.

17 Petersen, O.H., Sutton, R. and Criddle, D.N. (2006) Failure of calcium microdomain generation and pathological consequences. *Cell Calcium*, **40**, 593-600.

18 Sauvanet, C., Duvezin-Caubet, S., di Rago, J.P. and Rojo, M. (2009) Energetic requirements and bioenergetic modulation of mitochondrial morphology and dynamics. *Semin Cell Dev Biol.*

19 Miller, K.E. and Sheetz, M.P. (2004) Axonal mitochondrial transport and potential are correlated. *J Cell Sci*, **117**, 2791-2804.

20 Matsuda, N., Sato, S., Shiba, K., Okatsu, K., Saisho, K., Gautier, C.A., Sou, Y.S., Saiki, S., Kawajiri, S., Sato, F., Kimura, M., Komatsu, M., Hattori, N. and Tanaka, K. (2010) PINK1 stabilized by mitochondrial depolarization recruits Parkin to damaged mitochondria and activates latent Parkin for mitophagy. *J Cell Biol*, **189**, 211-221.

21 Hajek, P., Chomyn, A. and Attardi, G. (2007) Identification of a novel mitochondrial complex containing mitofusin 2 and stomatin-like protein 2. *J Biol Chem*, **282**, 5670-5681.

22 Lemasters, J.J. (1984) The ATP-to-oxygen stoichiometries of oxidative phosphorylation by rat liver mitochondria. An analysis of ADP-induced oxygen jumps by linear nonequilibrium thermodynamics. *J Biol Chem*, **259**, 13123-13130.

23 Bradford, M.M. (1976) A rapid and sensitive method for the quantitation of microgram quantities of protein utilizing the principle of protein-dye binding. *Anal Biochem*, **72**, 248-254.

24 Elmore, S.P., Nishimura, Y., Qian, T., Herman, B. and Lemasters, J.J. (2004) Discrimination of depolarized from polarized mitochondria by confocal fluorescence resonance energy transfer. *Arch Biochem Biophys*, **422**, 145-152.

25 Laird, N.M. and Ware, J.H. (1982) Random-effects models for longitudinal data. *Biometrics*, **38**, 963-974.

26 Chang, D.T. and Reynolds, I.J. (2006) Mitochondrial trafficking and morphology in healthy and injured neurons. *Prog Neurobiol*, **80**, 241-268.

27 Chen, L.B. (1988) Mitochondrial membrane potential in living cells. *Annu Rev Cell Biol*, **4**, 155-181.

28 Halestrap, A.P., Woodfield, K.Y. and Connern, C.P. (1997) Oxidative stress, thiol reagents, and membrane potential modulate the mitochondrial permeability transition by affecting nucleotide binding to the adenine nucleotide translocase. *J Biol Chem*, **272**, 3346-3354.

29 Bernardi, P., Krauskopf, A., Basso, E., Petronilli, V., Blachly-Dyson, E., Di Lisa, F. and Forte, M.A. (2006) The mitochondrial permeability transition from in vitro artifact to disease target. *FEBS J*, **273**, 2077-2099.

30 Scorrano, L., Ashiya, M., Buttle, K., Weiler, S., Oakes, S.A., Mannella, C.A. and Korsmeyer, S.J. (2002) A distinct pathway remodels mitochondrial cristae and mobilizes cytochrome c during apoptosis. *Dev Cell*, **2**, 55-67.

31 Lemasters, J.J., Theruvath, T.P., Zhong, Z. and Nieminen, A.L. (2009) Mitochondrial calcium and the permeability transition in cell death. *Biochim Biophys Acta*, **1787**, 1395-1401.

32 Zorov, D.B., Juhaszova, M. and Sollott, S.J. (2006) Mitochondrial ROS-induced ROS release: an update and review. *Biochim Biophys Acta*, **1757**, 509-517.

33 Malka, F., Guillery, O., Cifuentes-Diaz, C., Guillou, E., Belenguer, P., Lombes, A. and Rojo, M. (2005) Separate fusion of outer and inner mitochondrial membranes. *EMBO Rep*, **6**, 853-859.

34 Mattenberger, Y., James, D.I. and Martinou, J.C. (2003) Fusion of mitochondria in mammalian cells is dependent on the mitochondrial inner membrane potential and independent of microtubules or actin. *FEBS Lett*, **538**, 53-59.

35 Elmore, S.P., Qian, T., Grissom, S.F. and Lemasters, J.J. (2001) The mitochondrial permeability transition initiates autophagy in rat hepatocytes. *FASEB J*, **15**, 2286-2287.

36 Priault, M., Salin, B., Schaeffer, J., Vallette, F.M., di Rago, J.P. and Martinou, J.C. (2005) Impairing the bioenergetic status and the biogenesis of mitochondria triggers mitophagy in yeast. *Cell Death Differ*, **12**, 1613-1621.

37 Abeliovich, H. (2007) Mitophagy: the life-or-death dichotomy includes yeast. *Autophagy*, **3**, 275-277.

38 Tolkovsky, A.M. (2009) Mitophagy. *Biochim Biophys Acta*, **1793**, 1508-1515.

39 Cartoni, R., Leger, B., Hock, M.B., Praz, M., Crettenand, A., Pich, S., Ziltener, J.L., Luthi, F., Deriaz, O., Zorzano, A., Gobelet, C., Kralli, A. and Russell, A.P. (2005) Mitofusins 1/2 and ERRalpha expression are increased in human skeletal muscle after physical exercise. *J Physiol*, **567**, 349-358.

40 Soriano, F.X., Liesa, M., Bach, D., Chan, D.C., Palacin, M. and Zorzano, A. (2006) Evidence for a mitochondrial regulatory pathway defined by peroxisome proliferator-activated receptor-gamma coactivator-1 alpha, estrogen-related receptor-alpha, and mitofusin 2. *Diabetes*, **55**, 1783-1791.

41 Bach, D., Naon, D., Pich, S., Soriano, F.X., Vega, N., Rieusset, J., Laville, M., Guillet, C., Boirie, Y., Wallberg-Henriksson, H., Manco, M., Calvani, M., Castagneto, M., Palacin, M., Mingrone, G., Zierath, J.R., Vidal, H. and Zorzano, A. (2005) Expression of Mfn2, the Charcot-Marie-Tooth neuropathy type 2A gene, in human skeletal muscle: effects of type 2 diabetes, obesity, weight loss, and the regulatory role of tumor necrosis factor alpha and interleukin-6. *Diabetes*, **54**, 2685-2693.

42 Chen, H., Chomyn, A. and Chan, D.C. (2005) Disruption of fusion results in mitochondrial heterogeneity and dysfunction. *J Biol Chem*, **280**, 26185-26192.

43 Amiott, E.A., Lott, P., Soto, J., Kang, P.B., McCaffery, J.M., DiMauro, S., Abel, E.D., Flanigan, K.M., Lawson, V.H. and Shaw, J.M. (2008) Mitochondrial fusion and function in Charcot-Marie-Tooth type 2A patient fibroblasts with mitofusin 2 mutations. *Exp Neurol*, **211**, 115-127.

44 Baloh, R.H., Schmidt, R.E., Pestronk, A. and Milbrandt, J. (2007) Altered axonal mitochondrial transport in the pathogenesis of Charcot-Marie-Tooth disease from mitofusin 2 mutations. *J Neurosci*, **27**, 422-430.

45 Guillet, V., Gueguen, N., Verny, C., Ferre, M., Homedan, C., Loiseau, D., Procaccio, V., Amati-Bonneau, P., Bonneau, D., Reynier, P. and Chevrollier, A. (2010) Adenine nucleotide translocase is involved in a mitochondrial coupling defect in MFN2-related Charcot-Marie-Tooth type 2A disease. *Neurogenetics*, **11**, 127-133.

46 Loiseau, D., Chevrollier, A., Verny, C., Guillet, V., Gueguen, N., Pou de Crescenzo, M.A., Ferre, M., Malinge, M.C., Guichet, A., Nicolas, G., Amati-Bonneau, P., Malthiery, Y., Bonneau, D. and Reynier, P. (2007) Mitochondrial coupling defect in Charcot-Marie-Tooth type 2A disease. *Ann Neurol*, **61**, 315-323.

47 Jahani-Asl, A., Germain, M. and Slack, R.S. (2010) Mitochondria: joining forces to thwart cell death. *Biochim Biophys Acta*, **1802**, 162-166.

48 Jiang, G.J., Pan, L., Huang, X.Y., Han, M., Wen, J.K. and Sun, F.Z. (2005) Expression of HSG is essential for mouse blastocyst formation. *Biochem Biophys Res Commun*, **335**, 351-355.

49 Detmer, S.A. and Chan, D.C. (2007) Complementation between mouse Mfn1 and Mfn2 protects mitochondrial fusion defects caused by CMT2A disease mutations. *J Cell Biol*, **176**, 405-414.

50 Narendra, D., Tanaka, A., Suen, D.F. and Youle, R.J. (2008) Parkin is recruited selectively to impaired mitochondria and promotes their autophagy. *J Cell Biol*, **183**, 795-803.

51 Poole, A.C., Thomas, R.E., Andrews, L.A., McBride, H.M., Whitworth, A.J. and Pallanck, L.J. (2008) The PINK1/Parkin pathway regulates mitochondrial morphology. *Proc Natl Acad Sci U S A*, **105**, 1638-1643.

52 Deng, H., Dodson, M.W., Huang, H. and Guo, M. (2008) The Parkinson's disease genes pink1 and parkin promote mitochondrial fission and/or inhibit fusion in Drosophila. *Proc Natl Acad Sci U S A*, **105**, 14503-14508.

53 Park, J., Lee, G. and Chung, J. (2009) The PINK1-Parkin pathway is involved in the regulation of mitochondrial remodeling process. *Biochem Biophys Res Commun*, **378**, 518-523.

54 Yang, Y., Ouyang, Y., Yang, L., Beal, M.F., McQuibban, A., Vogel, H. and Lu, B. (2008) Pink1 regulates mitochondrial dynamics through interaction with the fission/fusion machinery. *Proc Natl Acad Sci U S A*, **105**, 7070-7075.

55
requ
Nat

56
of n
350

55 Ziviani, E., Tao, R.N. and Whitworth, A.J. (2010) Drosophila parkin requires PINK1 for mitochondrial translocation and ubiquitinates mitofusin. *Proc Natl Acad Sci U S A*, **107**, 5018-5023.

56 Mouli, P.K., Twig, G. and Shirihai, O.S. (2009) Frequency and selectivity of mitochondrial fusion are key to its quality maintenance function. *Biophys J*, **96**, 3509-3518.

CHAPTER IV

IN-VITRO KNOCK DOWN OF MITOFUSINS IN MUTANT *MFN2* CANINE FIBROBLAST CELLS

Chapter IV

In-vitro Knock down of mitofusins in mutant *MFN2* canine fibroblast cells

ABSTRACT

The most well investigated function of mitofusins is mediating outer mitochondrial membrane fusion. *MFN2* mutations associated with CMT2A2 vary in their impact on mitochondrial fusion. MFN1, a cellular paralogue of MFN2, complements the fusion defects attributed to some CMT2A2 MFN2 mutants. To confirm that the novel $MFN2^{\Delta E539}$ mutation observed in dogs is the underlying cause of the *in-vivo* phenotype, and to determine the fusion ability of this mutant, mitofusin specific knock down experiments in cultured primary dog fibroblasts have been performed. Knock down of *MFN1* expression resulted in hyper fragmented mitochondria of punctate shape and almost uniform diameter in cells derived from affected dogs. Knock down of both mitofusins in normal dog primary fibroblasts generated a similar phenotype to *MFN1* knock down in affected dog fibroblasts. In conclusion, mutant $MFN2^{\Delta E539}$ cannot promote mitochondrial fusion which confirms its dysfunction as the molecular basis of the fetal-onset neuroaxonal dystrophy (FNAD) phenotype observed in dogs.

Introduction

Mitofusins are mitochondrial outer membrane GTPase proteins. MFN1 and 2 share 66.2% sequence homology and control mitochondrial fusion (1). MFNs can form homo- and hetro-dimers with MFNs on adjacent mitochondrial membranes. Mitochondrial fusion is an energy dependent process that requires GTP hydrolysis. While MFNs interact with MFNs on outer mitochondrial membranes, MFN1 also interacts with OPA1 on the inner mitochondrial membrane during fusion (2). OPA1 is another dynamin-related GTPase of the mitochondrial inner membrane and is involved in fusion of the inner membrane. MFN1 has 8-fold the GTPase activity of MFN2 to meet its membrane tethering demands (3). Dimerization of MFNs is proposed to be through the C-terminal heptad repeat region that forms a coiled coil domain (4). Antiparallel coiled-coil domains on two different mitochondria outer membranes would interact and under GTP hydrolysis membranes would fuse. Accumulating data suggest that MFNs have converging and diverging functions (5, 6). MFN1 has higher tethering efficiency than MFN2 which suggest a more specific role in mitochondrial fusion. This is evident in MFN1 knockout fibroblasts showing more severe mitochondrial fragmentation when compared to MFN2 knockout mitochondria (7). MFN2 has been shown to be involved in many functions aside from mitochondrial fusion and is localized also in the cytoplasmic leaflet of ER membranes (8). MFN1 and MFN2 expression ratios vary from tissue to tissue, and MFN2 displays a tissue specific expression pattern more than MFN1 (7, 9-11). MFN1 and MFN2 have

been shown to be upregulated in different tissues at early developmental stages (12, 13). Both MFN knock out mouse models are embryonic lethal, primarily due to different placental defects (7). Conditional knockout mouse models with late gestational onset of deficiency of either MFN also show a distinguishable phenotype (14). MFN1 conditional knockout mice are born alive, fertile, and can survive for a minimum of 1 year. In contrast, about one third of *MFN2* conditional knockout mice die within 1 day of birth, while the rest die by day 17. The MFN2 conditional knockout mice that survive longer than a few days show movement disorders and defects in cerebellar development. This striking difference between conditional knock out phenotypes provides a valuable insight that MFNs have different roles during development and maturation.

Rescuing of mutant MFN2 fusion defects *in-vitro* has been successful when *MFN1* was used (15). Wild type MFN2 fails to rescue MFN2 fusion defective mutants, however, which highlights the importance of MFN1 and the role of MFN heterodimers in mitochondrial dynamics. In light of these observations this chapter analyzes the fusion function of the $MFN2^{\Delta 539}$ mutant in an *MFN1* knock down system. Moreover, knock down of *MFN2* transcription is performed to investigate impact on phenotype. The aim is to ascertain whether mutant MFN2 implements its primary fusion function and whether loss of this function contributes to the disease phenotype observed.

Materials and Methods

Antisense silencing oligomer selection and transfection

Double stranded RNA interference oligomers (dsiRNA) against dog *MFN1* and *MFN2* genes were selected from pre-designed oligo sets (Integrated DNA Technologies, Inc., Coralville, IA). For each gene, three 27-mer dsiRNAs (D1-D3) were tested individually, in pairs and all three together in a 12-well format. All dsiRNA oligomers were checked for similarities with dog gene sequences using the National Center for Biotechnology Information (NCBI) website BLAST engine (http://blast.ncbi.nlm.nih.gov/Blast.cgi). Each oligmer was used at 20nM concentration whether in combination with other oligos or alone. Knock down experiments were all performed in duplicates. A scrambled non-coding oligomer (NC1) was used as a dsiRNA transfection control. TYE is another control oligo that is fluorescently labeled to assay for successful cellular uptake and was used at 10nM where mentioned in results. Successful silencing was analyzed by qRT-PCR according to the protocol detailed in chapter II, and results were analyzed using the standard curve method. Prior to transfections, fibroblasts were seeded at 5 – 10 x 10^4 cells/ml dilution in 12-well culture plates or 35mm glass bottom culture dishes (MatTek corp., Ashland, MA). Wells and dishes were supplemented with full primary fibroblast growth medium consisting of high glucose DMEM, 10% FBS, 1% L-glutamine, and 1% penicillin/streptomycin antibiotic solution (Invitrogen Corp., Carlsbad, CA), and incubated at 37°C with 5% CO_2. At ~50% confluence, cells are incubated in full growth medium without

antibiotics overnight. Lipofectamine 2000 (Invitrogen Corp., Carlsbad, CA) reagent was used for transfection according to manufacturer's optimized protocol for RNAi experiments. Lipofectamine reagent and dsiRNA oligomers are separately diluted in Opti-MEM (Invitrogen Corp., Carlsbad, CA), a reduced serum medium, and incubated at room temperature for 5 minutes. Appropriate volumes are used according to culture dish dimensions and growth capacity. Diluted Lipofectamine and dsiRNA oligomers are then combined to a final concentration of 20nM for each dsiRNA and incubated at room temperature for 20 minutes. Suspensions are gently mixed by pipetting once prior to addition into culture dishes/wells. Cells were incubated at 37°C with 5% CO_2, and medium was changed to full growth medium with antibiotics 24 hours after transfection. On the third day following medium change, cells were prepared for RNA extraction according to protocol detailed in chapter III, or prepared for live cell imaging.

Live cell-imaging

DsiRNA transfected cells cultured in 35mm glass cover slip bottom dishes were incubated with 0.5µM mitotracker green (MTG) (Invitrogen Corp., Carlsbad, CA) for 1 hour in full growth medium at 37°C and 5% CO_2. Cells were washed three times in fresh full medium and mounted in a disc incubator maintained at 37°C. Images were captured with Olympus Fluoview 1500 confocal microscope (Olympus America Inc., Center Valley, PA) using 60X PlanApo objectives at 1.0 or higher digital zoom when magnification was required.

Results

Selection of dsiRNAs against MFNs

Antisense oligomers against *MFNs* were assayed for optimal knockdown of *MFNs* in primary CF cultures. All dsiRNA oligomers contained 27 RNA bases (table 4-1). NC1 control oligomer transfection at 20 and 40nM concentrations showed a slight decrease in expression of either *MFN* when compared to untreated control cells. Higher concentration of NC1 (60nM) caused an increase in *MFN1* expression. Cultured primary fibroblast survival and proliferation were unaffected by dsiRNA transfection and continued to thrive under optimal incubation conditions. Among the three antisense oligomers against *MFN1*, oligo D3 showed the most efficient knockdown of *MFN1* when compared to NC1 (20nM) transfected cells (Figure 4-1 top). As for dsiRNA against *MFN2*, oligos D2 and D3 in combination (20nM each) gave the best *MFN2* knockdown result when compared to NC1 (40nM) transfected cells (Figure 4-1 bottom). The dsiRNA selection experiment was repeated once and confirmed the pilot experiment results. In subsequent experiments *MFN1* oligo D3 duplex (20nM) and *MFN2* oligos D2 and D3 (20nM each) in combination were used in knock down experiments to assay for phenotype *in-vitro.*

Table 4-1. Control and dsiRNA oligomers used in screening knock down of mitofusins *in-vitro*.

DsiRNA name	Duplex sequence
NC1 negative control	S 5'- CGU UAA UCG CGU AUA AUA CGC GUA T -3' A 5'- AUA CGC GUA UUA UAC GCG AUU AAC GAC -3'
TYE 563 DS labeled transfection control	S 5'- TCC UUC CUC UCU UUC UCU CCC UUG UGA -3' A 5'- TCA CAA GGG AGA GAA AGA GAG GAA -3'
***MFN1* Duplex 1 (D1)**	S 5'- GCU AAA CAG AUA CUA GAU ACU GUG A -3' A 5'- UCA CAG UAU CUA GUA UCU GUU UAG CUC -3'
Duplex 2 (D2)	S 5'- GGG AAG AUC AAA UUG AUA GAC UGG A -3' A 5'- UCC AGU CUA UCA AUU UGA UCU UCC CUC -3'
Duplex 3 (D3)	S 5'- AGA AUA UAU GGA AGA CGU ACG CAG A -3' A 5'- UCU GCG UAC GUC UUC CAU AUA UUC UGG -3'
***MFN2* Duplex 1 (D1)**	S 5'- UGA AGA CAC CUA CAG GAA UGC GGA A -3' A 5'- UUC CGC AUU CCU GUA GGU GUC UUC AAG -3'
Duplex 2 (D2)	S 5'- CCC GGU UAC GAC AGA AGA ACA GGT T -3' A 5'- AAC CUG UUC UUC UGU CGU AAC CGG GUC -3'
Duplex 3 (D3)	S 5'- CGA GCA ACG GGA AGA GCA CUG UAA T -3' A 5'- AUU ACA GUG CUC UUC CCG UUG CUC GUC -3'

S = Sense, A = Antisense

Figure 4-1. Screening of dsiRNA *MFN* knockdown efficiencies. Expression level (y-axis) of *MFN1* (**top**) and *MFN2* (**bottom**) in primary dog fibroblast cells after transfection with different dsiRNA duplexes (x-axis).

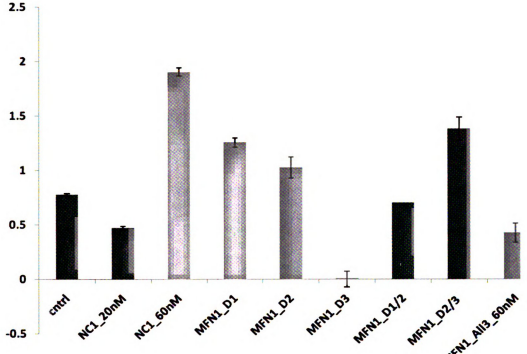
2.5
2
1.5
1
0.5
0
-0.5
cntrl
NC1_20nM
NC1_60nM
MFN1_D1
MFN1_D2
MFN1_D3
MFN1_D1/2
MFN1_D2/3
MFN1_All3_60nM

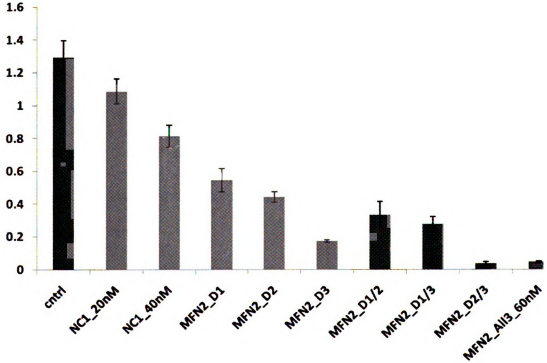
1.6
1.4
1.2
1
0.8
0.6
0.4
0.2
0
cntrl
NC1_20nM
NC1_40nM
MFN2_D1
MFN2_D2
MFN2_D3
MFN2_D1/2
MFN2_D1/3
MFN2_D2/3
MFN2_All3_60nM

Effects of MFN knock down on primary CF mitochondria

MFN1 knock down using dsiRNA in cultured primary fibroblast cells generated a distinct phenotype in homozygous *MFN2*$^{\Delta E539}$ cells when compared to homozygous wild type. Hyper-fragmented mitochondria were abundant throughout the cell forming punctate spheres of almost identical diameters (figure 4-2). Wild type *MFN2* cells transfected with *MFN1* dsiRNA did not show any altered phenotype which verifies that the *MFN1* knock down phenotype generated in affected pup fibroblasts is due to the *MFN2*$^{\Delta E539}$ mutation.

MFN2$^{\Delta E539}$ shows only trace expression in fibroblasts compared to normal fibroblast MFN2 expression as realized in chapter II. Therefore, it was hypothesized that knockdown of *MFN2* and *MFN1* in normal fibroblasts should result in a similar phenotype to *MFN1* knock down in homozygous *MFN2*$^{\Delta E539}$ fibroblasts. Indeed, normal fibroblasts treated with dsiRNAs against *MFN1* and *MFN2* showed an abundance of hyper-fragmented mitochondria (Figure 4-3). The conclusion from these results is that the level of MFN2$^{\Delta E539}$ expression remaining in mutant fibroblasts cannot complement the fusion defect caused by *MFN1* knock down.

To confirm the association of observed phenotype with dsiRNA uptake a fluorescently labeled duplex was used in knock down experiments. Knock down of MFN1, and MFNs in combination with 10nM TYE (ds red tagged duplex)

generated similar phenotypes as the above mentioned experiments. Cells transfected with *MFN1* dsiRNA showed hyper fragmented mitochondria in affected fibroblast cells. Most of normal fibroblast cells showed TYE563 signal without any apparent altered mitochondrial morphology. Some affected cells did show TYE563 signal without hyper fragmented mitochondria phenotype. However, all cells displaying mitochondrial hyper fragmentation were positive for TYE563 duplex uptake. Cells negative for TYE563 did not have an altered mitochondrial phenotype in affected fibroblast cells. Knock down of both MFN in presence of TYE563 resulted in hyper fragmented mitochondria in both genotypes assayed, with the altered mitochondrial morphology always associating with TYE563 uptake. In addition, in both genotypes there were some cells that were positive for TY563 uptake without any change in mitochondrial morphology.

Figure 4-2. *MFN1* knock down in cultured primary fibroblast cells of normal and affected pups. **A.** Normal fibroblasts mitochondrial morphology is maintained when untreated with an oligo and when transfected with NC1 mock oligo or with *MFN1*_D3 duplex. **B.** Affected fibroblasts mitochondrial morphology is maintained when transfected with NC1, however, when transfected with *MFN1*_D3 duplex hyper fragmentation of mitochondria is visible. Last frame is a magnified image of hyper fragmented mitochondria induced by *MFN1* knockdown.

A.
Untreated
NC1
MFN1_D3 duplex

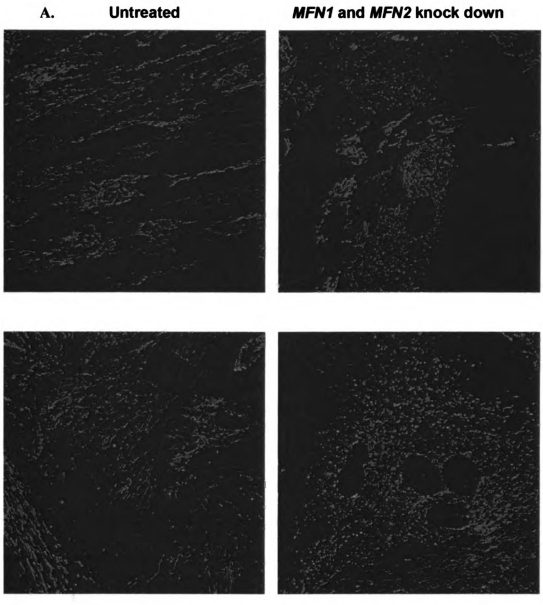

Figure 4-3. Cultured fibroblasts were transfected with a combination of *MFN1*(D3) and *MFN2* (D2/3) expression silencing duplexes. **A.** Normal fibroblasts display hyper fragmented mitochondria upon knock down of both mitofusins. **B.** Affected fibroblasts displayed the same hyper fragmented mitochondria when both mitofusins are knocked down.

Discussion

MFN1 is a cellular paralogue to MFN2 that has been shown to complement the MFN2 fusion function. We have specifically knocked down *MFN1* expression in cultured primary fibroblasts with homozygous $MFN2^{\Delta E539}$ mutation. Knock down of *MFN1* caused mitochondrial hyper fragmentation and loss of any tubular mitochondria of any length. This phenotype is attributed to complete loss of fusion abilities. Such a phenotype has been reported in *MFN1* knock out mouse embryonic fibroblast cells (7). MFN1 fusion promoting properties are superior to those of MFN2 (3). Although wild type *MFN2* over expression does rescue *MFN1* null phenotype (7), our $MFN2^{\Delta E539}$ mutant could not in an *MFN1* knock down model. Whether it is due to loss of fusion abilities or due to decreased MFN2 expression remains to be resolved. The result seen in *MFN1* knocked down fibroblast cells might be confounded in tissues with increased dependence on MFN2 than MFN1. We have shown in addition to other reports that nervous system tissues, muscle, and heart have increased *MFN2* expression when compared to *MFN1* (7, 9-11). Such tissues when affected by a mutant *MFN2* might not have sufficient MFN1 expression to maintain proper mitochondrial fusion.

Double knock down of mitofusins in normal and affected cultured primary fibroblast cells support the profound $MFN2^{\Delta E539}$ decrease in protein expression. Knock down of wild type *MFN2* and *MFN1* resulted in a similar phenotype to

MFN1 knock down in MFN2$^{\Delta E539}$ affected fibroblast cells. The fact that different cells require different mitochondrial dynamics suggests that MFN-mediated mitochondrial morphology and distribution is an influential event in cellular homeostasis (16). Moreover, the various functions of MFN2 aside from fusion might be the cause of the FNAD phenotype seen in MFN2$^{\Delta E539}$ mutants because different cells have different energy demands and require different mitochondrial responses to cellular stimuli (17). MFN2 functions of interest that could have a major impact on nervous system derived tissues include induction of the mitophagy cascade and axonal transport. Either or both functions might be compromised in our MFN2$^{\Delta E539}$ beyond rescue by MFN1 (18).

References

1 Santel, A. and Fuller, M.T. (2001) Control of mitochondrial morphology by a human mitofusin. *J Cell Sci*, **114**, 867-874.

2 Cipolat, S., Martins de Brito, O., Dal Zilio, B. and Scorrano, L. (2004) OPA1 requires mitofusin 1 to promote mitochondrial fusion. *Proc Natl Acad Sci U S A*, **101**, 15927-15932.

3 Ishihara, N., Eura, Y. and Mihara, K. (2004) Mitofusin 1 and 2 play distinct roles in mitochondrial fusion reactions via GTPase activity. *J Cell Sci*, **117**, 6535-6546.

4 Koshiba, T., Detmer, S.A., Kaiser, J.T., Chen, H., McCaffery, J.M. and Chan, D.C. (2004) Structural basis of mitochondrial tethering by mitofusin complexes. *Science*, **305**, 858-862.

5 Eura, Y., Ishihara, N., Yokota, S. and Mihara, K. (2003) Two mitofusin proteins, mammalian homologues of FZO, with distinct functions are both required for mitochondrial fusion. *J Biochem*, **134**, 333-344.

6 Zorzano, A. and Pich, S. (2006) What is the biological significance of the two mitofusin proteins present in the outer mitochondrial membrane of mammalian cells? *IUBMB Life*, **58**, 441-443.

7 Chen, H., Detmer, S.A., Ewald, A.J., Griffin, E.E., Fraser, S.E. and Chan, D.C. (2003) Mitofusins Mfn1 and Mfn2 coordinately regulate mitochondrial fusion and are essential for embryonic development. *J Cell Biol*, **160**, 189-200.

8 de Brito, O.M. and Scorrano, L. (2008) Mitofusin 2: a mitochondria-shaping protein with signaling roles beyond fusion. *Antioxid Redox Signal*, **10**, 621-633.

9 Bach, D., Pich, S., Soriano, F.X., Vega, N., Baumgartner, B., Oriola, J., Daugaard, J.R., Lloberas, J., Camps, M., Zierath, J.R., Rabasa-Lhoret, R., Wallberg-Henriksson, H., Laville, M., Palacin, M., Vidal, H., Rivera, F., Brand, M. and Zorzano, A. (2003) Mitofusin-2 determines mitochondrial network architecture and mitochondrial metabolism. A novel regulatory mechanism altered in obesity. *J Biol Chem*, **278**, 17190-17197.

10 Rojo, M., Legros, F., Chateau, D. and Lombes, A. (2002) Membrane topology and mitochondrial targeting of mitofusins, ubiquitous mammalian homologs of the transmembrane GTPase Fzo. *J Cell Sci*, **115**, 1663-1674.

11 Santel, A., Frank, S., Gaume, B., Herrler, M., Youle, R.J. and Fuller, M.T. (2003) Mitofusin-1 protein is a generally expressed mediator of mitochondrial fusion in mammalian cells. *J Cell Sci*, **116**, 2763-2774.

12 Jiang, G.J., Pan, L., Huang, X.Y., Han, M., Wen, J.K. and Sun, F.Z. (2005) Expression of HSG is essential for mouse blastocyst formation. *Biochem Biophys Res Commun*, **335**, 351-355.

13 Chang, D.T. and Reynolds, I.J. (2006) Differences in mitochondrial movement and morphology in young and mature primary cortical neurons in culture. *Neuroscience*, **141**, 727-736.

14 Chen, H., McCaffery, J.M. and Chan, D.C. (2007) Mitochondrial fusion protects against neurodegeneration in the cerebellum. *Cell*, **130**, 548-562.

15 Detmer, S.A. and Chan, D.C. (2007) Complementation between mouse Mfn1 and Mfn2 protects mitochondrial fusion defects caused by CMT2A disease mutations. *J Cell Biol*, **176**, 405-414.

16 Kuznetsov, A.V., Hermann, M., Saks, V., Hengster, P. and Margreiter, R. (2009) The cell-type specificity of mitochondrial dynamics. *Int J Biochem Cell Biol*, **41**, 1928-1939.

17 Kuznetsov, A.V. and Margreiter, R. (2009) Heterogeneity of mitochondria and mitochondrial function within cells as another level of mitochondrial complexity. *Int J Mol Sci*, **10**, 1911-1929.

18 Misko, A., Jiang, S., Wegorzewska, I., Milbrandt, J. and Baloh, R.H. (2010) Mitofusin 2 is necessary for transport of axonal mitochondria and interacts with the Miro/Milton complex. *J Neurosci*, **30**, 4232-4240.

CHAPTER V

CONCLUSIONS AND FUTURE DIRECTIONS

Chapter V

Conclusions and future directions

In this project I analyzed a novel mutation in the MFN2 gene on the molecular and cellular levels. The phenotype generated by this mutation was presented as a dog model of fetal onset neuroaxonal dystrophy. The novel MFN2 mutation is located within a highly conserved region of unknown function. I have shown that transcription of the mutant allele is active in both carriers and homozygous mutants. However, neuroaxonal dystrophy phenotype is only present in homozygous mutants, while carriers are normal. Rigorous anatomical and histological analysis of different isolated tissues identified pathology confined to the nervous system. The cerebellum, brainstem, spinal cord, and peripheral nerves show extensive degeneration and hypoplasia. Only a speculation can be made at this point to whether the degeneration is caused by death of properly formed tissues, or it is due to lack of developmental progress. A future experiment to target this issue is to collect tissues at different time points during development. Histological and molecular analysis of affected tissues would reveal the start of tissue damage and the molecular change in expression that dictates such adverse effects. It is hypothesized that ratio of MFN1 to MFN2 is altered in nervous system tissues during development and maturity, which might explain mutant MFN2 association with neuropathies.

Protein expression of mutant MFN2 was nearly undetectable in all assayed affected pup tissues except for cultured DRG cells. Remaining questions to be addressed is when and how is mutant $MFN2^{\Delta E539}$ protein expression being lost. Direct evidence of active transcription has been shown, but whether it is accurately translated has not been assayed. In addition, loss of protein expression can be attributed to dysfunctional protein post-translational modifications that could trigger specific degradation. Post translational modifications include addition of functional groups, linkage to other accessory peptides, amino acid conversions, and structure conformational changes. Moreover, targeting of mutant MFN2 to mitochondrial and ER membranes could be lost which would lead to specific accumulation of mutant MFN2. Mutant MFN2 aggregates might trigger proteolytic networks in the cell and lead to loss of protein expression. To address these possibilities pulse chase experiments would be performed to monitor transcript translation, protein modification and folding, protein targeting, and ultimately protein turnover in a cell culture system. Another future experiment would take advantage of detectable mutant $MFN2^{\Delta E539}$ in DRG cells to analyze its protein interaction network. Co-immunoprecipitation of $MFN2^{\Delta E539}$ from DRG cells lysate followed by mass spectroscopy would detect any alterations in partner proteins when compared to wild type MFN2.

Results indicate no apparent abnormalities spurred on by mutant $MFN2^{\Delta E539}$ when assaying for mitochondrial morphology, distribution, respiration, and recycling. Several of those assays utilized in-*vitro* conditions favoring growth and maintenance of homeostasis. A future experiment would involve assaying for a differential response to cellular stress, a state that might represent the developmental stages *in-vivo*. Such cellular stress can be through serum starvation, glucose starvation, oxidative stress, or calcium overload. It would be interesting to assay cellular responses to these stimuli in cells relevant to disease pathology, such as cultured primary DRG cells. Screening for a differential phenotype would involve the methods employed here and other methods relevant to neuronal cells, such as time-lapse imaging to assay for axonal transport, and axonal mitochondria density.

MFN1 knockdown experiment showed that residual $MFN2^{\Delta E539}$ protein in primary fibroblasts cannot maintain mitochondrial fusion. Therefore, $MFN2^{\Delta E539}$ either lacks mitochondrial fusion ability or its level of expression is insufficient to maintain fusion, and is rendered dysfunctional in association with FNAD phenotype. An interesting future experiment would be knocking down of MFN1 in cultured DRG cells from affected pups. MFN1 and MFN2 both were shown to be involved in mitochondrial axonal transport. Whether $MFN2^{\Delta E539}$ expressed in DRG is capable of maintaining axonal transport, when MFN1 is knocked down remains to be investigated. Moreover, mitochondrial fusion in neurons is more

dynamic and heavily regulated. Since cultured DRG cells maintain some $MFN2^{\Delta E539}$ expression it would be important to assay its fusion abilities under MFN1 is knock down conditions. It is also of value to look at MFN1 protein levels in nervous system tissues to delineate tissue specific dependence. Defined nervous system structures and specialized neuronal cells have been shown to have different patterns of mitofusin expression. This would reflect on mitochondrial fusion and other overlapping functions between MFN1 and MFN2. It is important to characterize MFN levels in nervous system cellular structures in the FNAD pup, specifically those of critical impact on nervous system development and organ innervations.

These conclusions taken together highlight the importance of the conserved region in which the mutation lies. Furthermore it emphasizes the need to fully analyze MFN2 structural and functional attributes in different cells, at different stages of development and maturation. On my part I have pinned $MFN2^{\Delta E539}$ as the molecular basis of the pathogenesis seen in FNAD. However, the mechanism of pathogenesis remains to be resolved by future experiments.

APPENDIX A

Inherited neuroaxonal dystrophy in dogs causing lethal, fetal-onset motor system dysfunction and cerebellar hypoplasia

John C. Fyfe[1, 2 *], Raba' A. Al-Tamimi[1], Rudy J. Castellani[3], Diana Rosenstein[2#], Daniel Goldowitz[4], Paula S. Henthorn[5]

[1] Laboratory of Comparative Medical Genetics, Department of Microbiology & Molecular Genetics, Michigan State University, East Lansing, MI 48824 USA

[2] Department of Small Animal Clinical Sciences, College of Veterinary Medicine, Michigan State University, East Lansing, MI 48824 USA

[3] Department of Pathology, School of Medicine, University of Maryland, Baltimore, MD 21201 USA

[4] Department of Medical Genetics, University of British Columbia, Vancouver, BC, V5Z 4H4 Canada

[5] Section of Medical Genetics, School of Veterinary Medicine, University of Pennsylvania, Philadelphia, PA 19104 USA

Running Title: Fetal-onset neuroaxonal dystrophy in dogs

Associate Editor: John L. R. Rubenstein, University of California at San Francisco

Key words: brainstem, spinal cord, peripheral neuropathy, spheroid, fetal akinesia

* **Corresponding author** and to whom reprint requests may be addressed:

John C. Fyfe, DVM, PhD
Laboratory of Comparative Medical Genetics
2209 Biomedical Physical Sciences
Michigan State University
East Lansing, MI 48824
Voice: 517-884-5348
Fax: 517-353-8957
Email: fyfe@cvm.msu.edu

Grant Sponsors: National Institute of Neurologic Disease and Stroke (NS41989), the National Institute of Research Resources (RR02512), and the Purebred Dog Endowment Fund of the College of Veterinary Medicine, Michigan State University.

ABSTRACT

Neuroaxonal dystrophy in brainstem, spinal cord tracts, and spinal nerves accompanied by cerebellar hypoplasia was observed in a colony of laboratory dogs. Fetal akinesia was documented by ultrasonographic examination. At birth, affected puppies exhibited stereotypical positioning of limbs, scoliosis, arthrogryposis, pulmonary hypoplasia, and respiratory failure. Regional hypoplasia in the central nervous system was apparent grossly, most strikingly as underdeveloped cerebellum and spinal cord. Histopathologic abnormalities included swollen axons and spheroids in brainstem and spinal cord tracts; reduced cerebellar foliation, patchy loss of Purkinje cells, multifocal thinning of the external granular cell layer, and loss of neurons in the deep cerebellar nuclei; spheroids and loss of myelinated axons in spinal roots and peripheral nerves; increased myocyte apoptosis in skeletal muscle; and fibrofatty connective tissue proliferation around joints. Breeding studies demonstrated that the canine disorder is a fully penetrant, simple autosomal recessive trait. The disorder demonstrated a type and distribution of lesions homologous to that of human infantile neuroaxonal dystrophy (INAD), most commonly caused by mutations of *PLA2G6*, but alleles of informative markers flanking the canine *PLA2G6* locus did not associate with the canine disorder. Thus, fetal-onset neuroaxonal dystrophy in dogs, a species with well-developed genome mapping resources, provides a unique opportunity for additional disease gene discovery and understanding of this pathology.

ABBREVIATIONS

FADS, fetal akinesia deformation sequence; **FNAD**, fetal-onset neuroaxonal dystrophy; **INAD**, infantile neuroaxonal dystrophy; **NAD**, neuroaxonal dystrophy; **PCH 1**, pontocerebellar hypoplasia type 1; ***PLA2G6***, phospholipase A2 group VI gene.

INTRODUCTION

Neuroaxonal dystrophy (NAD) is a nonspecific, but histologically distinct, neurodegenerative pathology of the central and/or peripheral nervous system. NAD is characterized by localized swellings (spheroids) and atrophy of axons (Summers et al., 1995). NAD can occur in chronic vitamin E deficiency, insulin deficient diabetes, aging, and exposure to certain toxins (Schmidt et al., 1991, 1997). Autosomal recessive forms of NAD have been described in humans and other species, but even within a species, there is variation in age of onset, clinical manifestations, lesion distribution, and electron microscopic description of spheroids (Sisó et al., 2006). Mechanisms by which these lesions develop are unknown.

In human infantile NAD (INAD, OMIM #256600; a.k.a. Seitelberger disease) the onset of clinical signs typically occurs between 6 and 18 months of age, first showing cognitive and motor regression, hypotonia, and progressive paraplegia (Carrilho et al., 2008; Kurian et al., 2008). A few INAD patients, however, have signs of disease at birth including fetal immobility (Janota 1979; Jennekens et al., 1984; Tachibana et al., 1986; Hunter et al., 1987; Chow and Padfield 2008). Severe cerebellar atrophy and/or Purkinje cell loss is an additional pathological hallmark of human INAD and is observed in some animal NADs as well (Woodard et al., 1974; Cork et al., 1983; Carmichael et al., 1993; Bouley et al., 2006; Nibe et al., 2007). Mutations in the gene encoding phospholipase A2, group VI (*PLA2G6*) are found in ~ 80 % of human INAD patients (Khateeb et al., 2006; Gregory et al., 2008; Wu et al.,

2009). Engineered abrogations of *Pla2g6* (a.k.a. *iPLA$_2\beta$*) expression in mice have produced orthologous models of human INAD, but they produce late-onset disease (Shinzawa et al., 2008; Malik et al., 2008). Identification of the INAD disease gene has not yet revealed a mechanism by which axons become dystrophic because the physiologic role of PLA2G6 in the nervous system is poorly understood. At one time, deficiency of a lysosomal hydrolase, α-N-acetylgalactosaminidase (α-NAGA; Schindler disease type I), was implicated as a cause of INAD, but this conclusion has since been contradicted (Bakker et al., 2001).

Here we report a neurodevelopmental disorder in dogs characterized by fetal-onset NAD throughout the brainstem, spinal cord and peripheral nerves. The canine disorder manifests as fetal akinesia late in gestation and respiratory failure at birth, both due to lower motor neuron dysfunction, and is accompanied by cerebellar hypoplasia. The phenotype is a fully penetrant, simple autosomal recessive trait. Alleles of informative markers flanking the canine *PLA2G6* locus are not associated with alleles of the disease locus in this family. Characterization of the canine disorder sets the stage for linkage mapping to determine the underlying genetic lesion and to gain further insight into the pathogenesis of neuroaxonal dystrophy.

MATERIALS AND METHODS

Animals: Dogs used in this study were members of a breeding colony maintained initially at University of Pennsylvania and later at Michigan State University. All protocols for routine housing and care, breeding and whelping, cesarean sections, perfusion, and euthanasia were approved by the respective Institutional Animal Care and Use Committees of the two institutions and were designed according to the principles described in the NIH Guide for the Care and Use of Laboratory Animals. Euthanasia was performed by parenteral administration of an overdose of sodium pentobarbital.

Ultrasonography: Abdominal ultrasonographic examination was performed on trained dogs in dorsal recumbency without sedation using an Aloka 500 ultrasound system (ALOKA, Inc., Wallingford, CT). Pregnant dogs were examined between 49 and 60 days of gestation. Day of gestation was calculated in each case by monitoring changes in vaginal epithelial cytology and serum progesterone concentration to estimate the day of ovulation, a procedure that allowed prediction of the time of full-term whelping to within ± 12 hours.

Antibody characterization: Antibodies and dilutions used in this study are listed in Table 1. Anti-glial fibrillary acid protein (GFAP), anti-neuron specific enolase (NSE), and anti-calbindin antibodies were used as cell-type markers for astrocytes, neurons, and Purkinje cells, respectively. Each demonstrated cells of characteristic morphology and distribution as described previously in

dog CNS tissues (Aoki et al., 1992; Sisó et al., 2003; Hwang et al., 2008; Sago et al., 2008). On western blots of newborn dog brainstem homogenate, these antibodies recognized single bands of 52, 48, and 28 kDa, respectively, as previously reported in other species (Marangos et al., 1975; Toma et al., 2001; Zhao et al., 2008).

Activated caspase-3 antibody was raised against a synthetic KLH-coupled peptide (CRGTELDCGIETD) adjacent to Asp175 in human caspase-3, and is a well-defined marker of apoptosis in mammalian tissues (Ribera et al., 2002). The immunizing peptide is identical in dog caspase 3, as well as in most other mammals. The antibody recognizes 17-19 kDA fragments, but not the full-length caspase 3 on western blots of human and mouse cell line homogenates (manufacture's fact sheet). On western blots of D-17 canine osteosarcoma cells (ATCC ® cat no. CCL-183™) treated with doxorubicin, but not of untreated cells, we detected a 17 kDa band. For antigen retrieval de-paraffinized slides were incubated for 30 min at 99 C in 10 mM sodium citrate buffer, pH 6.0. Staining was abolished by preincubating the primary antibody with cleaved caspase-3 (Asp175) blocking peptide (Cell Signaling Technology, Beverly, MA; cat. no.1050), or by substituting the primary antibody with normal goat serum. The SMI-312 antibody used here is a pan neurofilament (NF) marker that detects phosphorylated NF (Sternberger and Sternberger, 1983) in axons of fetal and newborn humans (Ulfig et al., 1998; Haynes et al., 2005). SMI-312 is a cocktail of monoclonal antibodies directed against extensively

phosphorylated epitopes on axonal NF-M and NF-H. SMI-312 stained axons throughout the CNS in the pups of this study in a pattern similar to NSE staining. In particular, however, SMI-312 did not stain neuronal perikarya, as has been described, in normal pup tissue, congruent with its specificity for phosphorylated NF. On western blots of detergent extracts of newborn dog brainstem, SMI-312 detected 200 and 160 kDA bands. None of the antibodies used exhibited residual staining when the primary antibody was omitted or replaced with irrelevant serum in the procedure. Because expression of various proteins and tissue structures develop rapidly in fetal and newborn pup CNS and skeletal muscle, sections from affected pups were assessed in comparison to sections of tissue from normal littermates, rather than by reliance on usual patterns of staining observed in older dogs.

Histopathology: For light microscopy, affected newborn and littermate control tissues were fixed by immersion in 100 mM sodium phosphate-buffered 1.25 M (4%) formaldehyde, pH 7.0 (NBF), paraffin or plastic (glycol methacrylate) embedded, and sectioned. In some animals, rapid fixation of the CNS was accomplished by NBF perfusion via the proximal aorta. Sections were obtained from all organs and all levels of the neuraxis. The entire brainstem and cerebellum of some dogs were examined in serial frontal and sagittal sections at 100 μm intervals. Routine stains included hematoxylin-eosin (H&E), luxol-fast blue, Klüver-Barrera, periodic acid-Schiff (PAS), Gomori's iron stain (Prussian blue), Holme's silver stain, Masson's trichrome, and cresyl echt violet in paraffin

sections, and toluidine blue in plastic sections. For electron microscopy, tissues were fixed by overnight immersion in100 mM sodium phosphate-buffered (pH 7.2) 400 mM (4 %) gluteraldehyde, postfixed in 100 mM sodium phosphate-buffered (pH 7.2) 40 mM (1 %) osmium tetroxide, dehydrated in graded alcohols, and embedded in Poly/Bed 812-Araldite resin. Sections were cut, stained sequentially in uranyl acetate and citrate-buffered lead nitrate, and examined on a Philips 301 transmission electron microscope. Sections comparing normal and affected pup tissues were stained identically, and tissue comparisons between dogs were reproduced at identical total magnifications. Photomicrographs were taken with a Kodak DCS Pro 14n digital camera. Uneven illumination was corrected by background division in Image Arithmetic (http://www.t3i.nl/myblog/?page_id=7) and contrast and brightness were adjusted globally in Adobe® Photoshop® CS2. Multiple-image figures were assembled in the Microsoft® PowerPoint® 2000 SP-3 program and cropped, sized, and saved as TIFF files in Adobe® Photoshop® 6.0

Statistics: Significance of quantitative data comparing organs from affected pups and normal littermates was determined using Student's t-test. Significance of data from prospective breeding experiments was determined using the χ^2 (Chi squared) test for goodness-of-fit. Where numbers or diameters of axons in a nerve are reported, they were determined on only one side of an affected or normal pup, rather than on both sides of the same individual.

Analysis of molecular markers: The canine *PLA2G6* locus was located on dog chromosome 10 (chr10:29,581,962-29,631,860) by BLAT search (Kent, 2002) of the May 2005 assembly (http://genome.ucsc.edu/) using the human cDNA (NM_003560.2) as query sequence. Polymorphic markers flanking the locus and separated by 15.34 Mb were analyzed in a subset of dogs in the pedigree. Primers for FH2293 were 5'-GAATGCCCTTCACCTTGAAA-3' and 5'-AGGAAAAGGAGAGATGATGCC-3'. Primers for C10.781 were 5'-ACCTCCAAGATGGCTCTTGA-3' and 5'-ACGTCGAGCTCCTGGCAT-3'. PCR conditions were those recommended by Richman et al (2001) and Mellersh et al (1997). Fluorescent labels on the forward primers allowed electrophoresis and allele calling from standard capillary electrophoresis, performed by a core facility.

RESULTS

Clinical findings: In a dog-breeding colony maintained for investigation of inherited disorders (He et al., 2003), certain matings produced a minority of offspring exhibiting characteristic malposition of limbs, scoliosis (fig.A.1, panels A and B, respectively), and death at birth due to inspiratory failure. Axial and appendicular joints were fixed (arthrogryposis) at birth preventing voluntary movement, though some affected pups retained slight lateral movement of the tail and gaping motions of the mandible. Jaw motion was interpreted to be part of an inspiratory reflex, but there was no coordinated excursion of the thoracic wall or diaphragm, and the lungs did not inflate spontaneously. When positive pressure ventilation (PPV) was applied, however, the thorax expanded, the diaphragm was displaced abdominally, and the lungs inflated. Tissues of the mouth and paws that were cyanotic before PPV turned pink and stayed so as long as PPV was maintained, indicating that pulmonary gas exchange and peripheral blood circulation were intact. The heart contracted, and blood circulated for many minutes after birth in affected pups, even when PPV was not applied, but no affected pup ever developed spontaneous respiration.

Affected puppies were detectable by abdominal ultrasonographic and/or radiographic examination of the pregnant dam several days before birth, (canine gestation is 63 days from the day of ovulation). During ultrasonographic examinations performed variously 10-2 days prior to birth, normal fetuses responded to proximity of the ultrasound probe with increased movements of limbs and trunk, but some littermates did not respond with

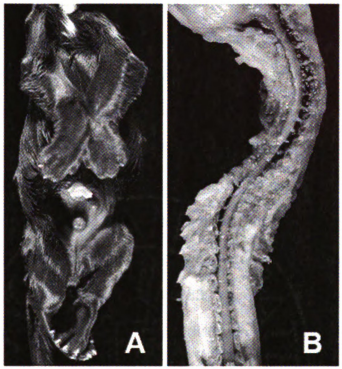

Figure A.1. Abnormal morphology at birth. Panel **A** shows the ventral view of a puppy affected with fetal-onset neuroaxonal dystrophy (FNAD) demonstrating the invariant and locked position of limbs. Panel **B** shows a dorsal view of the partially dissected cervical to lower lumbar segments of spinal cord lying in the scoliotic vertebral column. The pup's head is to the top of both panels.

movement. Cardiac morphology and contraction rate appeared normal in the immobile fetuses, as did all other abdominal and thoracic organs. Scoliosis in several affected fetuses was observed by abdominal radiograph of the dams at 56 days of gestation, suggesting that fixation of axial joints had already occurred in this individual. Two fetuses were immobile when examined by ultrasound at 57 days of gestation, and their joints were fixed when obtained by cesarean section at 60 days of gestation. In contrast, at 53 days of gestation, the joints of 5 affected pups obtained by cesarean section retained passive mobility (clinical status determined by histopathologic examination retrospectively). Pterygia, indicative of joint immobility from an early stage of development (Davis and Kalousek 1988; Cox et al., 2003), were never observed in affected pups. In this disorder, therefore, immobility and subsequent fixation of joints likely occurs late in gestation.

Postmortem findings: At birth, all affected pups exhibited multiple contractures of axial and appendicular joints. Examination did not reveal airway blockage. Severing the phrenic nerve caused immediate spasmodic contraction of the ipsilateral diaphragm in normal littermates sacrificed at birth, but not in affected pups, suggesting that failure to inspire was due to lack of innervation or intrinsic dysfunction of respiratory muscles. Despite a wide range in each group, the mean birth weight of affected puppies (193 ± 36 g, mean ± SD, range 124-288 g; n = 26) was less ($p<2x10^{-5}$) than that of normal littermates (237 ± 38 g, range 149-316 g; n = 38). Total lung wet weight was significantly

less in the affected pups (3.8 ± 0.9 g vs. 8.6 ± 1.7 g; $p<8x10^{-11}$) even when normalized to body weight (0.021 ± 0.005 vs. 0.036 ± 0.007; $p<7x10^{-9}$), indicative of pulmonary hypoplasia. The difference in lung weight was far greater than could be attributed to increased blood content likely present in the normal pups' lungs.

Gross morphologic abnormalities of other internal organs were confined to the CNS. Cerebral hemispheres of affected pups showed mild generalized volume reduction compared to normal littermates euthanized at birth, but otherwise demonstrated no malformation or encephaloclastic lesions. Serial coronal sections of the cerebral hemispheres showed well-developed gray and white matter structures in both affected and control pups, and the extent of myelination was similar. The weight of the formalin-fixed cerebrum with diencephalon of affected pups was ~ 75% of that of normal littermates sacrificed at birth (5.2 ± 0.74 g, n = 19 vs. 6.8 ± 1.1 g, n = 10; $p<0.002$). The brainstem of affected animals was similarly reduced in weight (~75%) but also without focal lesions or gross evidence of malformation. Strikingly, however, the cerebellum in affected dogs was markedly reduced in size compared to those in control animals (fig.A.2, panels A and C), with a rudimentary folial pattern in both the cerebellar vermis and lateral cerebellar hemispheres. Weight of the formalin-fixed cerebellum of affected pups was less than 50% of littermate controls (0.15 ± 0.02 g, n = 19 vs. 0.32 ± 0.06 g, n = 10; $p<10^{-5}$). Throughout its length, the cross-sectional area of spinal cord in affected pups was ~ 35% that of normal controls, and the reduction in area affected white

and grey matter nearly equally (fig.A.2, panels B and D). Dorsal and ventral spinal roots and peripheral nerves of affected pups were reduced in diameter and more translucent than those of control pups.

Histological abnormalities of the CNS were apparent by light microscopy of routinely stained sections, but lesions were confined to specific nerve tracts and nuclei. Specifically, no microscopic differences between affected pups and controls were detected in the cerebral hemispheres. The neuronal layers were formed similarly in both groups, including the placement of large pyramidal neurons. In frontal lobe coronal sections, the frontal neocortex, cingulated gyrus, corona radiata, caudate, and putamen showed intact neuronal populations. More posteriorly, the cerebral neocortex, hypothalamus, optic nerves, mamillothalamic tract, crus of fornix, hippocampus, parahippocampal gyrus, habenular nucleus, pituitary, subthalamic nucleus, and zona incerta were anatomically intact and devoid of pathological lesions in affected and control pups. Active myelination ("myelination gliosis") was present within the white matter, and neither qualitative nor quantitative differences in glial acidic fibrillary protein (GFAP) immunoreactivity were detected in the cerebral hemispheres of affected pups and controls.

In contrast to the above, there was extensive pathology in the cerebellum, brainstem, spinal cord and peripheral nerves. Brainstem sections in affected animals were remarkable for widespread neurodegeneration and the presence of swollen axons/spheroids (neuroaxonal dystrophy) in nuclei and tracts of the extrapyramidal components of the motor system (fig.A.3). In

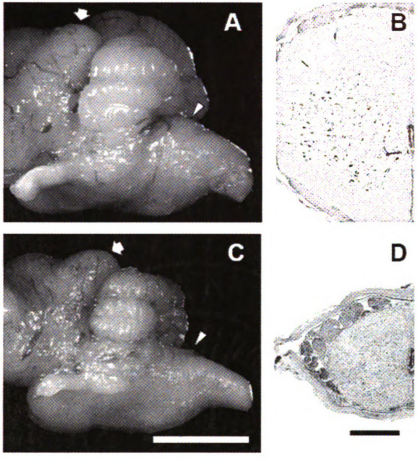

Figure A.2. Cerebellar and spinal cord hypoplasia. Panels **A** and **C** show the left lateral view of cerebellum and brainstem of a newborn normal pup and an affected littermate, respectively. In each panel the fat arrow indicates the caudal colliculus, and the arrowhead indicates the obex (bar in panel **C** = 5 mm, and panels **A** and **C** are presented at the same total magnification). Panels **B** and **D** show cross-sections of spinal cord cervical segment 6 of a newborn normal pup and an affected littermate, respectively (bar in panel **D** = 500 μm, and panels **B** and **D** are presented at the same total magnification). There was a similar degree of hypoplasia throughout the length of affected pup spinal cord.

longitudinal section, axonal swellings observed in the CNS were 5-12 μm in diameter, tapered at both ends, and 20-120 μm long. They were eosinophilic on H&E, blue/grey on cresyl violet, blue on Klüver-Barrera, grey/black on Holmes' silver, red on PAS stains before and after diastase digestion, and were almost unstained on the hematoxylin counterstain used during immunohistochemical staining. In cross-section, dystrophic axons were round, and they were variously homogeneous, palely vacuolated, or more intensely stained centrally on H&E, PAS, and Holmes' silver stained sections. The identity of spheroids as swollen axons was confirmed by intense immunostaining for neuron-specific enolase (NSE, fig.A.3, panel E) and absence of staining for GFAP (fig.A.3, panel F). Some, but not all, dystrophic axons in the brainstem and spinal cord stained intensely for phosphorylated neurofilaments (fig.A.3, panel D). Electron microscopy of dystrophic brainstem axons revealed axon-filling accumulations of small, pleomorphic, membrane-bound vesicles containing variously electron-dense fragments of organelles and amorphous material (fig.A.3, panels G and H). Some mitochondrial fragments were contained in double membrane vesicles and were in various stages of degeneration, suggestive of ongoing mitophagy. There were whorls of disorganized intermediate filaments among the vesicles in some spheroids, consonant with the variable neurofilament immunostaining indicated above. Neuroaxonal dystrophy was prominent throughout the mesencephalic, pontine, and medullary tegmentum. Swollen axons were observed in lateral and medial ventral thalamic, red, and caudal olivary nuclei;

Figure A.3. Staining, antigenic, and morphologic characteristics of dystrophic axons. Axonal swellings stained pink with H&E (panel **A**, red nucleus) and PAS (panel **B**, rostral cerebellar peduncle shown, stained after diastase digestion), and grey to black with Holme's silver stain (panel **C**, arrowhead indicates a spheroid in the rostral cerebellar peduncle). Immunohistochemical staining was either strongly positive or negative (arrowheads) when the primary antibody (SMI 312) was directed at phosphorylated neurofilaments (panel **D**). Panels **E** and **F** show serial cross-sections of the ventral medial funiculus of cervical spinal cord segment 6 immunostained for neuron-specific enolase (NSE) and GFAP, respectively. Dystrophic axons throughout the CNS uniformly stained positive for NSE but never for GFAP (see also fig.A.4). Bars in panels A-F = 20 μm. Transmission electron microscopy of dystrophic axons in the red nucleus (panel **G**) and medullary tegmentum (panel **H**) showed accumulations of membrane-bound vacuoles containing variably electron-dense amorphous material or organelles in various stages of degeneration (bars in panels **G** and **H** = 1 μm).

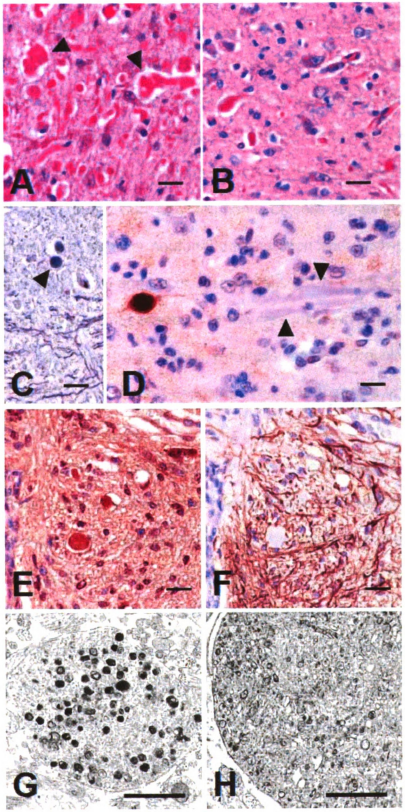
A
B
C
D
E
F
G
H

the cerebellorubral tract, the rubrospinal tract, the mesencephalic tract of the trigeminal nerve, and rostral and caudal cerebellar peduncles; and diffusely distributed in the reticular formation (fig.A.A.4). They were particularly obvious at midline decussations of the rostral and caudal cerebellar peduncles and the myencephalic reticular formation. The medullary reticular formation was conspicuously devoid of intact large neuron perikarya of the gigantocellular tegmental field in affected pups, with only remnants of cells remaining in normal positions. There were signs of neuronal degeneration and dystrophic axons in cranial nerve (CN) nuclei and tracts, respectively, of CN V, VII, IX, X, XI, and XII. These lesions were not observed in the cerebellar white matter, crus cerebri, pontine corticospinal tract, colliculi, pyramidal tracts, rostral olives, pontine nuclei, or CN III, IV, and VI. Iron deposition was not observed in the brainstem or any other part of the CNS.

In comparison to controls, the affected pup brainstem sections exhibited variably increased GFAP staining and astrocyte hypertrophy in the areas of the red nucleus, the decussation of the cerebellorubral tract, the transverse pontine fibers, throughout the medullary tegmentum, ascending and decussating fibers and the septae of the caudal olives, all along the course of CN VII, and throughout the nucleus ambiguous (fig.A.A.4). Areas that were consistently spared included the pyramids, superior olives, and the pontine nuclei. Despite widespread morphologic evidence of apoptotic cells (condensed, fragmented nuclei and darkly eosinophilic cytoplasm), there was very little activated caspase-3 staining of brainstem neurons and no more so in affected than in

Figure A.4. Brainstem neuroaxonal dystrophy and astrocytic reaction. Transverse sections through the red nucleus and nucleus of CN III (panels **A** and **B**), genu of CN VII nerve tract and nucleus of CN VI (panels **C** and **D**), nucleus and ascending fibers of CN VII (panels **E** and **F**), and caudal olive at the level of the obex (panels **G** and **H**) are shown. Panels **A**, **C**, **E**, and **G** were H&E stained; panels **B**, **D**, **F**, and **H** were GFAP immunostained (bars in all panels = 100 μm). In each panel, filled arrowheads point to examples of degenerating neuronal perikarya, and open arrowheads indicate swollen axons or spheroids. The roman numerals in some panels indicate cranial nerve nuclei. The dotted lines in panel **B** outline the apparently normal tract of CN III passing through the red nucleus. GFAP staining was greater than normal in panels **B** and **D** but was no different from staining in control pup sections in panels **F** and **H**.

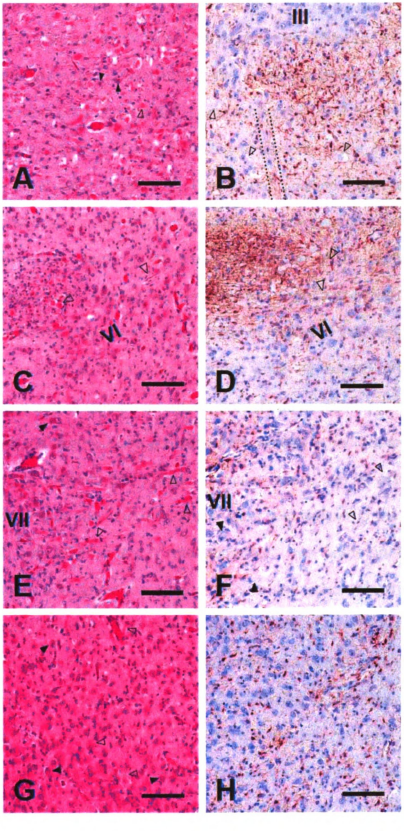
A
III
B
VI
C
VI
D
VII
E
VII
F
G
H

control pup sections. Sections of cerebellar cortex, including vermis and hemispheres, from affected pups were remarkable for reduced foliation, decreased neuronal precursor populations in the external granular cell layer, and decreased Purkinje cells and internal granular neurons (fig.A.5). Purkinje cell loss was patchy; many were degenerating or absent, but a subset of residual Purkinje cells were present in their usual position between the external and internal granular cell layers. Calbindin immunostain also revealed a dearth of Purkinje cell axons in the arbor vitae. None of the routine or immunohistochemical stains applied revealed swollen axons/spheroids in the cerebellum. The external granular cell layer varied in thickness from complete absence in some areas up to 35 microns in others, while the external granular layer in control pups was of uniform thickness throughout, at approximately 40 microns. Affected and normal pups showed approximately equal numbers of mitotic figures in the external and internal granular layers and of activated caspase-3 stained cells in the internal granular layer and deeper in the arbor vitae. Similarly, in both affected and normal pups there was exuberant GFAP staining of astrocytes throughout the arbor vitae with fine extensions through the internal granular, Purkinje, and external granular cell layers. In contrast, only affected pups showed morphologic or activated caspase-3 evidence of increased Purkinje cell apoptosis, and only in affected pups were there patches of astrocyte hypertrophy in the Purkinje and external granular layers (fig. 5, panels F and H). Positions of neurons of (deep) cerebellar nuclei were often observed as holes in the neuropil or mere remnants of cells (fig.A.5,

Figure A.5. Cerebellar histopathology. Tissue sections derived at birth of normal littermates (panels **A**, **C**, **E**, **G**) and FNAD affected pups (panels **B**, **D**, **F**, **H**, **I**, and **J**) are shown. Panels **A-H** and **I** show near-midline sagittal sections of cerebellum with the dorsal surface to the top and rostral to the left of each panel. Panels **A-D** show sections from pups taken by cesarean section at 60 days of gestation; other panels are from full-term pups. Sections in panels **A** and **B** are cresyl violet stained, (bars = 1 mm) and in panels **C** and **D** are calbindin immunostained (for Purkinje cells) with cresyl violet counterstain (bars = 200 μm). Sections in panels **E** and **F** are activated caspase-3 immunostained. Adjacent sections in panels **G** and **H** are GFAP immunostained. Panel **I** shows an H&E stained section of affected pup cerebellum adjacent to sections in **F** and **H**, and panel **J** shows an H&E stained transverse section through the dentate nucleus (bars in **E-J** = 100 μm).

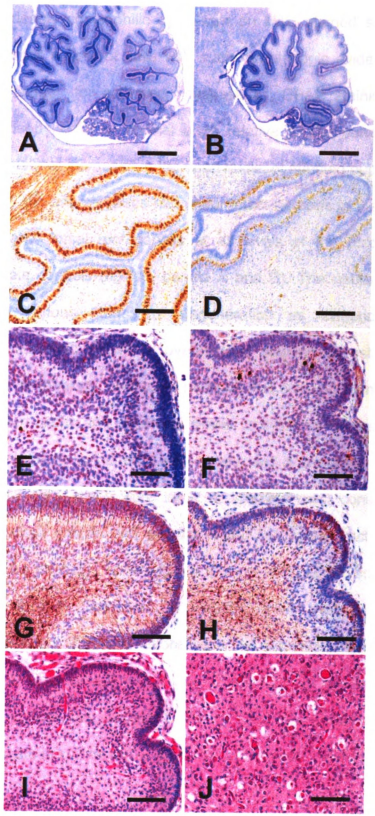
A
B
C
D
E
F
G
H
I
J

panel J). Remaining neurons in these nuclei exhibited pyknotic nuclear fragmentation and deeply eosinophilic cytoplasm on H&E stained sections. Some, but only a small subset of cells with such morphologic evidence of apoptosis also stained for activated caspase-3. GFAP staining was attenuated in the deep nuclei of normal pups relative to the surrounding neuropil but was somewhat increased in the deep nuclei of affected pups.

In spinal cord, the affected pups had fewer intact neurons in the lateral and ventral horns and dorsal root ganglia at all levels of the cord when compared to littermate controls (fig.A.6, panels A and B). The neurons that remained were in various stages of degeneration as evidenced by chromatolysis with eccentric nuclei or overall light staining (ghost cells), occasional apoptotic morphology, and some neurons that were surrounded by gliotic tissue. Swollen axons and spheroids similar to those in the brainstem were seen at all levels of the spinal cord white matter and occasionally in gray matter. In the cranial cord, these were in all funiculi but most consistently observed in the fasciculi gracilis and cunteatus and the spinal tract of the trigeminal nerve. More caudally, spheroids were most often observed in the lateral and ventral funiculi. Compared to controls, there were astrocyte hypertrophy and increased GFAP-immunoreactive cell processes throughout the lateral and ventral horns of spinal cord gray matter (fig.A.6, panels C and D). Neurons exhibiting activated caspase-3 staining were rare in affected pup sections of cord but were not observed at all in normal littermate sections.

Figure A.6. Spinal cord histopathology. Transverse sections of spinal cord segment C_6 of a normal littermate (panels **A** and **C**) and an FNAD affected pup (panels **B** and **D**) at birth are shown with Klüver-Barrera stain (panels **A** and **B**) or GFAP immunostain (panels **C** and **D**; bars in panels **A-D** = 500 μm). Transverse sections of spinal cord segment L_5 dorsal roots (panels **E** and **F**) and ventral roots (panels **G** and **H**) of a normal littermate (panels **E** and **G**) and an FNAD affected pup (panels **F** and **H**) at birth are shown (toluidine blue; bars = 20 μm). The greatly enlarged dorsal root axon of panel **F** is shown at higher magnifications in panels **I** (bar = 2 μm) and **J** (bar = 500 nm). Panel **J** shows the area bounded by the dashed line box in panel **I**.

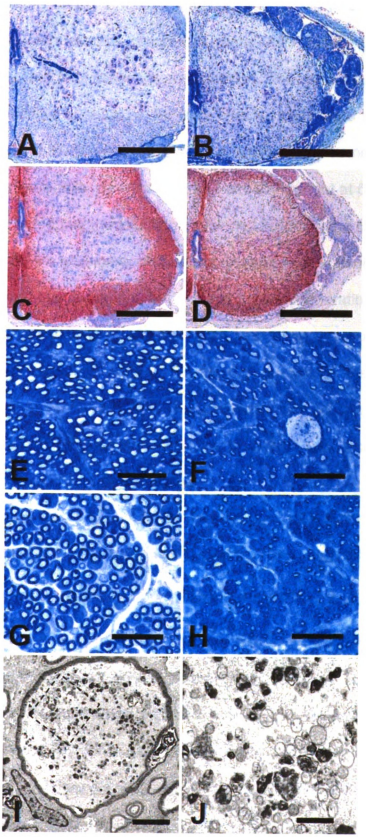
A
B
C
D
E
F
G
H
I
J

In order to observe earlier stages of disease progression in the CNS, two pregnancies were interrupted by cesarean section at 53 and 60 days of gestation, respectively, and fetal tissues were examined. The same cerebellar and brainstem abnormalities observed in full-term affected pups were seen in affected fetuses, although there were fewer swollen axons and less neuronal degeneration. Delayed cerebellar development was already evident at 53 days of gestation, but it appeared that the folia had developed further in the full term affected pups. In these, the youngest affected fetuses examined, neurons of the deep cerebellar nuclei were present, but signs of neurodegeneration were already evident. The spinal cord of affected pups was already reduced in diameter to ~70 % of normal controls at 53 days of gestation. The large neuronal perikarya of the ventral horn were in appropriately placed groups but already showed some mild degenerative changes, and there was increased astrocytosis in the lateral and ventral gray matter.

Dorsal and ventral spinal nerve roots in affected pups examined at birth were remarkable for the paucity of myelinated axons (fig.A.6, panels E-H). For instance, at the L_5 segment, an affected pup dorsal root had fewer than 50% of the myelinated axons of a normal littermate (1806 vs. 3793), and the number of ventral root axons was reduced to ~ 60% of normal (3156 vs. 5305). Numbers and morphology of Schwann cell nuclei appeared normal, and myelin sheaths had normal appearance. Dystrophic axans were present in spinal roots of affected pups as well (fig.A.6, panels F, I, and J). Electron microscopy of dorsal roots demonstrated some hugely dilated axons (5-15 μm diam. vs. 1-3 μm diam.

of surrounding axons in affected pups, as well as in normal littermates). They had intra-axonal accumulation of disordered neurofilaments, degenerating mitochondria, and small vacuoles containing amorphous material, but the myelin sheaths appeared normal.

Spheroids were also observed in peripheral nerves and intramuscular nerve branches of affected pups (fig.A.7). In the peroneal nerve, there were fewer myelinated axons overall (1235 ± 75 vs. 3051 ± 273), and the average diameter of remaining axons (excluding the obviously swollen axons with diameters > 6 μm) was less than that of normal pups (1.5 ± 0.5 μm vs. 2.8 ± 1.1 μm). In the phrenic nerve of affected pups, myelinated axon number was better preserved (1053 ± 65 vs. 1308 ± 27), but average axon diameters were again reduced (0.9 ± 0.3 μm vs. 1.5 ± 0.5 μm) (fig.A.7, panels A and B). Myelin sheaths appeared normal in the peripheral nerves examined.

In skeletal muscle of both affected and normal pups observed at birth, most muscle cells were small, though in some areas they varied in size with occasional hypertrophic cells, and some had central nuclei. In both, there was a mixture of myotubes and myofibers, and there were appropriate numbers of muscle spindles. Enzymatic histochemical fiber typing revealed almost entirely type II fibers, as previously described in newborn dog muscle (Braund and Lincoln 1981; Shelton et al., 1988). In affected pup muscle, however, there was increased space between fibers, sporadic or groups of small fibers, and increased numbers of fibers showing pyknotic and fragmented nuclei, suggestive of apoptosis (fig.A.7, panels G and H). This was confirmed by

Figure A.7. Peripheral nerve and skeletal muscle histopathology. Transverse sections of phrenic (panels **A** and **B**) and sciatic (panels **C** and **D**) nerves and semimembranosus muscle (panels **E-H**) of a normal littermate (panels **A, C, E,** and **G**) and an FNAD affected pup (panels **B, D, F,** and **H**) at birth. Panels **A** and **B** are toluidine blue stained (bars = 20 μm), and panels **C** and **D** are toluidine blue-carmine red stained (bars = 30 μm). Panels **E** and **F** are immunostained for activated caspase-3, and panels **G** and **H** are H&E stained (bars = 50 μm).

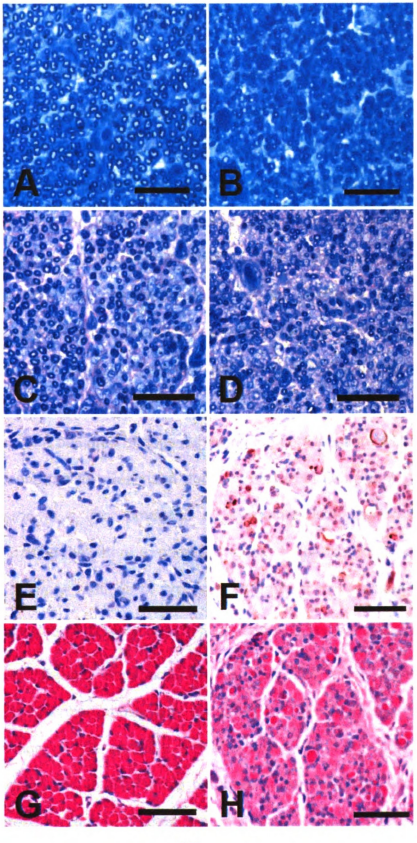
A
B
C
D
E
F
G
H

observation of increased numbers of myocytes in affected pup muscle staining positively for activated caspase-3 (7.4 ± 3.4/high power field vs. none observed in normal littermates) (fig.A.7, panels E and F).

Microscopic examination of the stifle in affected pups revealed multiple abnormalities previously described as secondary to joint immobilization (Akeson et al., 1987). The patellar tendon was 50-60 % the thickness of that in normal littermates, and femoral and tibial cortices were thinned. The origin of the patellar tendon exhibited disorganization of collagenous fibers, and its insertion on the tibia was compromised by loss of Sharpey's fibers and osteoclastic resorption of bone. There was early-stage proliferation of fibrofatty connective tissue within the joint space and among tissues caudal to the joint.

Clinical genetics: The pedigree of dogs exhibiting the constellation of clinical and neuroanatomic abnormalities described above is shown in figure 8. An affected pup first appeared in a litter produced by a brother-sister mating between offspring of a mating between a purebred giant schnauzer and a beagle. Subsequent to outcross matings of presumptive carriers to unrelated mongrel dogs (M_1-M_3), affected pups were born in litters with < 3 % neonatal mortality of other causes. All offspring were examined at birth. The gross phenotype of affected pups, as described above, was consistent and unambiguous. In the 33 prospective matings of this pedigree, 59 affected puppies, 34 male and 25 female, were among 230 total offspring produced in matings between obligate carriers. These results (25.7 % affected pups with even gender distribution) were

not statistically different from results expected under the hypothesis of simple autosomal recessive inheritance of a fully penetrant trait (χ^2=0.82, df=1, p>0.36 for affected vs. normal clinical status; χ^2=0.24, df=1, p>0.62 for gender distribution of affected offspring). These data indicate also that there was little or no embryonic or fetal loss of affected pups. Also of note is that the ratio of affected to total pups did not differ between matings in which alleles from different genetic backgrounds were segregating (26.4% vs. 25.4% on the left and right sides, respectively, of the pedigree in fig.A.8).

Molecular genetics: Eighty percent of human INAD patients exhibit mutations at the *PLA2G6* locus on chromosome 22. Therefore, we considered the canine orthologue as a candidate gene for FNAD in this family. Polymorphic markers flanking the canine *PLA2G6* locus (chr10: 29.58-29.63 Mb; CanFam2 assembly May 2005) were examined in a subset of the canine pedigree shown in figure 8. The obligate carriers, F274 and F284, were heterozygous at both markers (fig.A.9). Thirty-six offspring from matings of these dogs were genotyped. As expected for markers separated by ~15 Mb, the marker alleles recombined on 7 of 72 chromosomes (9.7 %). At least one affected pup exhibited each of the four possible unrecombined genotypes. Therefore, no hypothesized allele of *PLA2G6* was uniformly homozygous in affected pups, a criterion imposed by the simple autosomal recessive inheritance of this disorder observed in the breeding experiments described above. *PLA2G6* was excluded as a candidate disease gene in canine FNAD.

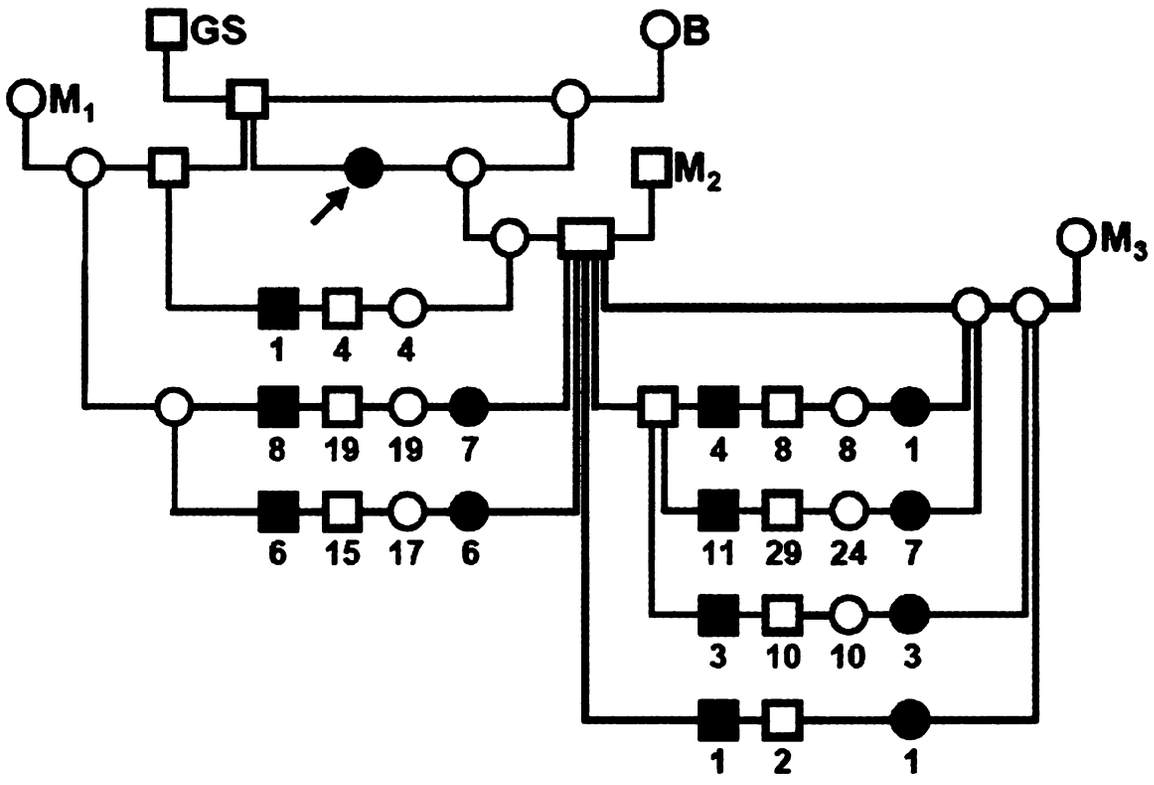

Figure A.8. Canine FNAD pedigree. Circles indicate females, squares indicate males, filled symbols indicate pups exhibiting the FNAD phenotype and open symbols indicate phenotypically normal dogs. Offspring of matings are arranged on a horizontal line connecting vertical lines descending from symbols for the sire and dam. Numbers below symbols indicate the number of offspring of the sex and phenotype indicated produced in multiple matings of the same parents. The arrow indicates the proposita. Dogs indicated **GS** and **B** were a purebred giant schnauzer and beagle, respectively, and **M_1-M_3** were three unrelated mongrels.

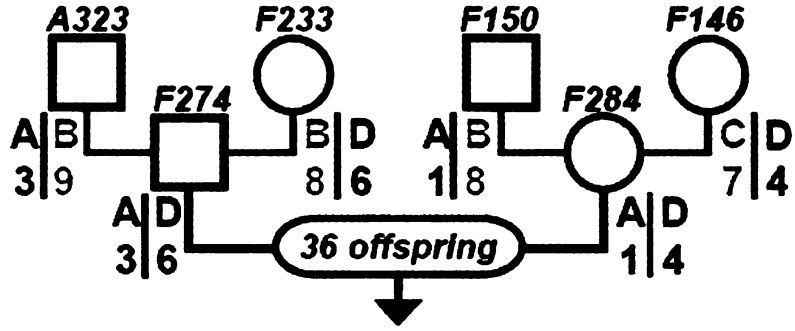

Genotype	No. Normal	No. Affected
A|A / 3|1	0	2
A|D / 3|4	5	2
D|A / 6|1	8	3
D|D / 6|4	8	1
Recombinant	6	1

Figure A.9. *PLAGA2* is excluded from the canine FNAD locus. Alleles of markers flanking the canine *PLAGA2* locus were examined in grandparents, parents and 36 offspring. Pedigree symbol conventions are as for figure 8, and marker genotypes of each grandparent or parent are below their respective symbols. Parental haplotype phase was deduced from grandparent genotypes. The table indicates the number of normal and affected offspring, respectively, that exhibited each of the nonrecombinant haplotypes or recombination on one chromosome. At least one affected pup exhibited each of the possible haplotype pairs, thus excluding the locus bounded by these markers from the disease locus.

DISCUSSION

In this report, fetal akinesia of affected pups, documented *in utero*, led to multiple joint contractures, pulmonary hypoplasia, and failure of respiration at birth. It is well demonstrated that any condition restricting fetal movement *in utero* may result in a constellation of morphologic abnormalities, including intrauterine growth retardation, facial anomalies, immobile joints, and limb malposition (Moessinger, 1983; Hall, 1986, 1997; Hageman et al., 1987; Folkerth et al., 1993; Bürglen et al., 1996; Riemersma et al., 1996; Brownlow et al., 2001). Such conditions can be extrinsic to the fetus (e.g. oligohydramnios) or intrinsic lesions (e.g. toxic, infectious, or genetic) that affect the kinesthetic pathways, motor neurons, the neuromuscular junction, or skeletal muscle. If fetal respiratory movements or swallowing are inhibited, the condition additionally results in pulmonary hypoplasia and polyhydramnios, respectively. Arthrogryposis multiplex congenita, multiple congenital contractures, Pena-Shokeir syndrome/phenotype, and most recently, fetal akinesia deformation sequence (FADS) have variously been used to describe these signs of etiologically heterogeneous fetal-onset disorders (Porter, 1995). At present, it is clear that when the FADS constellation of abnormalities is recognized in a patient, it is a description, rather than a diagnosis, and begs the question of cause. Therefore, fetal akinesia, joint contractures, pulmonary hypoplasia, and respiratory failure observed in the affected pups described here are interpreted as secondary features of motor unit dysfunction.

The etiology of fetal akinesia in this family is an inherited lesion that causes NAD and degeneration of spinal sensory and motor neurons, among others. It is a fully penetrant, autosomal recessive disorder. This family has genetic contributions from 5 unrelated dogs of widely different backgrounds, yet we observed no apparent alteration of the phenotype by modifying loci. The canine disorder is clinically and developmentally similar to the earliest-onset (fetal) cases of human INAD, described as connatal (Chow and Padfield 2008), but it is not caused by mutation of the canine *PLA2G6* locus. We prefer the term fetal-onset neuroaxonal dystrophy (FNAD) to describe the canine disorder as well as those of human patients whose clinical signs at birth indicate onset of this pathologic process during fetal life.

We suggest that a primary or secondary effect on motor neurons causes a failure to establish or, more probably, a loss of skeletal muscle innervation and the ensuing motor dysfunction observed as fetal akinesia. Our interpretation of the histopathology is that affected pups develop normally for a period, probably through the second trimester, but subsequently experience degeneration and dysfunction of a subset of CNS cells during the late fetal period. At birth the disorder is defined by multifocal neuroaxonal dystrophy with delayed or arrested development of specific CNS structures and accompanied by lower motor neuron degeneration, skeletal muscle dysfunction, and the consequent joint remodeling caused by immobility.

To our knowledge, there is no other animal model of FNAD. Spontaneously occurring familial disorders characterized by neuroaxonal

dystrophy have been described in various dog breeds (Cork et al., 1983; Griffiths et al., 1986; Sacre et al., 1993; Diaz et al., 2007; Jäderlund et al., 2007; Nibe et al., 2007, 2009), cats (Carmichael et al., 1993), sheep (Harper et al., 1991), horses (Miller and Collatos, 1997), and mice (Bouley et al., 2006). Each of these differs in at least some aspect of distribution of CNS lesions, integrity of myelin sheaths, or spheroid ultrastructure from what we report here. It is difficult, however, to make direct comparisons of the lesions because the neuronal pathology of the affected FNAD pups begins *in utero*, and the resultant motor dysfunction is lethal at birth. In all other descriptions of NAD in animals the onset of disease signs is at least some months after birth. The exceptions are those few human INAD patients that show signs at birth or prenatally. In the pathologically related human disorders, including idiopathic neurodegeneration with brain iron accumulation (NBIA) type 1 (OMIM #234200) and type 2 (OMIM #610217), the onset of disease is typically not until several years of age. Nor was iron accumulation observed in brainstem of the FNAD pups.

Canine FNAD affects neurons throughout the cerebellum, brainstem, spinal cord, and peripheral nerves, but the neuronal layers and nuclei of major CNS structures are in correct positions. The bulk of pathology occurs in synaptically connected neurons of the extrapyramidal motor control system, including proprioceptive input via sensory neurons and tracts, and in cranial and spinal nerves that carry axons of lower motor neurons to other than extra-ocular muscles. One possible scenario is that sensory input is lost initially, and neurons in the motor coordinating pathways and reflex arcs subsequently lose synaptic

activity or trophic molecules needed to maintain their integrity during development. Alternatively, the distribution of pathology may be due to a cell-autonomous defect that is most devastating to the particular subset of neurons involved. Most probably, however, the totality of observed pathology results from a mixture of mechanisms.

NAD is often attributed to disturbance of axonal transport (Coleman 2005; Saxena and Caroni 2007; DeVos et al., 2008), but in most cases causality has not been demonstrated. Additionally, swollen axons and spheroids are a feature of the neuropathology observed in mice expressing engineered or spontaneous mutations of genes whose products mediate basal macroautophagy and/or ubiquitin-mediated protein turnover (Saigoh et al., 1999; Komatsu et al., 2006, 2007; Hara et al., 2006). Studies in the *Lurcher* mouse, a model of excitotoxic neurodegeneration, indicate that an early response to axonal dystrophy in Purkinje cells is induction of autophagy to protect axons under metabolic stress (Wang et al., 2006). Whether disturbances of axonal transport overwhelm basal autophagy and/or ubiquitin-mediated protein turnover in neurons and lead to accumulation of axonal contents as spheroids, or whether these homeostatic processes interact in another way, remains to be determined.

The occurrence of dystrophic axons in the canine disorder is only partially coincident with astrocytic reaction or gliosis, suggesting that there may not be a cause and effect relationship and/or that dystrophic axons do not cause exuberant inflammation and are not rapidly cleared. The most consistent association between astrocytosis and signs of neurodegeneration (shrunken

cells, eccentric nuclei, and chromatolysis) was in the caudal olives and ventral and intermediate horns of spinal cord, suggesting a somewhat different degenerative mechanism in cells of those structures. A similar lack of coincident pathologies was that most neurons exhibiting morphologic evidence of apoptosis did not stain for activated caspase-3. However, all of these observations are essentially "snapshots" of ongoing pathologic processes taken at birth, and any lack of association may simply indicate temporally discrete stages of pathology in individual cells.

Pontocerebellar hypoplasia type 1 (PCH 1; a.k.a. pontocerebellar hypoplasia with spinal muscular atrophy; OMIM # 607596) is another autosomal recessive, fetal-onset disorder of CNS development with similarities to canine FNAD. In human PCH 1, the major subdivisions of the cerebellum are usually intact, albeit small, and there is loss of Purkinje and granular cells. Degeneration of the inferior (caudal) olivary nuclei, massive loss of ventral pontine neurons, and reactive gliosis in the brainstem are prominent. Lower motor neuron dysfunction is the feature that causes early lethality and distinguishes PCH 1 from all other types of PCH (Barth, 1993, 2000). In the earliest-onset cases of PCH 1, fetal akinesia leads to prominent morphologic abnormalities of the FADS complex. Death typically ensues in the immediate postnatal period due to generalized hypotonia and respiratory insufficiency requiring ventilatory support (Gorgen-Pauly et al., 1999; Muntoni et al., 1999; Ryan et al., 2000). The genetic basis of PCH 1 is unknown and most likely heterogeneous (Barth, 1993, 2000; Rudnik-Schöneborn et al., 2003). The

main similarities between canine FNAD and human PCH 1 are that both exhibit cerebellar hypoplasia and features of FADS that result from fetal-onset motor dysfunction. Two important differences between these disorders are that the pontine nuclei, which are largely intact in FNAD, degenerate in PCH 1, and NAD is not reported in PCH 1.

Mutations of *PLA2G6* cause most cases of human INAD (Gregory et al., 2008), but how these cause NAD is unknown. The recessive nature of human INAD and canine FNAD indicates that, in both instances, mutations cause a loss of gene function. Because canine FNAD is not due to mutation of *PLA2G6*, NAD is likely a stereotyped response of neurons to a variety of inherited dysfunctions, as well as to vitamin E deficiency and other insults, perhaps defining a common mechanism or pathway (Schmidt et al., 1991, 1997). At this time we are poised to take a positional-candidate cloning approach for identification of the gene mutation responsible for canine FNAD. The availability of high-resolution canine linkage and radiation hybrid maps, the assembled canine genome sequence with 7.6 X coverage, gene and SNP arrays, and now a large kindred segregating canine FNAD complete the set of needed resources for a whole-genome scan by linkage or association of markers.

ACKNOWLEDGEMENTS

The authors thank G. Diane Shelton and Brunhilde Wirth for helpful discussions, Thomas Van Winkle for initial histopathologic assessment, Thomas Mave for caesarian sections, the MSU Investigative HistoPathology Laboratory for tissue sections and stains, and Ralph Common for electron microscopy and photomicrographs. Dr. Rosenstein's present address is VCA South Shore Animal Hospital, 595 Columbian St, Weymouth, MA 02190. We are especially grateful to Donald F. Patterson for inspiration and guidance early in these investigations.

LITERATURE CITED

1. Akeson WH, Amiel D, Abel MF, Garfin SR, Woo SL-Y. 1987. Effects of immobilization on joints. Clin Orthop Relat Res 219:28-37.

2. Aoki T, Tanaka T, Watabe H. 1992. Purification and characterization of gamma-enolase from various mammals. Chem Pharm Bull (Tokyo) 40:1236-1239.

3. Bakker HD, de Sonnaville M-LCS, Vreken P, Abeling NGGM, Groener JEM, Keulemans JLM, van Diggelen OP. 2001. Human α-N-acetylgalactosaminidase (α-NAGA) deficiency: no association with neuroaxonal dystrophy? Eur J Hum Genet 9:91-96.

4. Barth PG. 1993. Pontocerebellar hypoplasias. An overview of a group of inherited neurodegenerative disorders with fetal onset. Brain & Devel 15:411-422.

5. Barth PG. 2000. Pontocerebellar hypoplasia--how many types? Eur J Paediatr Neurol 4:161-162.

6. Bouley DM, McIntire JJ, Harris BT, Tolwani RJ, Otto GM, DeKruyff RH, Hayflick SJ. 2006. Spontaneous murine neuroaxonal dystrophy: a model of infantile neuroaxonal dystrophy. J Comp Path 134:161-170.

7. Braund KG, Lincoln CE. 1981. Histochemical differentiation of fiber types in neonatal canine skeletal muscle. Am J Vet Res 42:407-415.

8. Brownlow S, Webster R, Croxen R, Brydson M, Neville B, Lin J-P, Vincent A, Newsom-Davis J, Beeson D. 2001. Acetylcholine receptor δ subunit mutations underlie a fast-channel myasthenic syndrome and arthrogryposis multiplex congenital. J Clin Invest 108:125-130.

9. Bürglen L, Amiel J, Viollet L, Lefebvre S, Burlet P, Clermont O, Raclin V, Landrieu P, Verloes A, Munnich A, Melki J. 1996. Survival of motor neuron gene deletion in the arthrogryposis multiplex congentia-spinal muscular atrophy association. J Clin Invest 98:1130-1132.

10. Carmichael KP, Howerth EW, Oliver Jr JE, Klappenbach K. 1993. Neuroaxonal dystrophy in a group of related cats. J vet Diagn Invest 5:585-590.

11. Carrilho I, Santos M, Guinarães A, Teixeira J, Chorão R, Martins M, Dias C, Gregory A, Westaway S, Nguyen T, Hayflick S, Barbot C. 2008. Infantile neuroaxonal dystrophy: What's most important for the diagnosis ? Eur J Paediatr Neurol 12:491-500.

12. Chow G, Padfield JH. 2008. A case of infantile neuroaxonal dystrophy-connatal Seitelberger disease. J Child Neurol 23:418-420.

13. Colman M. 2005. Axon degeneration mechanisms: commonality amid diversity. Nat Rev Neurosci 6:889-898.

14. Cork LC, Troncoso JC, Price DL, Stanley EF, Griffin JW. 1983. Canine neuroaxonal dystrophy. J Neuropathol Exper Neurol 42:286-296.

15. Cox PM, Brueton LA, Bjelogrlic P, Pomroy P, Sewry CA. 2003. Diversity of neuromuscular pathology in lethal multiple pterygium syndrome. Pediatr Dev Pathol 6:59-68.

16. Davis JE, Kalousek DK. 1988. Fetal akinesia deformation sequence in previable fetuses. Am J Med Genet 29:77-87.

17. DeVos KJ, Grierson AJ, Ackerly S, Miller CCJ. 2008. Role of axonal transport in neurodegenerative diseases. Ann Rev Neurosci 31:151-173.

18. Diaz JV, Duque C, Geisel R. 2007. Neuroaxonal dystrophy in dogs: Case report in 2 litters of papillion puppies. J Vet Intern Med 21:531-534.

19. Folkerth RD, Guttentag SH, Kupsky WJ, Kinney HC. 1993. Arthrogryposis multiplex congenita with posterior column degeneration and peripheral neuropathy: a case report. Clin Neuropathol 12:25-33.

20. Gregory A, Westaway SK, Holm IE, Kotzbauer PT, Hogarth P, Sonek S, Coryell JC, Nguyen TM, Nardocci N, Zorzi G, Rodriguez D, Desguerre I, Bertini E, Simonati A, Levinson B, Dias C, Barbot C, Carrilho I, Santos M, Malik I, Gitschier J, Hayflick SJ. 2008. Neurodegeneration associated with genetic defects in phosphlipase A_2. Neurology 71:1402-1409.

21. Griffiths IR, Duncan ID. 1979. The central nervous system in canine giant axon neuropathy. Acta Neuropathol 46:169-172.

22. Gorgen-Pauly U, Sperner J, Reiss I, Gehl HB, Reusche E. 1999. Familial pontocerebellar hypoplasia type I with anterior horn cell disease. Eur J Paediatr Neurol 3:33-38.

23. Hageman G, Willemse J, van Ketel BA, Verdonck AFMM.1987. The pathogenesis of fetal hypokinesia: a neurological study of 75 cases of congenital contractures with emphasis on cerebral lesions. Neuropediatrics 18:22-33.

24. Hall JG. 1986. Analysis of Pena Shokeir phenotype. Am J Med Genet 25:99-117.

25. Hall JG. 1997. Arthrogryposis multiplex congenita: etiology, genetics, classification, diagnostic approach, and general aspects. J Pediatr Orthop Part B 6:159-166.

26. Hara T, Nakamura K, Matsui M, Yamamoto A, Nakahara Y, Suzuki-Migishima R, Yokayama M, Mishima K, Saito I, Okano H, Mizushima N. 2006. Suppression of basal autophagy in neural cells causes neurodegenerative disease in mice. Nature 441:885-889.

27. Harper PA, Morton AG. 1991. Neuroaxonal dystrophy in Merino sheep. Aust Vet J 68:152-153.

28. Haynes RL, Borenstein NS, Desilva TM, Folkerth RD, Liu LG, Volpe JJ, Kinney HC. 2005. Axonal development in the cerebral white matter of the human fetus and infant. J Comp Neurol 484:156-167.

29. He Q, Fyfe JC, Schäffer AA, Kilkenney A, Werner P, Kirkness EF, Henthorn PS. 2003. Canine Imerslund-Gräsbeck syndrome maps to a region orthologous to HSA14q. Mamm Genome 14:758-764.

30. Hunter AGW, Jimenez CL, Carpenter BF, MacDonald I. 1987. Neuroaxonal dystrophy presenting with neonatal dysmorphic features, early onset of peripheral gangrene, and a rapidly lethal course. Am J Med Genet 28:171-180.

31. Hwang IK, Choi JH, Li H, Yoo KY, Kim DW, Lee CH, Yi SS, Seong JK, Lee IS, Yoon YS, Won MH. 2008. Changes in glial fibrillary protein immunoreactivity in the dentate gyrus and hippocampus proper of adult and aged dogs. J Vet Med Sci 70:965-969.

32. Jäderlund KH. Örvind E, Johnsson E, Matiasek K, Hahn CN, Malm S, Hedhammar Å. 2007. A neurologic syndrome in golden retrievers presenting as a sensory ataxic neuropathy. J Vet Intern Med 21:1307-1315.

33. Janota I. 1979. Neuroaxonal dystrophy in the neonate. Acta Neuropathol 46:151-154.

34. Jennekens FGI, Barth PG, Fleury P, Veldman H, Keuning JF, Westdorp J. 1984. Axonal dystrophy in a case of connatal thalamic and brain stem degeneration. Acta Neuropathol 64:68-71.

35. Kent WJ. 2002. BLAT - the BLAST-like alignment tool. Genome Res 12:656-664.

36. Khateeb S, Flusser H, Ofir R, Shelef I, Narkis G, Vardi G, Shorer Z, Levy R, Galil A, Elbedour K, Birk OS. 2006. *PLA2G6* mutation underlies infantile neuroaxonal dystrophy. Am J Hum Genet 79:942-948.

37. Komatsu M, Waguri S, Chiba T, Murata S, Iwata J, Tanida I, Ueno T, Koike M, Uchiyama Y, Kominami E, Tanaka K. 2006. Loss of autophagy in the central nervous system causes neurodegeneration in mice. Nature 441:880-884.

38. Komatsu M, Wang QJ, Holstein GR, Friedrich, Jr VL, Iwata J, Kominani E, Chait BT, Tanaka K, Yue Z. 2007. Essential role for autophagy protein Atg7 in the maintenance of axonal homeostasis and the prevention of axonal degeneration. Proc Nat Acad Sci, USA 104:14489-14494.

39. Kurian MA, Morgan NV, MacPherson L, Foster K, Peake D, Gupta R, Philip SG, Hendriksz C, Moton JEV, Kingston HM, Rosser EM, Wassmer E, Gissen P, Maher ER. Phenotypic spectrum of neurodegeneration associated with mutations in the *PLA2G6* gene (PLAN). Neurology 70:1623-1629.

40. Malik I, Turk J, Mancuso DJ, Montier L, Wohltmann M, Wozniak DF, Schmidt RE, Gross RW, Kotzbauer PT. 2008. Disrupted membrane homeostatis and accumulation of ubiquinated proteins in a mouse model of infantile neuroaxonal dystrophy caused by *PLA2G6* mutations. Am J pathol 172: 406-416.

41. Marangos PJ, Zomzely-Neurath C, Luk DC, York C. 1975. Isolation and characterization of the nervous system-specific protein 14-3-2 from rat brain. Purification, subunit composition, comparison to the beef brain protein. *J Biol Chem* 250: 1884-1891.

42. Mellersh CS, Langston AA, Acland GM, Fleming MA, Ray K, Wiegand NA, Francisco LV, Gibbs M, Aguirre GD, Ostrander EA. 1997. A linkage map of the canine genome. Genomics 46:326-336.

43. Miller MM, Collatos C. 1997. Equine degenerative myeloencephalopathy. Vet Clin North Am Equine Pract 13:43-52.

44. Moessinger AC.1983. Fetal akinesia deformation sequence: an animal model. Pediatrics 72:857-863.

45. Muntoni F, Goodwin F, Sewry C, Cox P, Cowan F, Airaksinen E, Patel S, Ignatius J, Dubowitz V. 1999. Clinical spectrum and diagnostic difficulties of infantile pontocerebellar hypoplasia type I. Neuropediatrics 30:243-248.

46. Nibe K, Kita C, Morozumi M, Awamura Y, Tamura S, Okuno S, Kobayashi T, Uchida K. 2007. Clinicopathological feature of canine neuroaxonal dystrophy and cerebellar cortical abiotrophy in papillion and papillion-related dogs. J Vet Med Sci 69:1047-1052.

47. Nibe K, NakyamaH, Uchida K. 2009. Immunohistochemical features of dystrophic axons in Papillion dogs with neuroaxonal dystrophy. Vet Pathol 46:474-483.

48. Porter HJ. 1995. Lethal arthrogryposis multiplex congenital (fetal akinesia deformation sequence, FADS). Pediatr Pathol Lab Med 15:617-637.

49. Ribera J, Ayala V, Esquerda JE. 2002. c-Jun-like immunoreactivity in apoptosis is the result of a crossreaction with neoantigenic sites exposed by caspase-3-mediated proteolysis. J Histochem Cytochem 50: 961-972.

50. Richman M, Mellersh CS, André C, Galibert F, Ostrander EA. 2001.Characterization of a minimal screening set of 172 microsatellite markers for genome-wide screens of the canine genome. J Biochem Biophys Methods. 47:137-149.

51. Riemersma S, Vincent A, Beeson D, Newland C, Hawke S, Vernet-der Garabedian B, Eymard B, Newsom-Davis J. 1996. Association of arthrogryposis multiplex congenital with maternal antibodies inhibiting fetal acetylcholine receptor function. J Clin Invest 98:2358-2363.

52. Rudnik-Schöneborn S, Sztriha L, Aithala GR, Houge G, Lægreid LM, Seeger J, Huppke M, Wirth B, Zerres K. 2003. Extended phenotype of pontocerebellar hypoplasia with infantile spinal muscular atrophy. Am J Med Genet 117A:10-17.

53. Ryan MM, Cooke-Yarborough CM, Procopis PG, Ouvrier RA. 2000. Anterior horn cell disease and olivopontocerebellar hypoplasia. Pediatr Neurol 23:180-184.

54. Sago K, Tamahara S, Tomihari M, Matsuki N, Asahara Y, Takei A, Bonkobara M, Washizu T, Ono K. 2008. In vitro differentiation of canine celiac adipose tissue-derived stromal cells into neuronal cells. J Vet Med Sci 70:353-357.

55. Saigoh K, Wang Y-L, Suh J-G, Yamanishi T, Sakai Y, Kiyosawa H, Harada T, Ichihara N, Wakana S, Kikuchi T, Wada K. 1999. Intragenic deletion in the gene encoding ubiquitin carboxy-terminal hydrolase in *gad* mice. Nat Genet 23:47-51.

56. Sacre BJ, Cummings JF, de Lahunta A. 1993. Neuroaxonal dystrophy in a Jack Russell terrier pup resembling human infantile neuroaxonal dystrophy. Cornell Vet 83:133-142.

57. Saxena S, Caroni P. 2007. Mechanisms of axon degeneration: From development to disease. Prog Neurobiol 23:174-191.

58. Schmidt RE, Coleman BD, Nelson JS. 1991. Differential effect of chronic vitamin E deficiency on the development of neuroaxonal dystrophy in rat gracile/cuneate nuclei and prevertebral sympathetic ganglia. Neurosci Lett 123:102-106.

59. Schmidt RE, Dorsey D, Parvin CA, Beaudet LN, Plurad SB, Roth KA. 1997. Dystrophic axonal swellings develop as a function of age and diabetes in human dorsal root ganglia. Neuropathol Exp Neurol 56:1028-1043.

60. Shelton GD, Cardinet GH, Bandman E. 1988. Expression of fiber type specific proteins during ontogeny of canine temporalis muscle. Musc & Nerve 11:124-132.

61. Shinzawa K, Sumi H, Ikawa M, Matsuoka Y, Okabe M, Sakoda S, Tsujimoto Y. 2008. Neuroaxonal dystrophy caused by group VIA phospholipase A_2 deficiency in mice: a model of human neurodegenerative disease. J Neuroscience 28:2212-2220.

62. Sisó S, Hanzlíček D, Fluehmann G, Kathmann I, Tomek A, Papa V, Vandevelde M. 2006. Neurodegenerative diseases in domestic animals: a comparative review. Vet J 171:20-38.

63. Sisó S, Tort S, Aparici C, Pérez L, Vidal E, Pumarola M. 2003. Abnormal neuronal expression of the calcium-binding proteins, parvalbumin, and calbindin D-28k, in aged dogs. J Comp Path 128:9-14.

64. Summers BA, Cummings JF, de Lahunta A. 1995. Veterinary Neuropathology. Mosby, St. Louis.

65. Tachibana H, Hayashi T, Kajii T, Takashima S, Sasaki K. 1986. Neuroaxonal dystrophy of neonatal onset with unusual clinicopathological findings. Brain Dev 8:605-609.

66. Toma JG, Akhavan M, Fernandes KJ, Barnabe-Heider F, Sadikot A, Kaplan DR, Miller FD. 2001. Isolation of multipotent adult stem cells from the dermis of mammalian skin. *Nat Cell Biol* **3**: 778-784.

67. Ulfig N, Nickel J, Bohl J. 1998. Monoclonal antibodies SMI 311 and SMI 312 as tools to investigate the maturation of nerve cells and axonal patterns in human fetal brain. Cell Tissue Res 291:433-443.

68. Wang QJ, Ding Y, Kohtz S, Mizushima N, Cristea IM, Rout MP, Chait BT, Zhong Y, Heintz N, Yue Z. 2006. Induction of autophagy in axonal dystrophy and degeneration. J Neurosci 26:8057-8068.

69. Woodard JC, Collins GH, Hessler JR. 1974. Feline hereditary neuroaxonal dystrophy. Am J Pathol 74:551-566.

70. Wu Y, Jiang Y, Gao Z, Wang J, Yuan Y, Xiong H, Chang X, Bao X, Zhang Y, Xiao J, Wu X. 2009. Clinical study and *PLA2G6* mutation screening analysis in Chinese patients with infantile neuroaxonal dystrophy. Eur J Neurol 16:240-245.

71. Zhao Y, Flandin P, Long JE, Cuesta MD, Westphal H, Rubenstein JL. 2008. Distinct molecular pathways for development of telencephalic interneuron subtypes revealed through analysis of Lhx6 mutants. J Comp Neurol 510:79-99.